African Journal of Environmental Science and Technology

Volume 11 Number 10, October 2017
ISSN 1996-0786

Academic Journals

ABOUT AJEST

The **African Journal of Environmental Science and Technology (AJEST)** (ISSN 1996-0786) is published monthly (one volume per year) by Academic Journals.

African Journal of Environmental Science and Technology (AJEST) provides rapid publication (monthly) of articles in all areas of the subject such as Biocidal activity of selected plant powders, evaluation of biomass gasifier, green energy, Food technology etc. The Journal welcomes the submission of manuscripts that meet the general criteria of significance and scientific excellence. Papers will be published shortly after acceptance. All articles are peer-reviewed

Contact Us

Editorial Office: ajest@academicjournals.org

Help Desk: helpdesk@academicjournals.org

Website: http://www.academicjournals.org/journal/AJEST

Submit manuscript online http://ms.academicjournals.me/

Editorial Board

African Journal of Environmental Science and Technology

Table of Contents: Volume 11 Number 10 October 2017

ARTICLES

academicJournals

Vol. 11(10), pp. 499-508, October 2017
DOI: 10.5897/AJEST2017.2360
Article Number: AA0247265921
ISSN 1996-0786

http://www.academicjournals.org/AJEST

African Journal of Environmental Science and Technology

Full Length Research Paper

Pig faeces digestion as compared to anaerobic co-digestion using waste waters sludge or bovine ruminal gastric content treatments

José Ramón Laines Canepa*, Shayla Montejo Olán, José Aurelio Sosa Olivier, Israel Ávila Lázaro and Gabriel Núñez Nogueira

División Académica de Ciencias Biológicas, Universidad Juárez Autónoma de Tabasco, Carretera Villahermosa-Cárdenas km 0.5 entronque con Bosques de Saloya, 86150, Centro, Tabasco, México.

Received 3 June, 2017; Accepted 17 August, 2017

Anaerobic co-digestion improves the pig faeces digestion process. This work presents anaerobic digestion of pig faeces (C) as compared to 2 co-substrates: Sludge (L) from waste waters and bovine ruminal gastric content (R). Pig faeces used were generated in a local farm at the Juarez Autonomous University of Tabasco (UJAT), with a total population of 148 animals. Analytical determinations were made on the substrate and co-substrates. Each treatment was performed in triplicate (9 experimental units), for 18 weeks. C+R co-digestion had the highest removal of chemical oxygen demand (COD) with 90%. Biogas production (0.012 L day^{-1}) was quantified for C and C+R, with concentrations of 70.87±8.65 and 71.89 ± 7.60% of methane (CH_4), respectively. For C+L, it was 0.009 L day^{-1}, with 77.89±6.74% of CH_4. Results obtained showed that co-digestion of C+L was better with regards to the quality of biogas from low hydrogen sulfide (H_2S) concentrations (70.33±6.36 ppm). The use of anaerobic co-digestion systems represents an alternative treatment for faeces generated in pig farms and other kinds of wastes to reduce the potential source of infection produced by these types of waste.

Key words: Biogas, digester, manure, pig faeces, rumen.

INTRODUCTION

Breeding of pig is an important and constantly growing activity in rural areas, which represents an option of food and economical resource. In a higher scale, pig activity is carried out in farms with the purpose of reproduction and sale of livestock. However, these activities generate water from washouts, food wastes, faeces and urine, with a high organic load, mostly disposed in natural aquatic environments in open landfill, without any treatment. Productions of pig worldwide generate 9% of the greenhouse gas (GHG) emissions in the livestock sector. In Mexico, 66,708.27 tons of faeces are produced per year with contribution of 27.80% (18.547 tons per year) from the pig sector (Gerber et al., 2013). In Tabasco, particularly in year 2015, 265,214 heads in 45,828

*Corresponding author. E-mail: josra_2001@yahoo.com.mx.

commercial production units was reported (SIAP, 2015). Montejo et al. (2015) reported that the average faeces generation on a daily basis in five different animal development stages (fattening, weaning, breeding, reproduction and maternity) is 100.96 kg; data was obtained in a survey made in pig farm at the Agriculture and Livestock Academic Division (DACA), Juarez Autonomous University of Tabasco (UJAT). Different alternatives have been given to solve these problems. Garzón and Buelna (2014) mentioned that pig exploitation requires a treatment system such as anaerobic digestion, considering wastes as useful resources in livestock production. Holm-Nielsen et al. (2009) pointed out that anaerobic digestion of animal wastes converts organic waste into two valuable products: biogas and digestate, which may be used as fuel in the generation of energy (heating and electricity), and as organic fertilizer, respectively. Chen et al. (2008) mentioned that anaerobic digestion offers the benefit of reducing the volume of wastes and the deactivation of pathogens. This technology has been successfully applied in the treatment of livestock food wastes, residual waters, and residuals sludge due to their capacity to reduce chemical oxygen demand (COD) and biochemical oxygen demand (BOD). Shah et al. (2015) defined co-digestion as a process where two substrates are anaerobically digested for biogas production. Chen et al. (2008) highlighted that the anaerobic co-digestion process, significantly improves the efficiency of waste treatment promoting the adaptation of the microorganisms to the inhibitor condition. Biogas production is largely supported by the substrate physical and chemical features, by total solid (TS) content, total volatile solids (TVS), fixed solids (FS) and ashes. Zhang et al. (2014), reported values of 29.96±0.26% of TS and 20.89±0.23% of TVS (dry base) for pig feces, while Chen et al. (2015) reported the use of pig faeces in anaerobic digestion, with total solids (TS) values of 20 and 35%, with a production of 2.40 L day^{-1} of biogas and a degradation of 56% of TS. Ye et al. (2013) reported rice straw co-digestion, kitchen wastes and pig manure in a concentration of 54 g TVS L^{-1}, with a yield of 383.9 L CH_4 kg^{-1} TVS. Kaparaju and Rintala (2005) used potato peelings in the co-digestion of pig manure with a ratio of 20 and 80%, respectively, reaching yields of 0.28 to 0.30 m^3 CH_4 kg^{-1} TVS. Borowski et al. (2014) evaluated the co-digestion of sludges in a wastewater treatment plant, pig faeces and bird manure (ratio of 70:20:10), reporting a performance of 336 L CH_4 kg^{-1} TVS, with 67% in volume of CH_4 and 29% in volume of carbon dioxide (CO_2). The purpose of this study was to evaluate the digestion eficiency of pig faeces generated in DACA with two different anaerobic co-digestion treatments using sludge from wastewater treatment plant or ruminal bovine stomach contents from a municipal slaughter house as co-substrates.

METHODOLOGY

Substrate and co-substrates acquisition

Pig faeces (C) were obtained from pig farm at the DACA UJAT (Figure 1a). Bovine ruminal gastric content (R) was obtained from the municipal slaughter house located in Cunduacán, Tabasco (Figure 1b). The sludge (L) was obtained from an Imhoff cone type wastewater treatment plant, located also in Cunduacán (Figure 1c). Composite samples were taken using the quarter method (SCFI, 1985a).

Physicochemical analyses

Each of the substrate samples and co-substrates were analyzed in triplicate for moisture percentage (SCFI, 1985b), TVS percentage (SCFI, 2015), FS and ash percentage (SCFI, 1984). TS determination was determined by the difference of 100% - % humidity according to Bux et al. (2012).

Experimental design

Three experimental units containing pig faeces, three pig faeces - sludges and three pig faeces-rumen units were displayed following a randomized design. Each experimental unit (EU) consisted of a 1 L reaction bottle connected to a 1 L Tedlar bag (Figure 2). Each reaction bottle was mixed at a rate of 500 rpm for 20 min using a Thermo Scientific grill 135935Q ® SP. Treatment were performed in triplicate. Each experimental unit was filled up to 80% (800 mL) in a ratio of 9:1 (Water: TVS), according to Gallardo et al. (2013). Each treatment design is described in Table 1, considering 10% of TVS on a dry basis.

Experimental monitoring

Biogas production was analyzed for 18 weeks. Different physicochemical parameters, like pH, oxide reduction potential (mV), dissolved oxygen (%) and chemical oxygen demand (mgL^{-1}) were measured during the experiment using Multiparametric Hanna® 9828 brand equipment, biogas characterization (% v/v), employing Dräger X-am model 7000 model Gas detection equipment and nutrients using Hanna® 83225 Multiparameter meter.

Statistical analysis

Analysis of variance (ANOVA) was performed with 95% confidence interval to determine differences in the three treatments tested (C, C + L and C + R), in the production of CH_4, CO_2 and H_2S. In the same way, Tukey multiple contrasts test was applied to find differences among treatment. STATGRAPHICS® Centurion XV package was used for the statistical analysis.

RESULTS AND DISCUSSION

Substrates and co-substrates analyses

Table 2 shows the substrate and co-substrates features.

Figure 1. Collection of substrates and co-substrates. (a) Swine Farm. (b) Municipal slaughter house. (c) Waste water treatment.

Figure 2. Reaction bottle connected to Tedlar bag.

pH behavior

C + L treatment started with a neutral pH, while C and C + R treatment started with a more basic pH (above 8, hydrolytic phase). After three weeks, pH values in all 3 treatments reduced to less than 7, remaining in this condition during a week (acidogenic phase), and increased gradually until pH was stabilized at week 12. At the end of the experiment, the pH values remained stable in a range below 8 (methanogenic phase), as shown in Figure 3. This behavior is in good agreement with Kaparaju and Rintala (2005), who suggested that the co-digestion process should have a pH between 7.1 and 8.1. The effect of pH during the 3 weeks, showed less inhibition in the activity of microorganisms resulting in a stable and undisturbed digestion and co-digestion (Chen et al., 2008; Rajagopal et al., 2013).

Oxide-reduction potential (ORP)

After three weeks, ORP values showed an average of -300 mV, highlighting the redox condition (Figure 4). This result is closely related to the recommended value suggested by Flotats et al. (2001), Liu et al. (2011) and Su et al. (2016), who considered that the ORP optimum for an anaerobic process should be less than -270 mV; however, a high redox potential (10.56 V) is a direct inhibition value (Chen et al., 2014).

Chemical oxygen demand (COD)

Treatment C had the lowest efficiency in COD removal values (Table 3) up to the end of the process, which is different from the report of Pazuch et al. (2017), with a value of 68%, but in a anaerobic-digestion process where cattle manure and crude glycerin were used. However, these results are similar to those shown by Nuchdang and Phalakornkule (2012) with values >80% that used anaerobic digestion and co-digestion of glycerol and pig manure.

Table 1. Types of treatments.

Treatments	Substrate (g)	Co-substrate (g)	Total	Treatments
C	125.62	-	125.62	(125.62)(0.6368)= 80.00
C+L	113.06	71.43	184.49	(113.06)(0.6368)+(71.43)(0.112)=79.99
C+R	113.06	9.89	122.95	(113.06)(0.6368)+(9.89)(0.8089)=79.99

C, Pig feces; L, sludge; R, bovine ruminal gastric content waste.

Table 2. Pig feces (C), sludge (L) and bovine ruminal gastric content (R) waste characteristics.

Analytical characteristics (%)	Substrate	Co-substrate	
	C	L	R
H	65.90±0.15	72.81±4.55	83.66±0.37
TS	34.10±0.15	27.19±4.55	16.34±0.37
TVS	63.68±1.07	11.2±0.88	80.89±1.22
FS	6.53±0.30	88.8±0.15	19.11±1.22
Ash	29.79±0.78	85.62±0.88	13.73±0.24

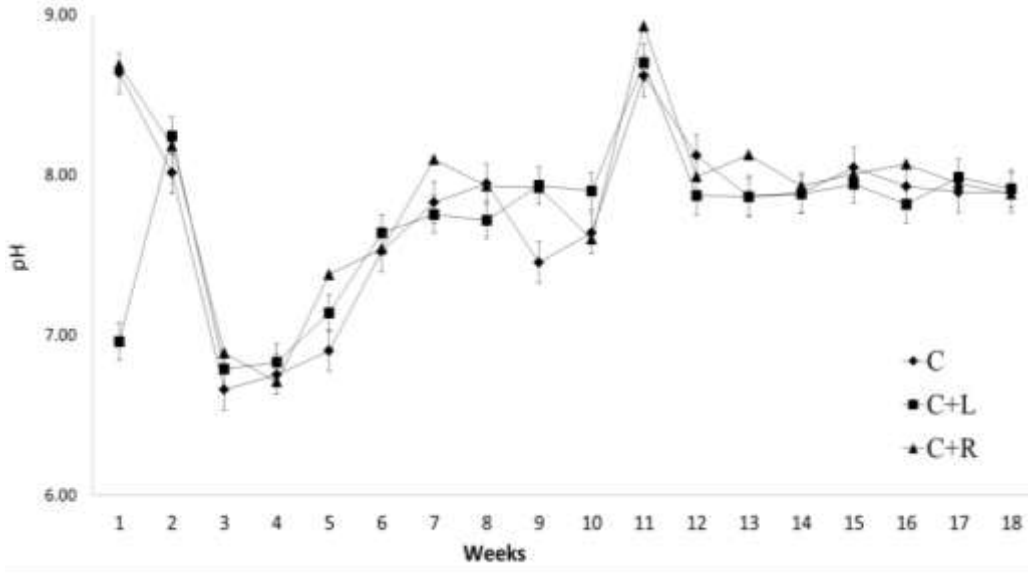

Figure 3. pH behavior for eighteen weeks.

Biogas characterization

The three main gas compounds in a biogas mixture are shown in Table 4. The proportion obtained (% v/v) highlighted high presence of H_2S in treatment C.

Biogas recovering

The biogas produced during this study was 0.012 L day^{-1} in C and C+R treatments, while in C+L, it was 0.009 L day^{-1}. In the C+L treatment, CH_4 and CO_2 content was greater than the values reported by Chen et al. (2015), Nuchdang and Phalakornkule (2012) and Sebola et al. (2015), where 65, 62 and 58% CH_4 was produced, respectively.

Nutrients

In Table 5, the nutritionals characteristics of the digestate, either at the beginning or end of the anaerobic co-

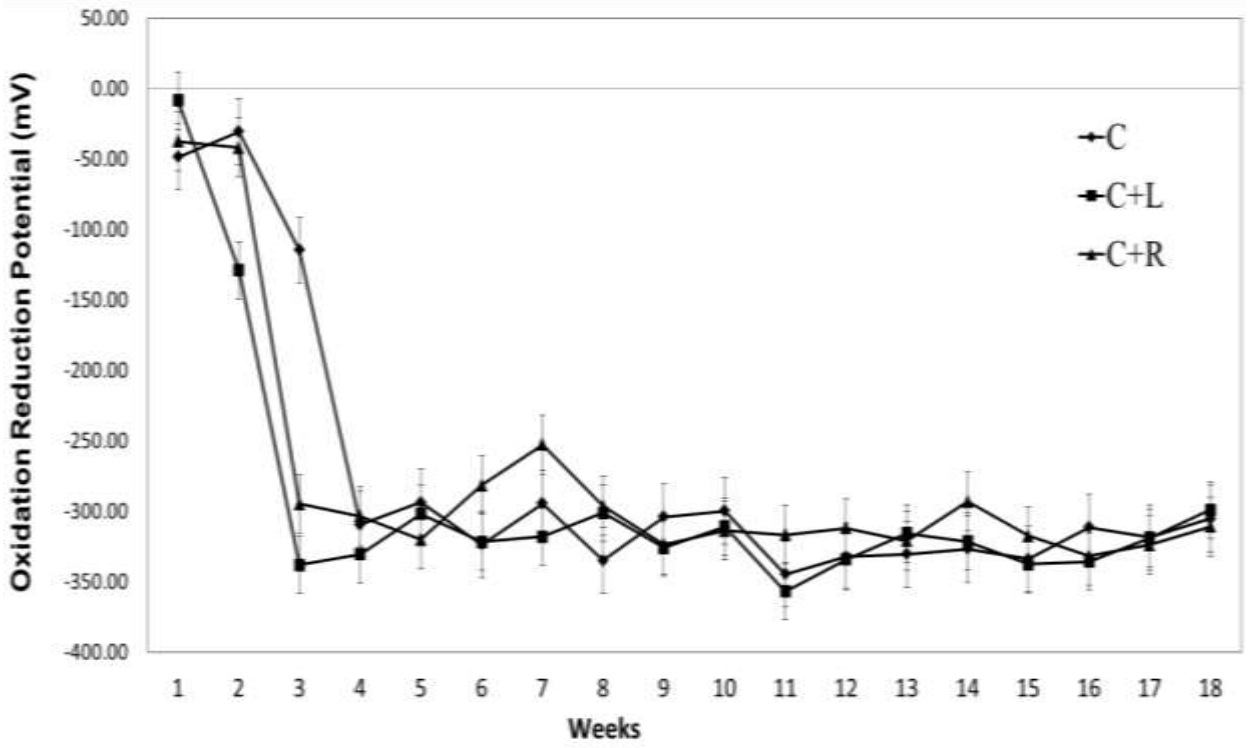

Figure 4. Oxide reduction potential values during the eighteen weeks.

Table 3. COD removal in the three treatments.

Treatments	COD (mg L^{-1})		COD removal (%)
	Initial	Final	
C	28000.0	5600.0	80.00
C+L	26433..3	3333.3	87.39
C+R	20266.7	2000.0	90.13

Table 4. Volumes of gas generated in the biogas.

Treatments	CH_4 (%)	CO_2 (%)	H_2S (ppm)
C	70.87 ± 8.65	29.12 ± 8.65	164.75±16.01
C+L	77.89 ± 6.74	22.11 ± 6.48	70.33±6.36
C+R	71.89 ± 7.60	28.11 ± 7.60	124.67±6.66

Table 5. Nutrient features of co digestion per treatment.

Nutrient	C			C+L			C+R		
(mg/L)	Start	End	%	Start	End	%	Start	End	%
(NO_3^-)	5106	2666	0.26	0	4000	0.40	0	0	0.00
(P_2O_5)	6693	4613	0.46	7440	4160	0.41	6000	3520	0.35
(K_2O)	2800	2533	0.25	3733	2400	0.24	2026	1866	0.18

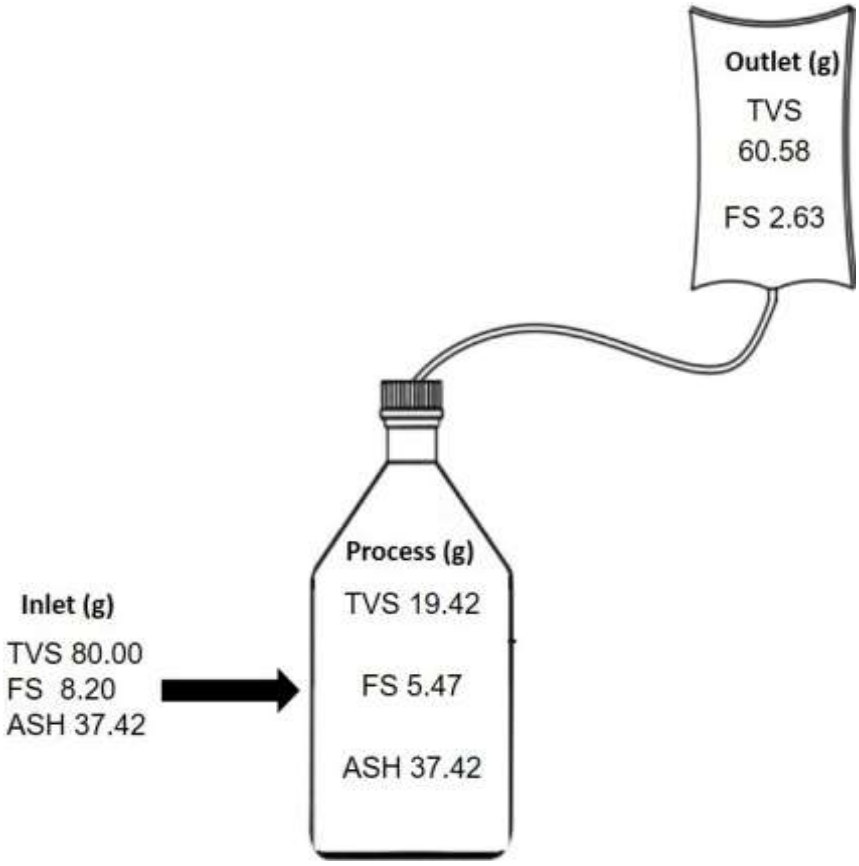

Figure 5. Mass balance of pig manure.

digestion experiment, are showed.

Mass balance for treatment

Treatment C contained 80 g of TVS, 8.20 g FS and 37.42 g ashes, giving a total of 125.62 g. The efficiency of the process showed 63.21 g (60.58 +2.63 g) as biogas production, with 62.31 g of biogas or digestate remaining inside the reactor. During this process, an amount of 71.66% of degradable solid (Figure 5) was removed.

For C+L treatment, 79.99 g TVS, 9.65 g of FS and 94.83 g of ashes were used, giving a total of 184.49 gas original substrate. The efficiency of the process showed 70.03 g (61.84 + 8.19 g) as biogas production, with 114.46 g of biogas or digestate remaining inside the reactor. During this process, 78.12% of degradable solids (Figure 6) were removed.

Finally, for C+R treatment, it was 79.99 g TVS, 7.91 g FS and 35.05 g ashes, giving a total of 122.95 g. The efficiency of the process showed 69.85 g (63.88 + 5.97 g) biogas production, with 53.1 g of biogas or digestate remaining inside the reactor. As a result, 79.46% of degradable solids (Figure 7) were removed.

Statistical analysis of CH_4 and CO_2 production

The analysis of one-way variance shows that there are no significant differences ($P = 0.38$) among CH_4 production in the three treatments (Figure 8). However, treatment of C + L had a greater CH_4 production, as compared to the other two treatments (C and C + R, respectively) tested. With regards to CO_2 production, one way analysis of variance showed no significant differences ($P = 0.38$) among treatments. C + L treatment had less CO_2 production (Figure 9).

Statistical analysis of H_2S production

ANOVA showed significant statistical differences ($P < 0.01$) among the three treatments evaluated (Figure 10). Tukey multiple contrast test showed significant differences among the three treatments evaluated in terms of the production of hydrogen sulfide. It was observed that the

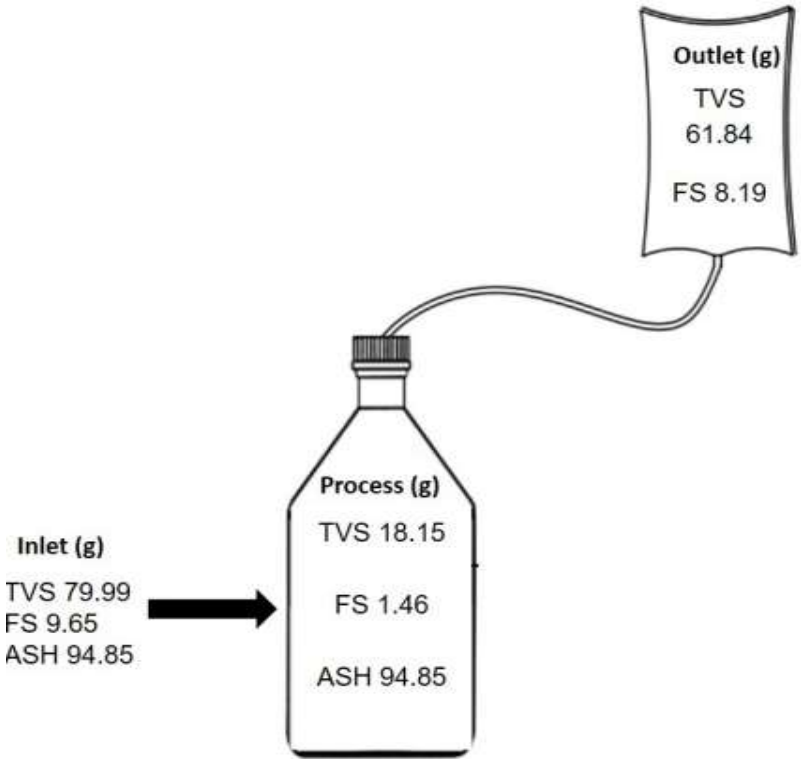

Figure 6. Mass balance of pig manure plus sludge.

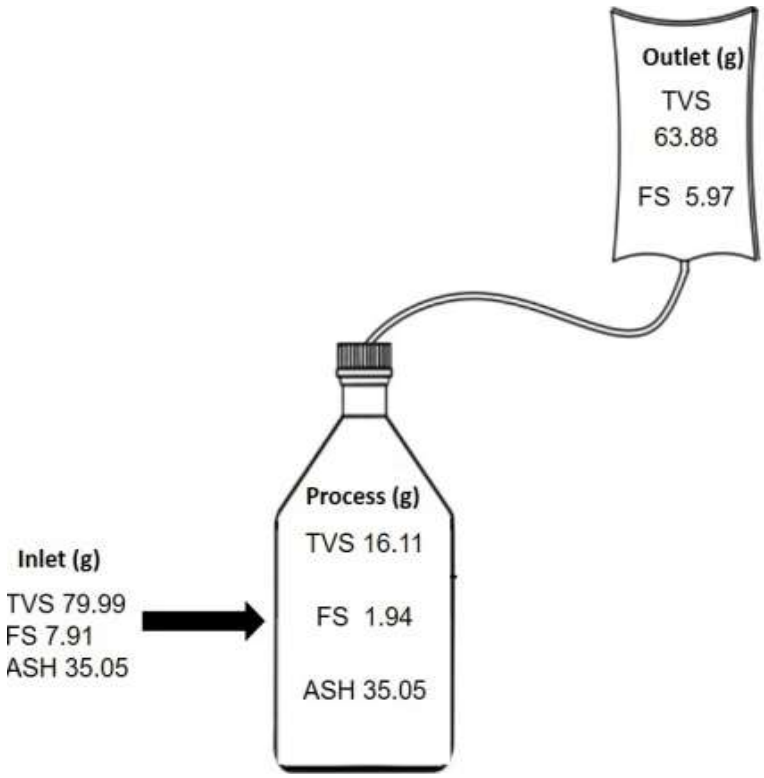

Figure 7. Mass balance of pig manure plus rumen.

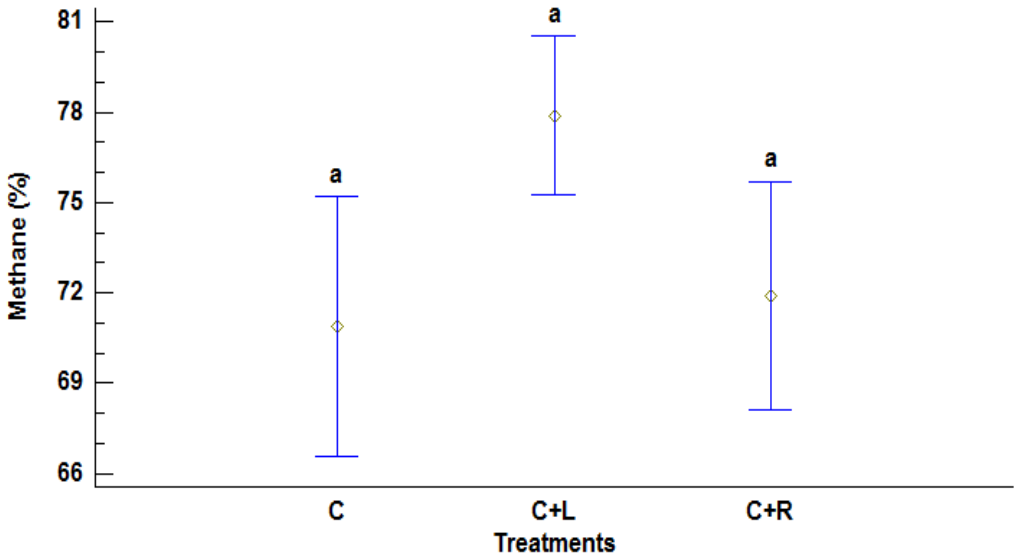

Figure 8. Treatment average values evaluated in the production of CH_4 ± standard error.

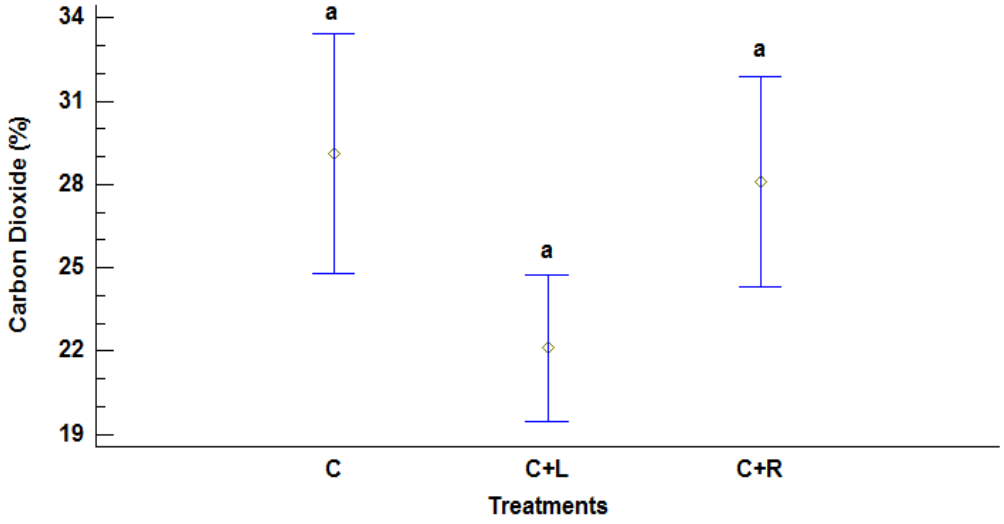

Figure 9. Average values of the treatments evaluated in the production of CO_2 ± standard error.

C + L treatment generated the lowest concentration of H_2S, followed by the C + R. The highest value of H_2S was obtained in treatment C.

Conclusions

The digestion eficiency of pig faeces by two different anaerobic co-digestion treatments using sludge from wastewater treatment plant or ruminal bovine stomach contents as co-substrates showed that the best treatment was C+L, resulting in higher CH_4 production, lower CO_2 and lowest H_2S production, respectively. Therefore, the use of wastewater sludge in anaerobic co-digestion processes promotes more suitable biogas production with pig faeces substrates. C+R treatment had less COD values, reaching 90% efficiency. According to these results, anaerobic digestion and co-digestion are suitable options in agricultural and livestock waste management, reducing waste production and volumes, allowing higher

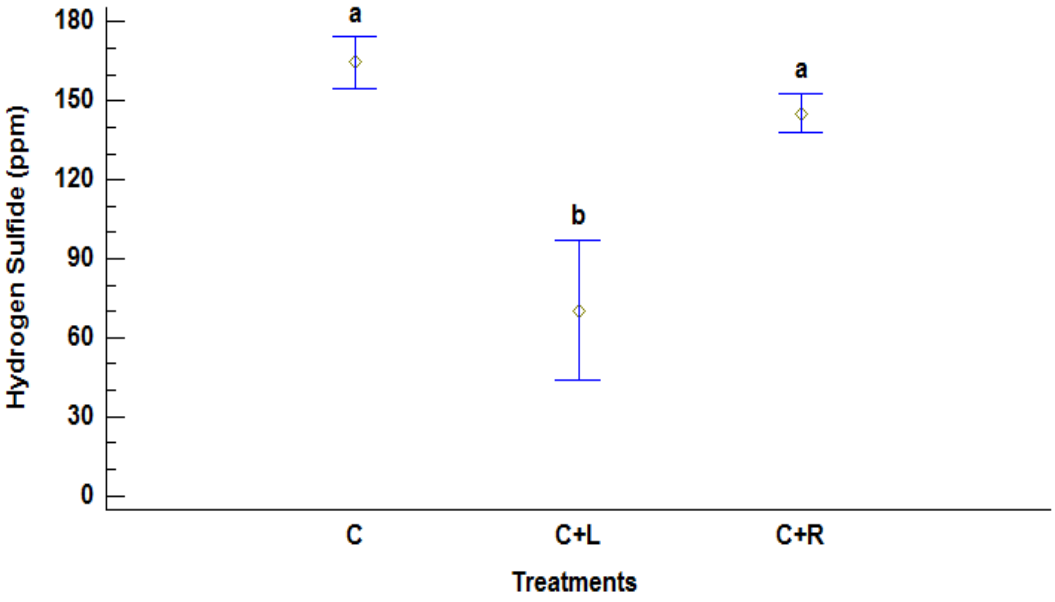

Figure 10. Average values of the treatments evaluated for the production of H_2S ± standard error.

recovery values and maximizing recycling with high calorific or energetic products, such as biogas.

CONFLICT OF INTERESTS

The authors have not declared any conflict of interests.

REFERENCES

Borowski S, Domański J, Weatherley L (2014). Anaerobic co-digestion of swine and poultry manure with municipal sewage sludge. Waste Manag. 34(2):513-521.

Bux M, Razaque A, Aslam M (2012). Biomethanization Potential of Waste Agricultural Biomass in Pakistan: A Case Study. Int. J. Biomass Renew. 1:32-37.

Chen C, Zheng D, Liu GJ, Deng LW, Long Y, Fan ZH (2015). Continuous dry fermentation of swine manure for biogas production. Waste Manag. 38(1):436-442.

Chen JL, Ortiz R, Steele TWJ, Stuckey DC (2014). Toxicants inhibiting anaerobic digestion: A review. Biotechnol. Adv. 32(8):1523-1534.

Chen Y, Cheng JJ, Creamer KS (2008). Inhibition of anaerobic digestion process: A review. Bioresour. Technol. 99(10):4044-4064.

Flotats X, Campos E, Palatsi J, Bonmatí A (2001). Digestión anaerobia de purines de cerdo y co-digestión con residuos de la industria alimentaria. Monografías de Actualidad 65:51-65.

Garzón-Zúñiga MA, Buelna G (2014). Caracterización de aguas residuales porcinas y su tratamiento por diferentes procesos en México. Revista Internacional de Contaminación Ambiental 30(1):65-79.

Gallardo-Izquierdo A, Laines-Canepa JR, Colomer-Mendoza FJ, Miralles-Montins T, Gómez-Parra A (2013). Biometanización de los rechazos procedentes del proceso de afino del compost. In V Simposio Iberoamericano de Ingeniería de residuos sólidos (p. 7). Mendoza, Argentina: Red Iberoamericana en Gestión y Aprovechamiento de Residuos. Retrieved from http://www.redisa.net/doc/artSim2013/TratamientoYValorizacionDeResiduos/Biometanizacion Rechazos Procedentes Afino Compost.pdf

Gerber PJ, Steinfeld H, Henderson B, Mottet A, Opio C, Dijkman J, Tempio G (2013). Enfrentando el cambio climático a través de la ganadería. Una evaluación global de las emisiones y oportunidades de mitigación. (FAO, Ed.),

Holm-Nielsen JB, Al Seadi T, Oleskowicz-Popiel P (2009). The future of anaerobic digestion and biogas utilization. Bioresour. Technol. 100(22):5478-5484.

Kaparaju P, Rintala J (2005). Anaerobic co-digestion of potato tuber and its industrial by-products with pig manure. Resour. Conserv. Recycl. 43(2):175-188.

Liu Y, Zhang Y, Quan X, Chen S, Zhao H (2011). Applying an electric field in a built-in zero valent iron – Anaerobic reactor for enhancement of sludge granulation. Water Res. 45(3):1258-1266.

Montejo S, Laines JR, Sosa JA, Hernández L, Ávila I (2015). Estudio De Generación Y Calculo Del Potencial De Biogás En La Granja Porcina De La División Académica De Ciencias Agropecuarias-Ujat. Kuxulkab', pp. 45-50.

Nuchdang S, Phalakornkule C, (2012). Anaerobic digestion of glycerol and co-digestion of glycerol and pig manure. J. Environ. Manag. 101:164-172.

Pazuch FA, Siqueira J, Friedrich L, Lenz AM, Nogueira CEC, de Souza SNM (2017). Co-digestion of crude glycerin associated with cattle manure in biogas production in the state of Paraná, Brazil. Acta Sci. Technol. 39(2):149-159.

Rajagopal R, Massé DI, Singh G (2013). A critical review on inhibition of anaerobic digestion process by excess ammonia. Bioresour. Technol. 143:632-641.

Sebola MR, Tesfagiorgis HB, Muzenda E (2015). Methane Production from Anaerobic Co- digestion of Cow Dung, Chicken Manure, Pig Manure and Sewage Waste. Proc. World Congress Eng. 1:1-7.

Secretaria de Comercio y Fomento Industrial (1984). NMX-AA-018-1984 Protección Al Ambiente-Contaminacion Del Suelo- Residuos Sólidos Municipales-Determinación de Cenizas, Diario Oficial de la Federación §.

Secretaria de Comercio y Fomento Industrial (1985a). NMX-AA-015-1985 Protección Al Ambiente - Contaminación Del Suelo - Residuos Sólidos Municipales- Muestreo-Método de Cuarteo, Diario Oficial de la Federación §.

Secretaria de Comercio y Fomento Industrial (1985b). NMX-AA-016-

1985 Protección Al Ambiente-Contaminación Del Suelo- Residuos Sólidos Municipales-Determinación de humedad, Diario Oficial de la Federación §.
Secretaria de Comercio y Fomento Industrial (2015). NMX-AA-034-SCFI-2015 Análisis De Agua - Medición De Sólidos Y Sales Disueltas En Aguas Naturales, Residuales Y Residuales Tratadas – Método De Prueba (Cancela a La Nmx-AA-034-SCFI-2001). Diario Oficial de la Federación §.
Shah FA, Mahmood Q, Rashid N, Pervez A, Raja IA, Shah MM (2015). Co-digestion, pretreatment and digester design for enhanced methanogenesis. Renew. Sustain. Energy Rev. 42:627-642.
SIAP (2015). Población ganadera. Secretaría de Agricultura, Ganadería, Desarrollo Rural, Pesca y Alimentación. Retrieved from https://www.gob.mx/cms/uploads/attachment/file/166003/porcino.pdf
Su H, Tan F, Xu Y (2016). Enhancement of biogas and methanization of citrus waste via biodegradation pretreatment and subsequent optimized fermentation. Fuel 181:843-851.
Ye J, Li D, Sun Y, Wang G, Yuan Z, Zhen F, Wang Y (2013). Improved biogas production from rice straw by co-digestion with kitchen waste and pig manure. Waste Manag. 33(12):2653-2658.
Zhang W, Wei Q, Wu S, Qi D, Li W, Zuo Z, Dong R (2014). Batch anaerobic co-digestion of pig manure with dewatered sewage sludge under mesophilic conditions. Appl. Energy 128:175-183.

academicJournals

Vol. 11(10), pp. 509-516, October 2017
DOI: 10.5897/AJEST2017.2275
Article Number: 20D5B3365923
ISSN 1996-0786

http://www.academicjournals.org/AJEST

African Journal of Environmental Science and Technology

Full Length Research Paper

Effects of soil bund on soil physical and chemical properties in Arsi Negelle woreda, Central Ethiopia

Dulo Husen[1*], Feto Esimo[2] and Fisiha Getechew[3]

[1]Fiche Soil Research Center, P.O. Box 109, Fiche, Ethiopia.
[2]Oromia Agricultural Research Institute, P.O.Box 81265, Addis Ababa, Ethiopia.
[3]Biosystems and Environmental Engineering Department, Hawassa University, P.O box 5, Hawassa, Ethiopia.

Received 4 January, 2017; Accepted 13 April, 2017

This study was conducted in Arsi Negelle woreda of West Arsi Zone, Oromia regional state. The main objective of the study was to investigate the impacts of soil bund on soil physical and chemical properties in Arsi Negelle woreda. The soil data was collected from sites namely: lowland, midland and highland and from soil bunds aged >4 years, <4 years and control of farmland. Three representative sites were selected purposively for soil sample collection. Stratified random sampling techniques were used for soil samples collection. Fifty-four disturbed and undisturbed soil samples were collected for soil properties analysis from two soil depths (10 and 20 cm). Statistical analysis was done following a completely randomized design (CRD) with factorial experiments and treatments as fixed effect and location of sampling as a random effects. The analysis was carried using R software. Regression analysis was used to relate physical properties of soil with each other. Tukey test was used for comparison of means of treatments when statistical significance is found at P ≤ 0.05. Bulk density (BD) and air-filled porosity (AFP) showed significance difference on treated and non-treated site, respectively. The mean of electric conductivity (EC), total nitrogen (TN), available phosphorous (AP) and organic carbon contents were recorded to be significantly higher (p≤ 0.05) on soil bund ages greater than 4 years (>4years) at both soil sampling depths. Aged soil bunds (treated plots) showed a significant changes on soil physical and chemical properties than control plots. The mean of total nitrogen (TN), available phosphorous (AP) and organic carbon contents were recorded significantly higher (p≤ 0.05) in lowland than highland at both soil sampling depths. In generally, ages of soil bunds and sites had significant effect on many soil physical and chemical properties. The sites and ages interaction had significant effect on bulk density (BD) at both depths at P ≤ 0.05. In conclusion, this study showed that soil bunds had significant effect on many physical and chemical properties of soil in the study area.

Key words: Soil bund, bulk density, saturated hydraulic conductivity, electrical conductivity, total nitrogen, organic carbon.

INTRODUCTION

Natural resource degradation and land degradation in particular has negative impact on the economy of developing countries including Ethiopia. This is because, the country heavily depends on their natural resource for

food self-sufficient, food security and economic development. Soil erosion and nutrient depletion are the most important forms of land degradation in Ethiopia (Tekle, 1999). The effects of soil erosion vary by management (conservation) and location. In general, it deteriorates chemical properties of soil by loss of organic and minerals containing plant nutrients that are necessary for life support system of soil resource (Zougmore, 2009).

Soil erosion also brings changes in physical properties such as texture, infiltration rate, bulk density, available water holding capacity and depth of favorable root growth. These changes has negative effect on most of the soil ecological function and services (Schjonning et al., 2009). The contributing factors for soil erosion in most parts of the country are poor agriculture activities (including intensive tillage, complete removal of crop residues, low levels of fertilizer application), lack of appropriate soil conservation measures and cropping practice (Abebayehu and Eyassu, 2011).

In central rift valley of Ethiopia, soil erosion is a serious problem because of fragile and easily erodible soil. The land of Arsi Negelle is well known for the devastating soil erosion problem that has resulted in a decline in agricultural productivity in the region (Titola, 2008). Arsi Negelle is located in central rift valley, where the ecosystem is fragile. Continuous cultivation with little protection measures exacerbated the level of soil erosion, and hence land productivity had declined significantly and farmers were cultivating the land without giving more attention to soil maintenances in the area. This caused the loss of top soil and reduced productivity capacity of the land and economy of the country. Physical soil and water conservation (SWC) measures such as soil bunds have been practiced in Arsi Negelle woreda for decades (from elders interviewed) as amelioration measures for soil erosion. Soil bunds are a common practice for physical soil and water conservation measures and many studies were conducted to address issues of its adoption and reduction in soil loss due to construction of the structure.

Most soil research focused on empirical soil loss, crop yield and largely based on study of perception of farmers to adaptation of soil and water conservation structures. Some of the key processes important for potential restoration of degraded soil have been studied, but largely in the study of farmers' perception. Limited knowledge of soil regeneration due to soil and water conservation structures, limits quantitative measures of severity of soil degradation. Thus, this research work focused on identifying the benefits of this structures and its impact on soil physical and chemical properties in the study area. Specific objectives are as follows:

1. To analyze the impacts of ages of soil bunds on soil physical and chemical properties
2. To analyze the impacts of sites on physical and chemical properties.

MATERIALS AND METHODS

Description of the study area

The study was conducted in Arsi Negelle woreda, which is located at 225 km south of the Addis Ababa. Geographically, it is situated in the central rift valley system between 7° 09'-7° 41' N longitude and 38°25'-38° 54' E latitude (Figure 1). Average annual temperature varies from 10 to 25°C, while the annual rainfall varies between 800 and 1200 mm (ORS, 2004). The altitude of the study area ranges from 1500 to 2300 m above sea level and falls in Weyna Dega Agro-ecological Zone. The Woreda has 43 rural and 3 urban kebeles. The study area is classified into three sites (lowland, midland and highland) based on temperature, rainfall, altitude and vegetation covers.

Experimental design and sampling

The three representative kebeles were selected purposively for each site (lowland, midland and highland) based on recommendation by woreda agricultural Expert and Development agent (DA) for soil sample collection. Stratified random sampling techniques were used for soil samples collection. In each selected kebele, three replicate field plots with two age groups (<4 years and >4 years) and control were identified within the similar slope. At each sampling plot, two undisturbed soil samples were collected at the center from 10 to 20 cm soil depths by using core samplers. Whereas, at each sampling plot, two disturbed soil samples were collected from four corners and one from the center by using auger from 10 to 20 cm soil depths, respectively. The collected soil samples were mixed to obtain representative composite samples approximately 1 kg of disturbed soil samples. From ages of soil bunds >4 years, <4 years and control, six soil samples were collected from each plots and 18 soil samples were collected from each site. A total of samples include 54 undisturbed (three sites × three treatments (two age groups of soil bund + without soil bund (control)) × three replications × two soil depths) and 54 disturbed soil samples were collected respectively.

Laboratory analysis

Before the actual measurement, excess soil was removed by spatula in field. The core soil samples were used for determinations of volumetric moisture content, bulk density, saturated hydraulic conductivity and air-filled porosity, whereas the disturbed soil samples were used for the analysis of soil texture and soil chemical properties. Standard methods were used for analyses of soil

*Corresponding author. Email: dulo.husen@gmail.com.

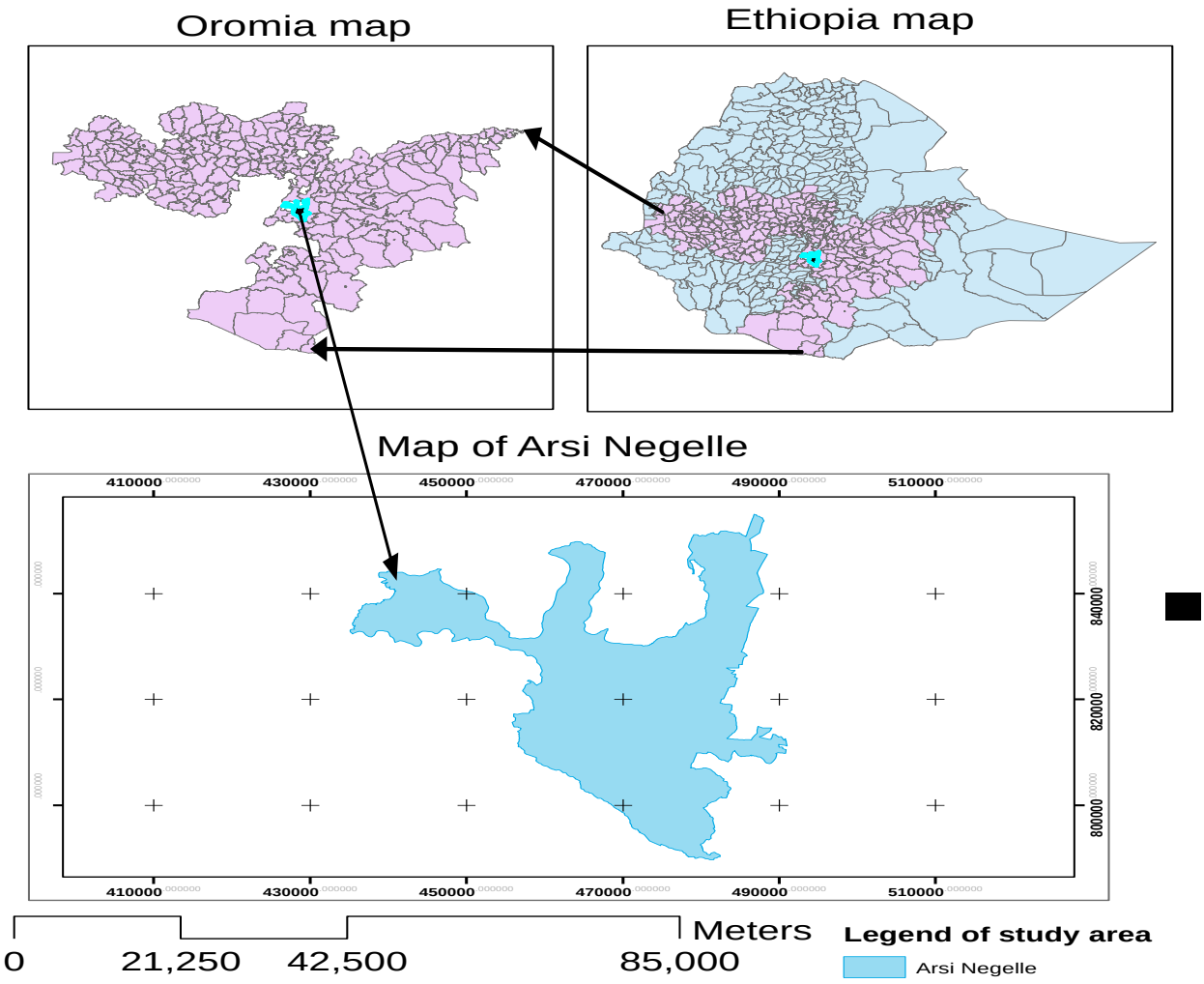

Figure 1. Arsi Negelle District map.

chemical properties and soil textural classes.

The cores samplers were covered with nylon cloth from the bottom, and saturated step-wise with capillary water from beneath. Then, the samples were used for measurement of saturated hydraulic conductivity, K_{sat} using constant head method as described in Klute and Dirksen (1986). The measurements of average value of water discharge (Q) (unit: $L^3 T^{-1}$) collected after it reached steady state, soil length (L), cross-sectional area of the soil sample (A) [unit: L^2], and hydraulic head (H) [L], were used to determine the K_{sat} (LT^{-1}) using Darcy's equation, which is given by:

$$K_{sat} = \frac{QL}{AH} \quad (1)$$

Statistical analysis

Prior to statistical analysis, the normality of datasets (data sets) was checked. Statistical analysis followed a completely randomized design (CRD) with factorial experiments. A linear mixed model with treatments (site and age) as fixed effect and location of sampling as a random effect was fitted for each sampling depths. A mixed model in R software was employed. Tukey test was used for comparison of means of treatments when statistical significance is at $P \leq 0.05$. Regression analysis was used to relate soil physical properties with each other.

RESULTS AND DISCUSSION

Impact of soil bund on selected soil physical properties

Soils were collected from three different sites (lowland, midland and highland) and three treatments (age>4 years, <4 years and control) and along with the interaction effect of treatments of both soils collected at

Table 1. Effects of soil bund ages and sites on selected soil physical properties.

Soil depth (cm)	Soil parameter	Age effect			Site effect			Site × age
		>4year	<4year	Control	Low land	Middle land	High land	
10	BD (g cm^{-3})	1.317^{c}	1.324^{b}	1.333^{a}	1.32^{b}	1.323^{b}	1.33^{a}	0.0039
	Θ_w(cm^3cm^{-3})	0.38^{a}	0.36^{a}	0.36^{a}	0.404^{a}	0.381^{a}	0.32^{b}	Ns
	ε_a(cm^3 cm^{-3})	0.121^{a}	0.141^{a}	0.14^{a}	0.097^{b}	0.121^{b}	0.183^{a}	Ns
	K_{sat} (mm hr^{-1})	37.69^{a}	39.26^{a}	35.94^{a}	39.3^{a}	38.7^{a}	34.9^{b}	Ns
20	BD (g cm^{-3})	1.321^{c}	1.326^{b}	1.334^{a}	1.323^{c}	1.328^{b}	1.33^{a}	0.0011
	Θ_w (cm^3cm^{-3})	0.417^{a}	0.353^{b}	0.38^{b}	0.41^{a}	0.39^{a}	$0.0.35^{b}$	0.0002
	ε_a(cm^3 cm^{-3})	0.084^{c}	0.15^{a}	0.114^{b}	0.090^{b}	0.1065^{b}	0.148^{a}	0.0002
	K_{sat} (mm hr^{-1})	37.75^{a}	39.1^{a}	36.5^{a}	41.3^{a}	40.37^{a}	31.63^{b}	Ns

Means with same letter in each row are not statistically significant at P<0.05, Ns= not significant. Site × age refers to the interaction between site and age.

10 and 20 cm soil sampling depth shown in Table 1.

Ages effects on selected soil physical properties

Bulk density (BD) was significantly difference at $p < 0.05$ among ages of structures. The untreated plots were found to exhibit significantly higher mean value of BD than treated plots at both depths (Table 1). Soil bund construction reduced loss of fertile soil and crop residues. Similar results were reported elsewhere, for instance Mulugeta and Karl (2010) conducted study on impact of conservation structures on key soil properties in south Gondar, and reported significantly higher mean value of BD in non-conserved plots than in the plot treated with soil and water conservation measures.

Volumetric moisture content (Θ_w) at sampling did not show significantly difference at p<0.05 among ages of structures at 10 cm soil depth, whereas significant impact for soil at 20 cm depth. The non-significant result at upper depth could be due to sampling condition.

Air-filled porosity (ε_a) in almost all cases higher in the soil bund conserved less than 4 years and non-conserved plot, although this was significantly difference at p<0.05 at 20 cm soil sampling depth among ages of structures, but not at 10 cm sampling depth. This might be due do to more moisture in conserved farm plot. The high values of air-filled porosity observed both in treated and non-treated soils indicate that the soil in the study area was generally suitable for plant growth even prior to the introduction of soil conservation measures.

For most combinations of depth and experimental treatments, the saturated hydraulic conductivity values of the soil considered under this study were considerably higher than 8.6 cm day^{-1}, which was established by McQueen and Shepherd (2002) as the critical limit for adequate hydraulic conductivity. However, the observed value of saturated hydraulic conductivity was rather low when compared with the extreme precipitation events in the study area. This situation inevitably increases the risk of surface runoff and eventually soil erosion, which was evidently observed in year 2016.

Sites effects on selected soil physical properties

Bulk density was significantly difference at $p < 0.05$ among sites of structures. The mean of bulk density was highest at highland and lowest at lowland. This might be due to maintenance problem of structures in highlands that washed away fertile and light soil and thereby exposed slightly heavier soil. The deposition of this washed away soil could occur at lowland and thereby reduced the bulk density of soil at the destination. In another study, Tan (1996) categorized the bulk density values, 1.0 to 1.5 gcm^{-3} as a favorable physical condition of soils for plant growth.

Volumetric moisture content (Θ_w) was significantly different at $p < 0.05$ among sites for both soil-sampling depths (Table 1). The mean of volumetric moisture content did not show significant differences at midland and lowland for both soil-sampling depths, because soil bunds at these locations were well maintained and promoted more water retention than in highlands.

The mean of air-filled porosity (ε_a) at sampling was higher at highland than midland and lowland for both soil-sampling depths. Soil conservation structure could have been expected to improve aeration condition of the soil, whereas, the condition observed here was contrary. This could be explained by high moisture holding capacity of deposited soil at these two locations and the samples were collected during rainy season at the time of high moisture content in the soil.

As expected, the mean of saturated hydraulic conductivity (K_{sat}) was higher at lowland and midland than highland for both soil-sampling depths. However, no

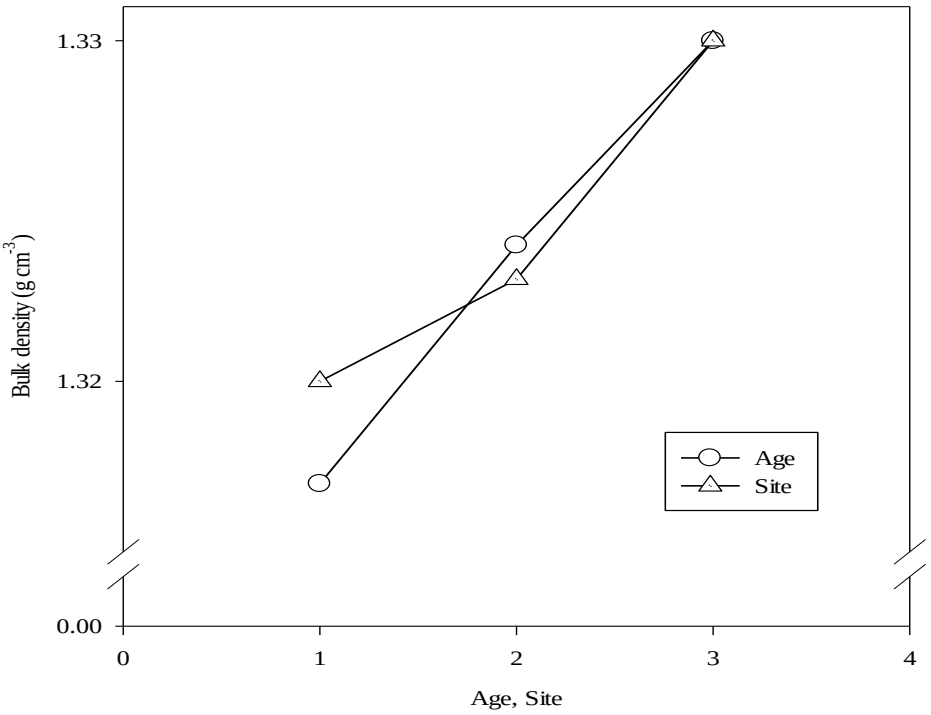

Figure 2. Bulk density of soil sample collected from 10 and 20 cm depth and interaction effects of age and site. Ages: 1 = ages of soil bund > 4year; 2 = ages of soil bund<4 year; 3 = Control. Sites: 1 = lowland; 2 = midland; 3 = highland.

significant differences were observed in saturated hydraulic conductivity between soils collected from midland and lowland. One reason for higher saturated hydraulic conductivity at midland and lowland could be proper maintenance of structures at these two sites than highland.

Ages interaction sites effects

In this study, for soil sampled at 20 cm depth, there was significant interaction between ages of structures and sites for bulk density, volumetric moisture content and air-filled porosity (Table 1). This trend was not true for soil collected from 10 cm soil depth except for bulk density. As can be seen from Figure 2, the two lines (one for age and the other for site) cross each other, this implies interaction.

Impact of soil bund on selected soil chemical properties

Soils were collected from three different sites (lowland, midland and highland) and three treatments (>4 year, <4 year and control) and along with the interaction effect of treatments of both soils collected at 10 and 20 cm soil sampling depth as shown in Table 2.

Ages effects on selected soil chemical properties

The mean of pH were not significantly different at $P<0.05$ for both soil sampling depth. In general, the mean of pH value of soil in the study area ranges from neutral to slightly alkaline (6.75 to 7.5) according to classification by SSSA (1996). The mean value of electric conductivity (EC) was significant difference at $P<0.05$ among ages of structures for both soil sampling depth.

Total nitrogen (TN) contents were significantly different at $P<0.05$ among the ages of soil bund for both soil sampling depths (Table 2). The treated farmland had also higher TN as compared to the non-treated farmland for both soil-sampling depths. Similar results were reported by Mulugeta and Karl (2010), who stated that physical soil and water conservation measures stabilizes the nitrogen fixing plants and thereby increase TN in conserved plot. In general, the total nitrogen content of the soil in the study area lies within very low to medium class according to Barber (1984). The low value of total nitrogen was observed both in the conserved and non-conserved plot; this indicates that the soil in the study

Table 2. Effects of soil bund age and site on selected soil chemical properties.

Soil depth (cm)	Soil parameter	Age effect			Site effect			Site x age
		>4year	<4year	Control	Low land	Middle land	High land	
10	EC (mmhos/cm)	0.24^{a}	0.19^{b}	0.16^{b}	0.203^{a}	0.17^{a}	0.22^{a}	0.0037
	pH	7.03^{a}	7.14^{a}	7.01^{a}	7.023^{ba}	6.67^{b}	7.5^{a}	Ns
	T N(%)	0.20^{a}	0.16^{a}	0.114^{b}	0.22^{a}	0.135^{b}	0.121^{b}	Ns
	A P(ppm)	10.9^{a}	7.14^{b}	4.1^{b}	11.57^{a}	8.5^{a}	2.1^{b}	Ns
	OC (%)	3.32^{a}	3.23^{a}	2.05^{b}	4.4^{a}	1.93^{b}	2.29^{b}	Ns
20	EC (mmhos/cm)	0.182^{a}	0.154^{ba}	0.127^{b}	0.145^{ba}	0.13^{b}	0.19^{a}	Ns
	pH	7.03^{a}	7.31^{a}	6.75^{a}	6.9^{b}	6.7^{b}	7.5^{a}	Ns
	T N (%)	0.155^{a}	0.122^{a}	0.07^{b}	0.16^{a}	0.09^{b}	0.09^{b}	0.0011
	AP (ppm)	8.03^{a}	3.7^{b}	3.4^{b}	9.96^{a}	4.42^{b}	0.71^{c}	Ns
	OC (%)	2.44^{a}	2.24^{ba}	1.62^{b}	2.96^{a}	1.63^{b}	1.714^{b}	Ns

Means with same letter in each row are not statistically significant at P<0.05, Ns = Not significant. Site × age is refers to the interaction between site and age.

area was generally poor in total nitrogen content. Moreover, the crop residue have impact on replenishing of total nitrogen content which was used as source of firewood.

Available phosphorous (AP) was significantly different at P<0.05 among the ages of soil bund for both soil sampling depths (Table 2). The mean of AP for treated farm land is greater than untreated farm land. The result agrees with the finding of Mulugeta and Karl (2010)who reported that AP was observed to be significantly different between the conserved and non-conserved fields. The variation is due to the soil organic matter content difference.

In general, according to Barber (1984), AP content of the cultivated land both for treated and untreated land is low. This could be one of the reasons why the yield in the area was very small as compared to yield reported in the media, although farmers use extension packages. Therefore, more has to be done in conserving macronutrients on cultivated land by using extension package.

There was significant difference at p<0.05 in mean value of organic carbon (OC) contents among treated and untreated farmland at both soil sampling depth (Table 2). This might show that the soil bund construction has played a positive role in conserving the soil organic carbon. The result agrees with the finding of Tadele (2011), who reported higher organic carbon in treated farmland and lower in untreated farmland. Even though, the soil bunds construction increased organic carbon, the mean of organic carbon on treated and untreated plot is almost equal or below the critical value of organic carbon. Loveland and Webb (2003) reported that a 2% of OC is a critical level for crop production and soil aggregate stability. In generally, more has to be done to conserve organic carbon, organic matter and others micronutrients.

Site effects on selected soil chemical properties

In general, pH, AP, TN and OC shows that there were significant differences at P<0.05 among sites at both soil sampling depths (Table 2). Whereas, the EC was not significantly different at p<0.05 in 10 cm soil sampling depth and significant difference at p<0.05 in 20 cm soil sampling depth (Table 2). In all the cases, the numeric values were highest at lowland except for pH and EC. During erosion, it can be hypothesized that top soil is washed away progressively with nutrients and the remaining soil become infertile. In addition, at site of deposition, the soil could have been fertile and contain more nutrients. The result of this study supports this hypothesis that soil bund constructed at lowland is well maintained. For chemical properties, the interaction effects between site and age were not significant difference at p<0.05, except for the case of EC at 10 cm soil depth and TN at 20 cm soil depth (Table 2).

Relationship between soil physical properties

Bulk density is one of the common parameters used to quantify this change. This is because of the ease of measurement of bulk density. They also used the changes in bulk density to quantify changes in other physical properties of soil. The only few field studies address the quantitative relationships between bulk density and saturated hydraulic conductivity. Exceptions are the work of Dexter (2004) who predicted changes into hydraulic conductivity due to increase in bulk density following passage of heavy agricultural machinery on soil. In this study, strong and significant relationship between saturated hydraulic conductivity and bulk density was

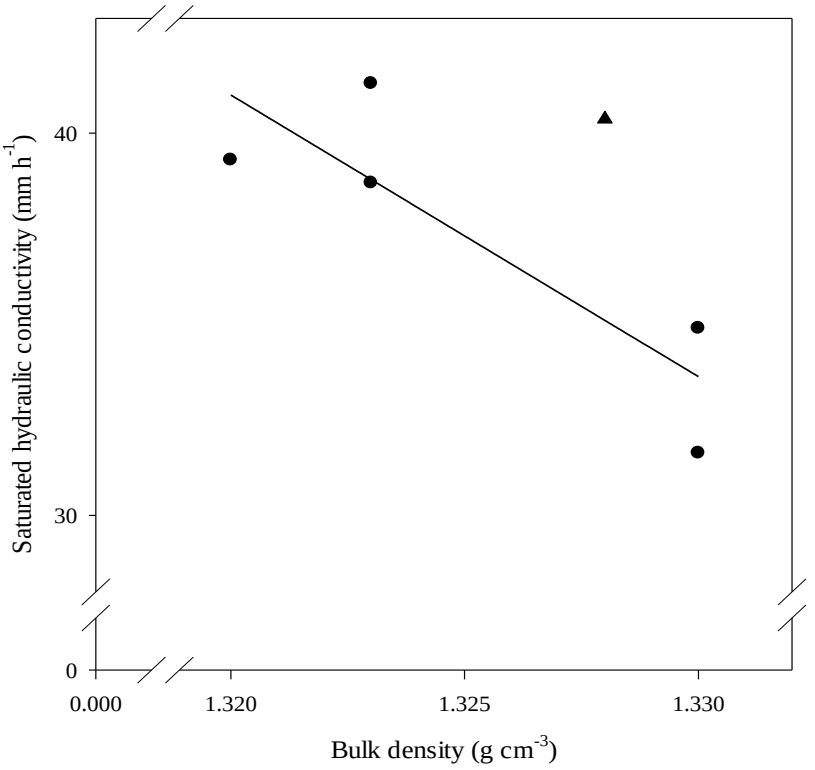

Figure 3. Saturated hydraulic conductivity versus BD. Measured values of the saturated hydraulic conductivity, Ksat, for soils collected from 10 and 20 cm depth.

obtained (Figure 3). The linear line in Figure 3 is the regression equation:

$$K_{sat} = -736.91\ BD\ (\pm 244.22) + 1013.72(\pm 323.65)$$

$$R^2 = 0.86; \quad p < 0.05 \qquad 2$$

Remarkably, the regression equation in this investigation was almost identical to the relationship found by Dexter (2004) for Polish soils that were collected from different sites of agricultural fields from 10 to 16 cm depths.

Conclusions and recommendations

The mechanisms in natural amelioration as well as artificial supplements to erode are nearly absent in subsoil layers. The results need efforts to minimize soil erosion. Hence, soil bund construction reduced soil erosion and increased production and productivity of soil unless soil erosion increased from time to time and reduced soil production potential. Thus, soil bund construction improved soil properties. Development strategy and program interventions designed to enhance agricultural productivity by promoting soil bund in land management in the study area need to take into account. There is an urgent need to restrict further increase in soil erosion risk. To have a whole picture of soil erosion (cause-and-effect chains), further studies are needed to link changes in physical properties to soil functions relevant for biomass production and environmental quality. In generally, the soil bund construction is mandatory to obtain sustainable development unless the fertility of soil is eroded and the land becomes degraded (out of production).

ACKNOWLEDGEMENTS

The authors acknowledge Oromia Agricultural Research Institute for granting MSc program.

REFERENCES

Abebayehu A, Eyassu E (2011). Soil nutrient Stock Evaluation under different land use types in the smallholder farming systems of Jimma Zone, Ethiopia Int. J. Agric. Res. 6(9):707-713.

Dexter AR, Czyz EA, Gate OP (2004). Soil structure and the saturated hydraulic conductivity of subsoils. Soil Till. Res. 79:185-189.
Klute A, Dirksen C (1986). Hydraulic conductivity and diffusivity Laboratory methods. p. 687-734. In A. Klute (ed.) Methods of soil analysis. Part 1. ASA and SSSA, Madison, WI.
Loveland P, Webb J (2003). Is there a critical level of organic carbon in the agricultural soil of temperate region: a review. Soil Till. Res. 70:1-18.
McQueen T, Shepherd G (2002). Physical changes and compaction sensitivity of a fine-textured, poorly drained soil (Typic Endoaquept) under varying durations of cropping, Manawatu Region, New Zealand. Soil Till. Res. 63:93-107
Mulugeta D, Karl S (2010). Assessment of integrated soil and water conservation measures on key soil properties in south Gondar, north-western Highlands of Ethiopia. J. Soil Sci. Environ. Manag. 1(7):164-176.
ORS (2004).The Oromia Regional State government: Socio Economic Profile of East Shoa Zone.
SSSA (Soil Science Society of America) (1996). In Glossary of soil science terms, (SSSA), Madison, WI, 1.
Stroosnijder L (2009). Modifying land management in order to improve efficiency of rainwater use in the African highlands. Soil Till. Res. 103:247-256.
Tadele A, Yihenew GS, Mitiku H, Yamoh C (2011). Effect of soil and water conservation measures on selected soil physical and chemica properties and Barley (Hordeum spp.) Yield. J. Environ. Sci. Eng. 5:1488-1493.
Tan HK (1996). Soil Sampling, Preparation and Analysis. Marcel Dekker, Inc., New York.
Tekle K (1999). Land degradation problems and their implications for food shortage in South
Titola T (2008). Environmental degradation and its implications for agricultural and rural development: The issue of land erosion. J. Sustain. Dev. Afr. 10(2):131.
Yihenew GS, Getachew A (2013). Effects of different land use systems on selected physico- chemical properties of soils in Northwestern Ethiopia. J. Agric Sci. 5:114-117.
Zougmore R, Mando A, Stroosnijder L (2009). Soil nutrient and sediment loss as affected by erosion barriers and nutrient source in Semi-Arid Burkina Faso. Arid Land Res. Manag. 23:85-101.

academicJournals

Vol. 11(10), pp. 517-531, October 2017
DOI: 10.5897/AJEST2017.2382
Article Number: 8126E4065928
ISSN 1996-0786

http://www.academicjournals.org/AJEST

African Journal of Environmental Science and Technology

Full Length Research Paper

Correlation and mapping of geothermal and radioactive heat production from the Anambra Basin, Nigeria

Kuforijimi Olorunsola* and Christopher Aigbogun

Department of Physics, Faculty of Science, University of Benin, Benin City, Edo State, Nigeria.

Received 4 July, 2017; Accepted 17 August, 2017

Twelve sheets of aeromagnetic and aeroradiometric data covered the study area. The data was used to investigate heat sources. The aeromagnetic data were combined to form a composite map- total magnetic intensity (TMI) anomaly map and aeroradiometric data of each radio-element were combined to produce the radioelements maps. Regional-residual separation of the total magnetic intensity data was performed using polynomial fitting method on the aeromagnetic data. The filtered residual data was Fourier transformed after dividing the whole area into thirty-five overlapping sections for spectral analysis, to determine Curie point depth, geothermal heat flow and magnetic trends. Calculation of ratios was used for the radio-elements to estimate the radioactive heat values in the study area, and the surface geology of the study area was delineated to outline each rock unit to match their density and corresponding radio-elements. The results of the analysis of aeromagnetic data showed that the shallow magnetic source ranges from 0.59 to 3.86 km, deeper source ranges from 8.03 to 19.85 km, Curie point depth values ranges from 14.64 to 38.62 km and geothermal heat flow values ranges between 37.54 and 99.02 mWm^{-2}. The results of the analysis of the radioactive heat production of the study area range between 0.01 and 5.43 μWm^{-3}. The highest heat produced was from the Shale with radioactive heat production as high as 5.43 μWm^{-3}. There are high geothermal heat flow and radioactive heat values in Aimeke and Ogobia.

Key words: Aeromagnetic, aero-radiometric, radioactive, geothermal.

INTRODUCTION

Aeromagnetic and aeroradiometric data were used to correlate the geothermal heat flow and radioactive heat production of the Anambra basin to ascertain if area with high geothermal heat flow values corresponds with that of the radioactive heat production. In this research work, Curie point depth was used to calculate the geothermal heat flow because of its importance in earth science (Artemieva et al., 2001; Megwara et al., 2012). The radioactive heat map was interpreted to know productive area based on the geographic projection of important towns. The digitized and georeferenced geological map of the study area outlined the rocks' boundaries. Apart

*Corresponding author. E-mail: kuforijimi@gmail.com.

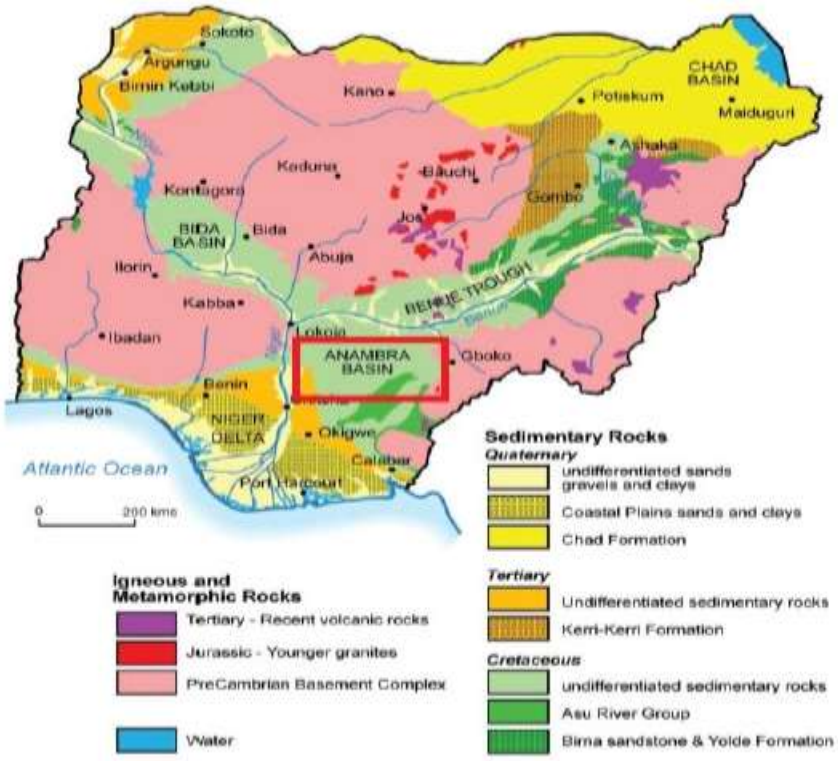

Figure 1. Geological map showing the study area in red (Source: MacDonald et al., 2014).

from geothermal exploration, radioactive heat can also be applied to detect uranium exploration (Killen et al., 2009; Grasty, 1979), identify sedimentary facies for oil and gas exploration (Myers et al., 1979; Bristow et al., 1989; Davies et al., 1996), detect radioactive contamination (Rybach et al., 1995; Sanderson et al., 1989) and mineral exploration (Mero, 1960). Radioactive decay of rocks is probably the greatest overall source of heat in the Earth's crust by a substantial factor, although, there are other sources that may be peculiar to specific area (Jessop, 1990). In some studies, radioactive heat production was calculated from concentrations of radio-elements measured in the laboratory by Fernández et al. (1998) and directly from gamma-ray log by Bücker and Rybach (1996) in order to get the accurate radioactive heat values. Also, radioactive heat production was assessed from airborne gamma-ray data (Salem et al., 2005; Richardson and Killen, 1980; Thompson et al., 1996).

The geological setting

The geology of the study area is presented in Figure 1. The area of study is bounded by latitudes 6°00'N and 7°30'N and longitudes 6°30'E and 9°00'E of the Anambra basin. The Anambra basin is an elongated NE – SW trends as marked out in Figure 2 and is located at the south-western fringe of the Anambra basin bordered on the west by the Precambrian basement complex rocks of western Nigeria and on the east by the Abakaliki Anticlinorium. The Asu River Group in the Abambra basin consists of shales, limestones and sandstone lenses of the Abakaliki Formation in the Abakaliki area and the Mfamosing Limestone in the Calabar Flank (Petters, 1982). The sedimentation in the Anambra basin started with the marine Albian Asu River Group, even though some pyroclastics of Aptian – Early Albian ages have been scarcely reported (Ojoh, 1992). The general stratigraphic cross-sections of this region are presented in Figure 2.

MATERIALS AND METHODS

Data acquisition and processing

Twelve sheets of 268 - 271, 287 - 290 and 301 - 304 covered the study area. They were measured and acquired on a scale of 1: 100,000 series by Fugro Airborne Surveys for Nigerian Geological Survey Agency (NGSA). The sheets were used as basic data for determining the nature of magnetic anomalies over the area. The survey was carried out along a series of North-South lines with a spacing of 3 km and an average flight elevation of 80 m above the

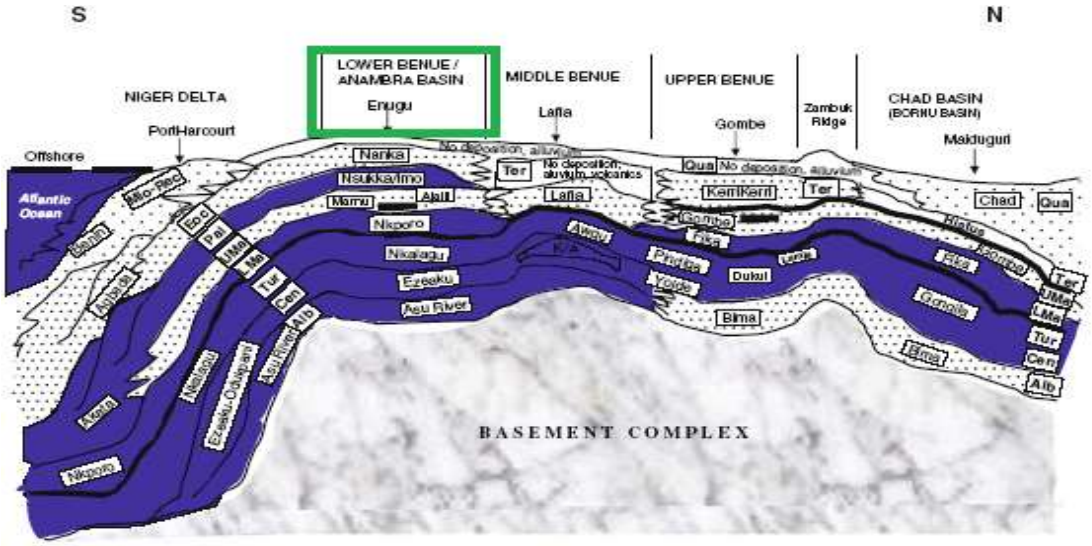

Figure 2. Idealized N-S stratigraphic cross-section across the Chad Basin-Benue Trough-Niger Delta showing Anambra basin underlain by basement complex depicting connected Trans-Atlantic seaway between the South Atlantic and the Tethys Sea during the Coniacian-Turonian (Source: Obaje, 2009).

sea level. The magnetic data was obtained from digitization of the total magnetic intensity contour maps at an interval of 0.0271 units at a flight line spacing of about 3 km. Also, the radiometric data for this study was obtained by windowing out the data of the same twelve (12) radiometric sheets. The radiometric data were acquired at a flight elevation of 80 m, line spacing and tie-line spacing were 500 and 5000 m, respectively.

Airborne magnetic data processing

A super (composite) map (Figure 3a and b) was produced after merging the data of each smaller map that covered the study area with "Oasis Montaj version 8.3"- a geospatial software and “Golden Surfer 11”- a contouring software with a grid cell size of 55 m (Dentith, 2011). The results are presented in three columns: longitudes, latitudes and magnetic values of the given data point, respectively, and each magnetic data was placed with their corresponding longitudes and latitudes. Magnetic field reduction to the equator (RTE) filter was performed since the study area is located within the low magnetic latitudes (that is, areas with geomagnetic inclination less than 15°) where a reasonable reduction to the pole (RTP) of magnetic data is not achievable (Anudu et al., 2014; Sheriff, 2002; Rajagopalan, 2003; Wijins et al., 2005; Fairhead and Williams, 2006; GETECH, 2007; Geosoft Inc., 2011a). A Butterworth low-pass filter was applied during the RTE transformation to eliminate high-wavenumber connected with noise in the data. The parameters used during RTE filtering are: geomagnetic inclination of -8.571°, geomagnetic declination of -1.779° and amplitude correction of -20, while the Butterworth low-pass filter parameters include: cut-off wavelength of 500 m and filter order of 8. The -8.571° and -1.779° are mean values of the geomagnetic inclination and declination, computed for the area based on the IGRF-11 model for year 2006 to 2007 as adopted by the International Association of Geomagnetism and Aeronomy (IAGA) (NOAA/NGDC, 2010; Anudu et al., 2014). This process converts the TMI anomaly map of the area into one with better directions of magnetization field and the reduction to the equator total magnetic intensity (RTE-TMI) anomaly map was produced. Two noticeable disturbances were observed: residual and regional, they were separated using polynomial filtering method. The filtered residual data was Fourier transformed and the area was divided into 35 overlapping sections (Figure 4) for spectral analysis (Udensi et al., 2004). Figure 5a and b show the plots of spectral energies against their corresponding wave-numbers of one of the 35 plots to calculate the values of the shallow magnetic source and deeper magnetic source depths for each sections. The Curie point depth was calculated using Equation 1:

$$Z_b = 2Z_O - Z_t \quad (1)$$

The value of the geothermal heat flow is expressed by Fourier’s law with Equation 2:

$$q = \left[\frac{dT}{dT}\right]\lambda \quad (2)$$

Tanaka et al. (1999, 2005) used the same equation to calculate geothermal heat flow, where (q) is the geothermal heat flow, (λ) is the coefficient of thermal conductivity, the Curie temperature (θ) can be obtained from the Curie point depth (Z_b) and the thermal gradient $(\frac{dT}{dZ})$ using the following equation:

$$\theta = \left[\frac{dT}{dT}\right]Z_b \quad (3)$$

The combination of Equations 2 and 3 gave:

$$q = \lambda\left[\frac{\theta}{Z_b}\right] \quad (4)$$

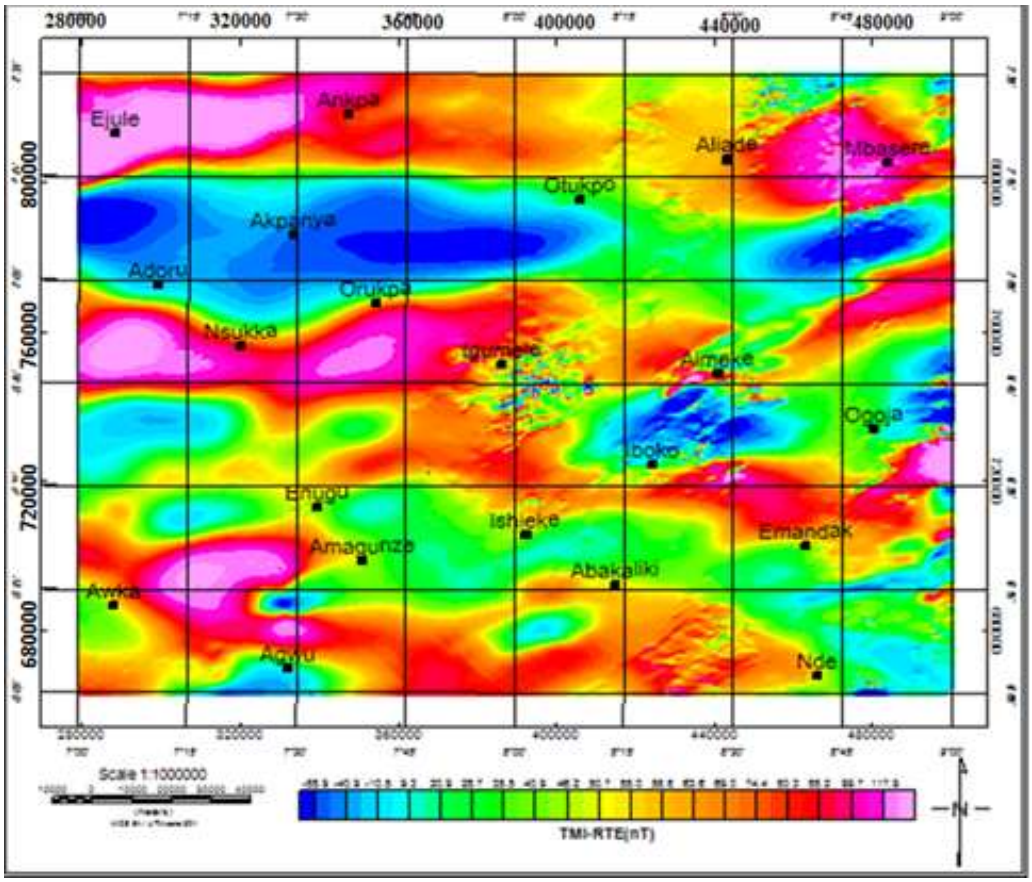

Figure 3a. Reduction to the Equator of total magnetic intensity (RTE-TMI) anomaly map of the study area.

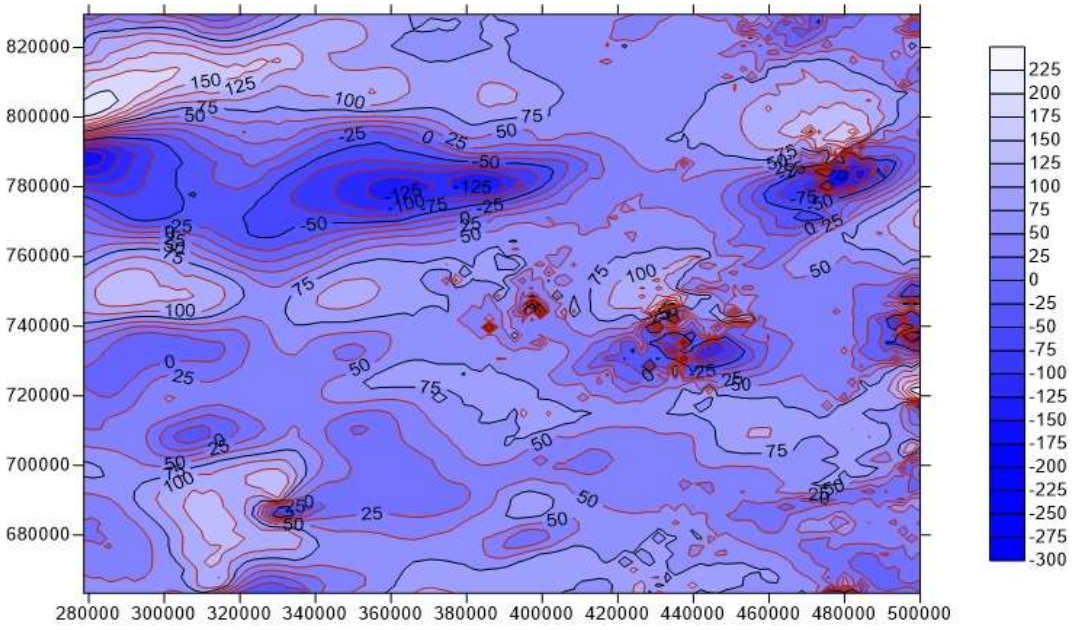

Figure 3b. Contour of total magnetic intensity (TMI) anomaly map of the study area (the axes are in degrees and contour interval is 25 nT, respectively).

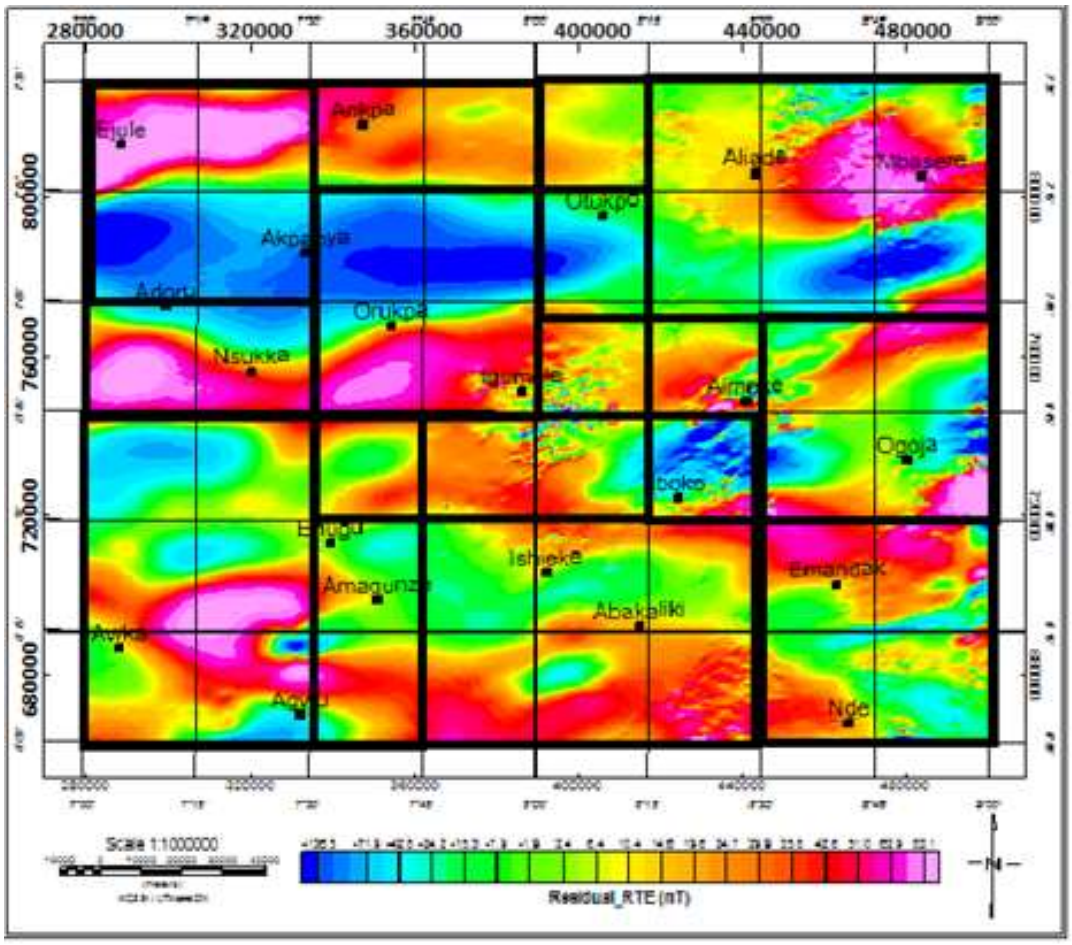

Figure 4. Residual magnetic anomaly map of the study area showing overlapping sections using the coordinates at the centre for each location.

Geothermal gradient is calculated as the ratio of Curie point temperature to Curie point depth: $(\frac{\theta}{Z_b})$ $^{o}Ckm^{-1}$.

In this study, 2.5 Wm^{-1} $°C^{-1}$ (Reiter et al., 1985) was taking as an average of thermal conductivity value, because the predominant lithology in this area is Shale.

Radiometric data processing

The radioactive heat values were calculated from the energy released from the Alpha, Beta and Gammay decay of rocks (Salem and Fairhead, 2011) using an empirical equation by Rybach (1976) expressed as:

$$A(\mu W/m^3) = \rho(0.0952\ C_u + 0.0256\ C_{Th} + 0.0348\ C_k) \quad (5)$$

Where, A = radioactive heat, ρ = density of rock adapted from Telford et al. (1990), C_u, C_{Th} and C_k are the concentrations of uranium (ppm), thorium (ppm) and potassium (%), respectively.

The method applied in this research is similar to that of Salem et al. (2005) where the rock unit boundaries were outlined to avoid mix-up while assigning densities to each rock unit with their corresponding radio-elements.

RESULTS

Figure 3a and b show the image of the total magnetic intensity and the contour map of the study area. The anomalies present in the study area were analyzed quantitatively from the combined data of 12. The total magnetic intensity (TMI) in the area is in the range of -300 to 225 nT, and is characterized by short-wavelength (high wave number), medium-wavelength (moderate wave number) and long-wavelength (low wavenumber) anomalies. The range of the TMI quite agrees with the work of Anudu et al. (2014) stating that the range of the TMI in the middle Benue Trough is in the range of -370 to 270 nT. Most of the anomalies in the TMI anomaly map have predominantly NE–SW and E–W trends. The residual magnetic anomaly map of the study area is

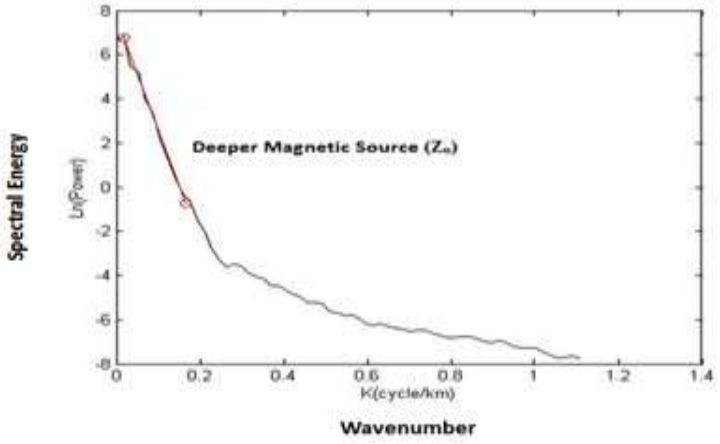

Figure 5a. Typical plot of spectral energy against wave-number showing deeper magnetic source depths.

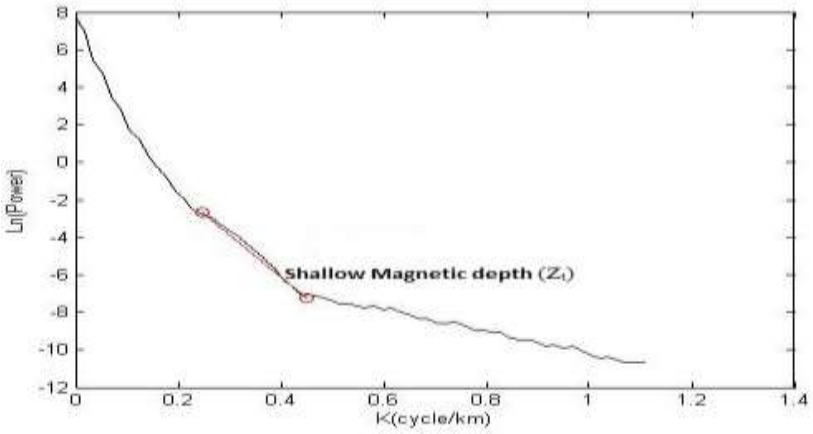

Figure 5b. Typical plot of spectral energy against wave-number showing shallow magnetic source depths.

presented in Figure 6 after the composite map has been reduced to the equator. Table 1 shows the values of the shallow magnetic sources, deeper magnetic sources, Curie point depths and geothermal heat flow derived from the power-density spectra energy of the study area. The results of the analysis showed that the shallow sources have depths varying from 0.59 to 3.86 km, while the deeper sources have depths ranging from 8.03 to 19.85 km and Curie point depth values ranging from 14.64 to 38.62 km. The geothermal heat flow values obtained from the Curie point depth and geothermal gradient values vary from 99.02 mWm^{-2} in the upper part around Enugu and Agwu and also very high around Aimeke to 37.54 mWm^{-2} in the lower part around Iboko in the study area. Figure 7 shows the geothermal heat flow map of the study area.

Correlation of thorium abundance, total magnetic intensity and geological maps

The thorium abundance values range from 4.3 to 24.6 ppm. Correlation of Figure 8a and b shows that high thorium concentration corresponds with high total magnetic intensity anomalies around Nsukka, Mbasere, Ekuaro, Ogobia, Aimeke, Abakaliki and Iboko while low thorium concentration corresponds with low magnetic intensity anomalies around Emandak, Igumale, Amagunze, Ankpa, and Akpanya. The Ogobia and Aimeke area shown in the geological map (Figure 8c) have occurrences of shales and basement complex; which are associated with thorium mineralization and basement granitic rocks which are associated with magnetic mineralization.

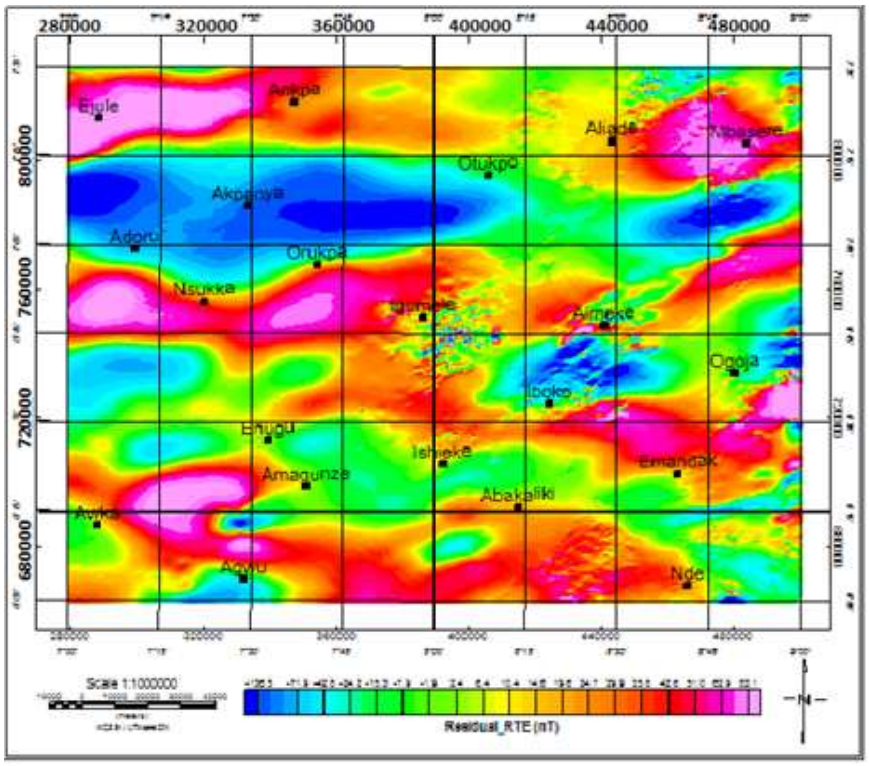

Figure 6. Residual magnetic field map of the study area. The x- y-axes are longitude and latitude in decimal degrees, respectively.

Correlation of uranium abundance, total magnetic intensity and geological maps

The uranium abundance values range from 0.6 to 6.8 ppm. Correlation of Figure 9a and b shows that high uranium concentration corresponds with high total magnetic intensity anomalies around Ogobia and Aimeke while low uranium concentration corresponds with low magnetic intensity anomalies around Ankpa and Akpanya. Ogobia and Aimeke area shown in the geological map (Figure 9c) has occurrence of shales and basement complex which are associated with uranium mineralization and basement granitic rocks which are associated with magnetic mineralization.

Correlation of potassium abundance, total magnetic intensity and geological maps

The potassium abundance values range from 0.0 to 1.3%. Correlation of Figure 10a and b shows that high potassium concentration corresponds with high total magnetic intensity anomalies around Ogobia, Iboko, Ishieke, Aimeke and Nde, while low thorium concentration corresponds with low magnetic intensity anomalies around Ankpa, Ejule, Akpanya, Nsukka and Ngwo. The Ogobia and Aimeke area shown in the geological map (Figure 10c) have occurrences of shales and basement complex; which are associated with potassium mineralization and basement granitic rocks which are associated with magnetic mineralization.

Radiometric anomalies hotspots

Based on the radiometric heat flow map (Figure 11) of the study area, Ogobia and Aimeke show high concentration values of potassium, uranium and thorium. These particular areas are suitable for geothermal resource because of the high values of the three radio-elements.

Qualitative and quantitative analysis of the radioactive heat analysis

The rock units with their average densities identified and assigned were used for the estimation of the radioactive heat production based on the concentrations of potassium, thorium and uranium within each rock unit. The average of the density of each rock unit was used in this research work as presented in Table 2. The boundary

Table 1. Summary of the results of the shallow depth, deeper depth, Curie point depth and geothermal heat flow for the 35 over-lapping cells and their corresponding longitudes and latitudes.

Sections	Latitude (°)	Longitude (°)	Shallow depth (Z_t) km	Deeper depth (Z_o) km	Curie point depth Z_b (km)	Geothermal heat flow (mWm^{-2})
1	6.25	7.25	3.57	10.37	17.16	84.50
2	6.25	7.50	2.43	9.51	16.60	87.36
3	6.25	7.75	1.41	8.03	14.64	99.02
4	6.25	8.00	1.04	10.24	19.44	74.58
5	6.25	8.25	1.18	12.65	24.12	60.13
6	6.25	8.50	1.28	13.67	26.06	55.64
7	6.25	8.75	1.22	9.52	17.40	81.37
8	6.50	7.25	1.08	12.38	23.69	61.22
9	6.50	7.50	0.98	10.14	19.31	75.10
10	6.50	7.75	1.50	9.48	17.47	82.99
11	6.50	8.00	0.81	10.74	20.66	70.17
12	6.50	8.25	1.17	9.68	18.18	79.75
13	6.50	8.50	1.13	10.19	19.25	75.32
14	6.50	8.75	1.01	8.01	16.02	96.57
15	6.75	7.25	0.59	17.32	34.04	42.60
16	6.75	7.50	3.86	16.23	28.60	50.69
17	6.75	7.75	1.53	15.85	30.18	48.05
18	6.75	8.00	1.43	11.31	21.19	68.43
19	6.75	8.25	1.30	10.98	20.65	70.21
20	6.75	8.50	1.43	11.08	20.73	69.94
21	6.75	8.75	1.71	8.44	15.18	95.55
22	7.00	7.25	1.00	13.48	25.97	55.84
23	7.00	7.50	2.08	17.20	32.33	44.85
24	7.00	7.75	1.07	19.85	38.63	37.54
25	7.00	8.00	1.11	15.87	30.63	47.34
26	7.00	8.25	1.12	11.32	21.52	67.37
27	7.00	8.50	1.67	9.90	18.13	79.99
28	7.00	8.75	0.94	10.35	19.76	73.36
29	7.25	7.25	0.81	11.79	22.76	63.70
30	7.25	7.50	0.99	14.09	27.21	53.29
31	7.25	7.75	1.34	10.27	19.19	75.56
32	7.25	8.00	1.44	11.35	21.27	68.18
33	7.25	8.25	1.27	12.12	22.96	63.15
34	7.25	8.50	0.94	11.47	22.01	65.89
35	7.25	8.75	0.97	14.05	27.13	53.45

of each rock unit was outlined with the concentrations of radio-elements (K (%), eU and eTh) (Figure 10). Summary of the results of the analysis of radioactive heat value for each rock unit is presented in Table 3 and illustrated as map in Figure 11. High radioactive heat concentrations were observed around Aimeke, Iboko, Mbashere, Ogobia and Nde. Radioactive heat production values for each rock unit were calculated based on Equation 5.

DISCUSSION

Figure 12 shows that the structural trends are in E-W direction and this agrees with the magnetic trend results. It is also an indication of the fault lines in the Anambra

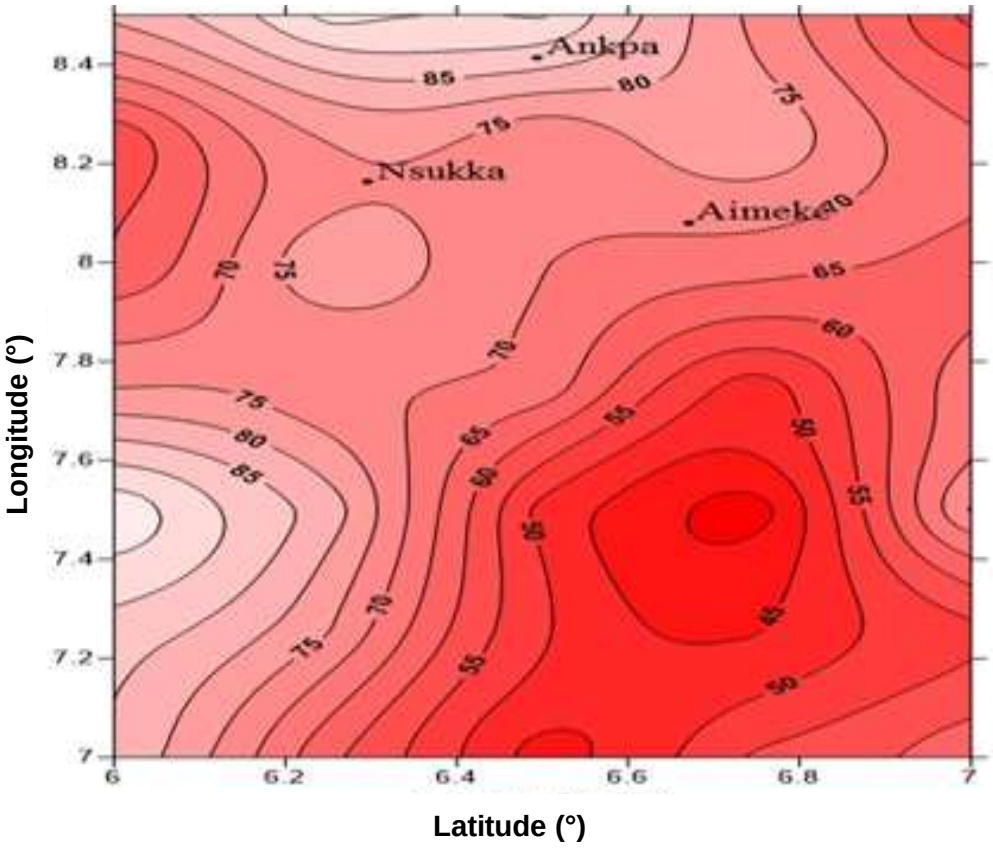

Figure 7. Geothermal Heat flow map of the study area (Contour interval is 5.0 mWm^{-2}).

basin. The green arrows indicate that the radioactive heat flows in E-W direction. Majority of the anomalies in the total magnetic map are mostly NE–SW and E–W trends. The radioactive results showed high concentration of uranium, thorium and potassium in Aimeke and Ogobia areas. Also, this research work provides new insights on the geothermal setting of the Anambra basin using airborne radiometric data. Radioactive heat production was mapped from the aero-radiometric data. The investigated basin has a range of radioactive heat production values which is above 4.0 μWm^{-3} for a high radioactive heat production (Alistair et al., 2014). Most of the radioactive heat is produced from uranium as its constant is more than twice of the constants of the other two radio-elements (Equation 5). The high concentration of uranium, potassium and thorium in Aimeke and Ogobia shows potentiality for geothermal energy production.

The radio-elements' maps showed that there is high concentration of thorium in Nsukka, Mbasere, Ekuaro, Ogobia, Aimeke, Abakaliki and Iboko. These areas have abundance of shale and sandstones. Potassium existence is correspondingly abundant in Ogobia, Iboko and Aimeke because of abundance of shale while high concentration of uranium was found around Ogobia and Aimeke.

Analysis of the radioactive heat map showed that Ogobia, Aimeke and Nde have high concentration of radioactive heat. The high concentration of uranium, potassium and thorium in Aimeke and Ogobia shows potentiality for geothermal energy production.

Ankpa has a high geothermal heat flow due to the occurrence of granitic rocks underlain the area. This particular area has a low radioactive heat value; this shows that the geothermal heat in Ankpa is not from radioactive heat values found in this study. This may be due to the heat from the mantle or the ambient heat in the hot granitic rocks in this area. The same thing is applicable to Enugu with high geothermal heat flow but low radioactive heat values; this may be due to the occurrence of coal underlain the area. The geothermal heat flow is at its highest value around Ogobia, Aimeke and Enugu. Based on the results from the analysis, there is likelihood that the study area may be prospective for geothermal energy utilization because heat flow values fall between 60 and 100 mWm^{-2} (Jessop et al., 1976) which is the acceptable standard for geothermal heat flow

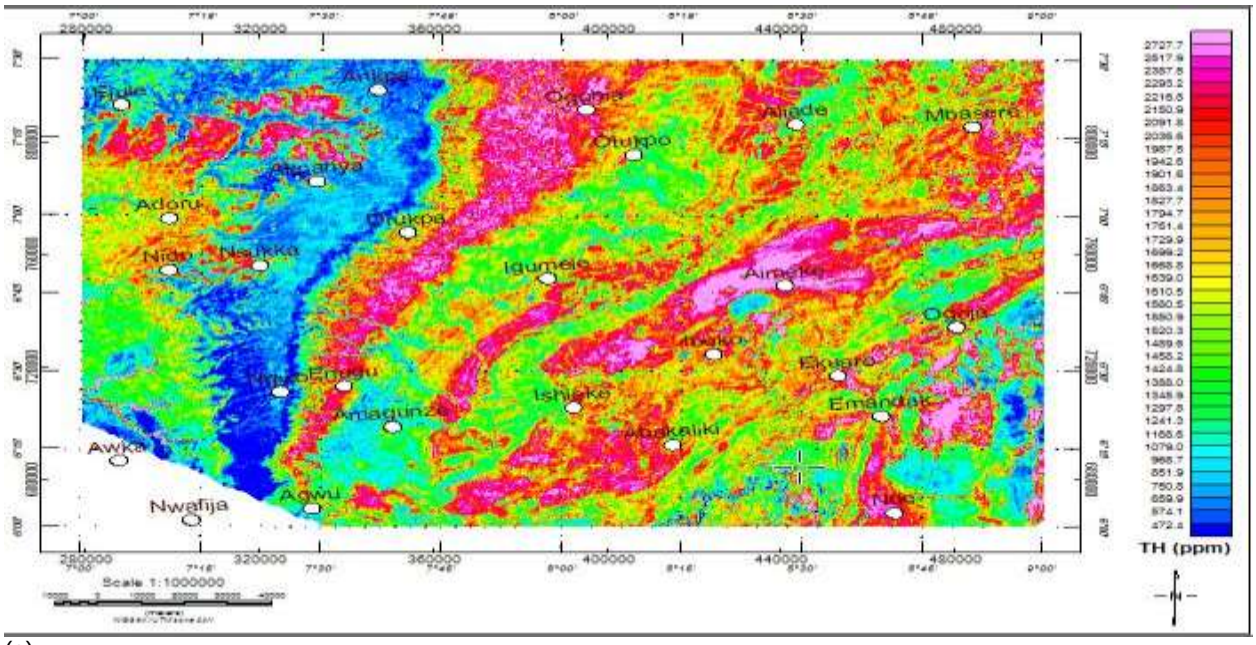

(a)

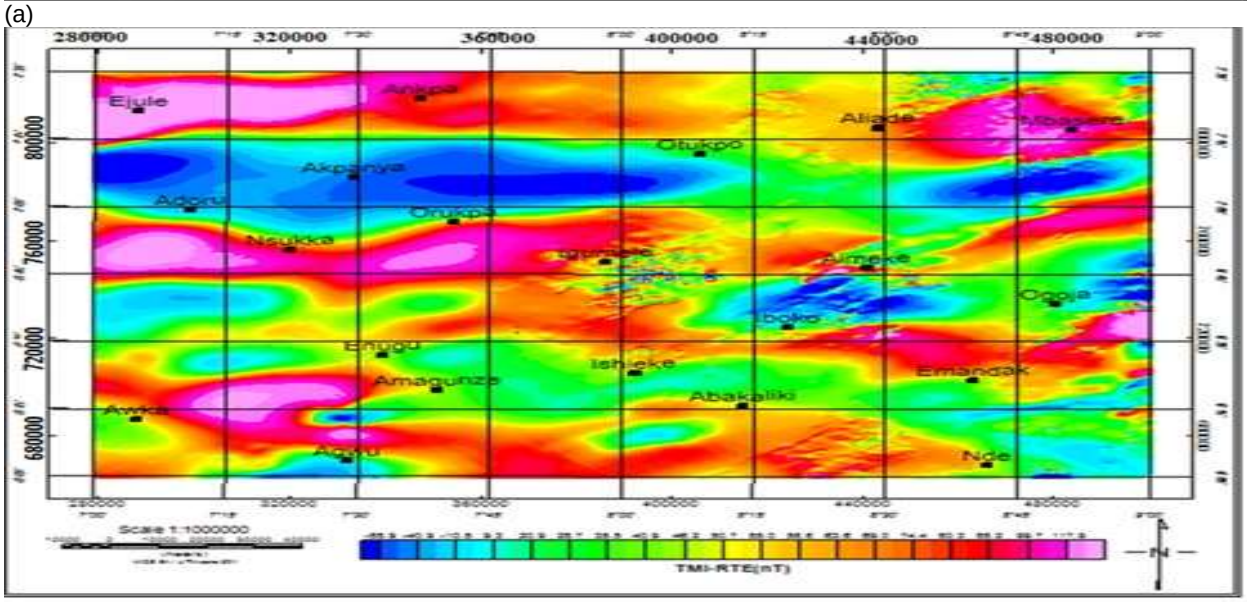

(b)

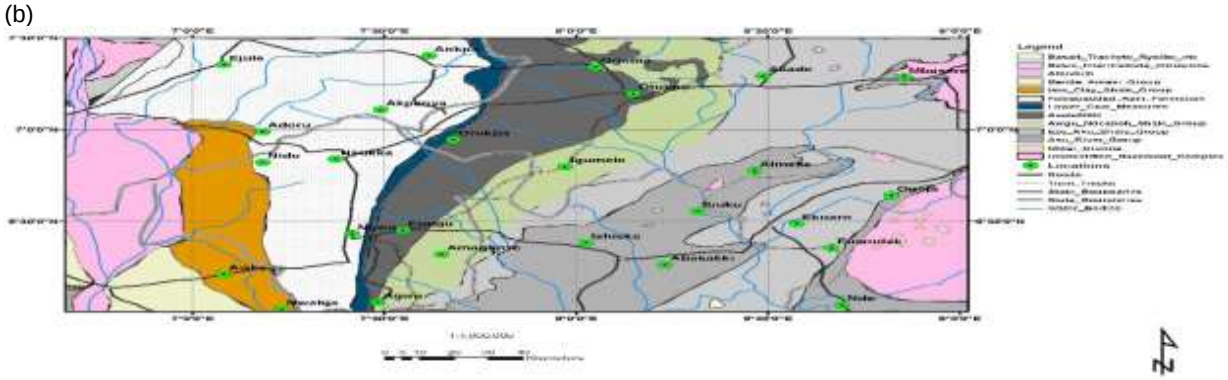

(c)

Figure 8. Correlation of (a) thorium abundance (b) total magnetic intensity and (c) geological maps of the study area.

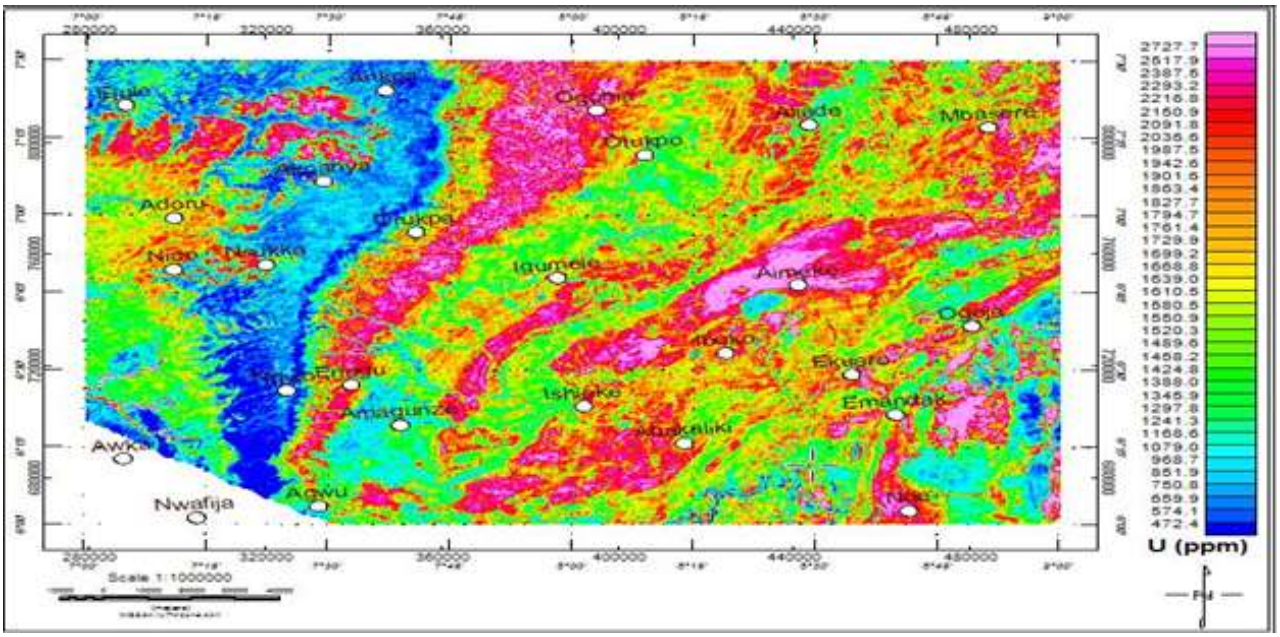

(a)

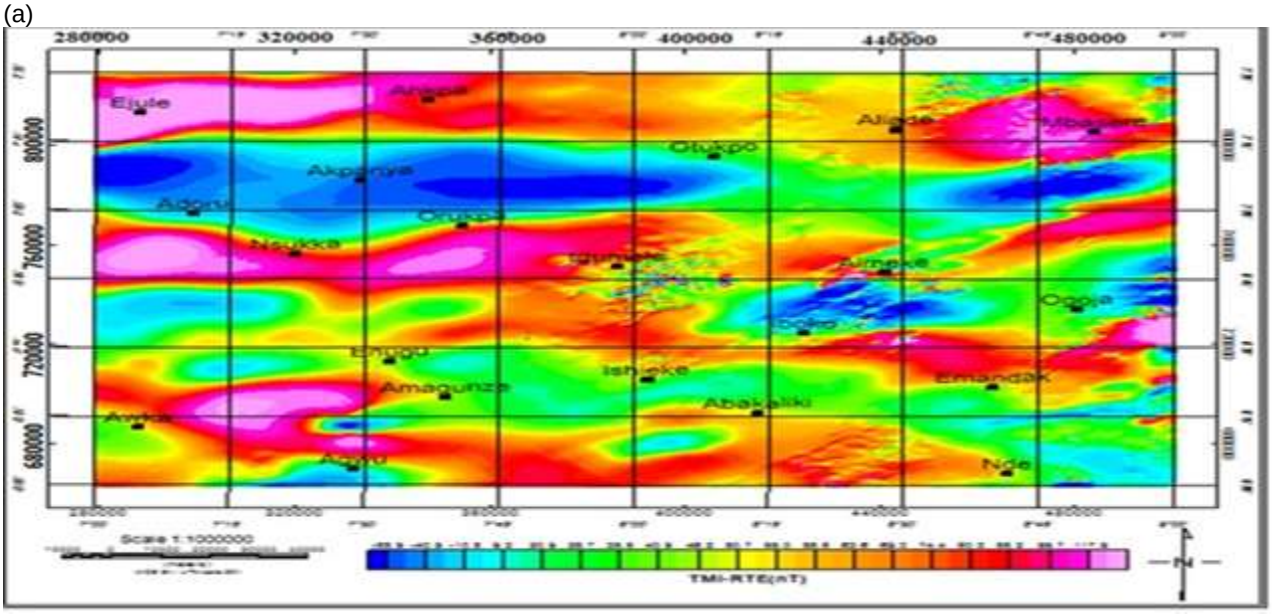

(b)

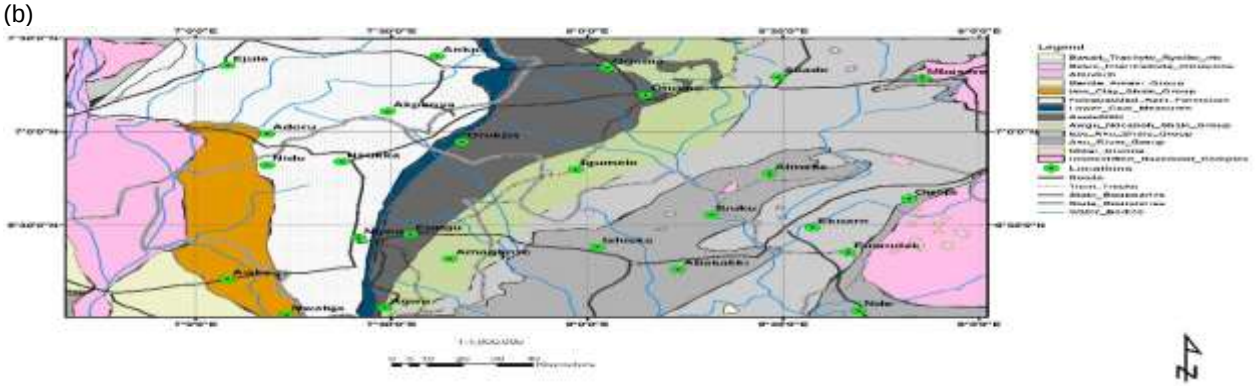

(c)

Figure 9. Correlation of (a) uranium abundance (b) total magnetic intensity and (c) geological maps of the study area.

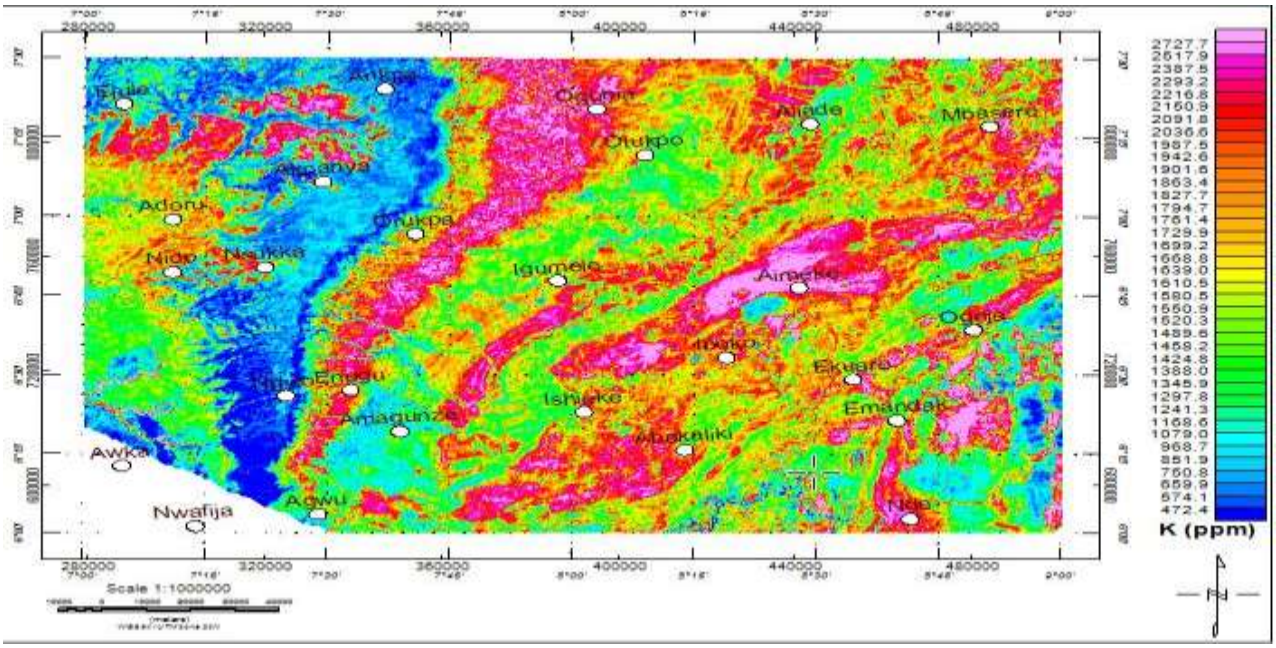

(a)

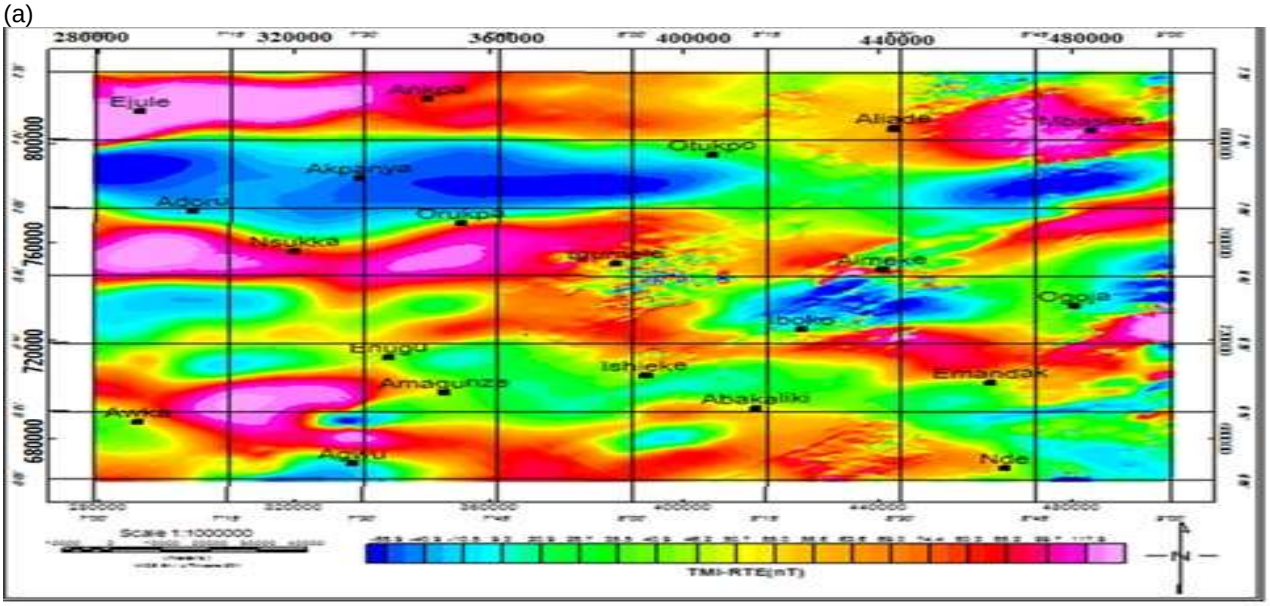

(b)

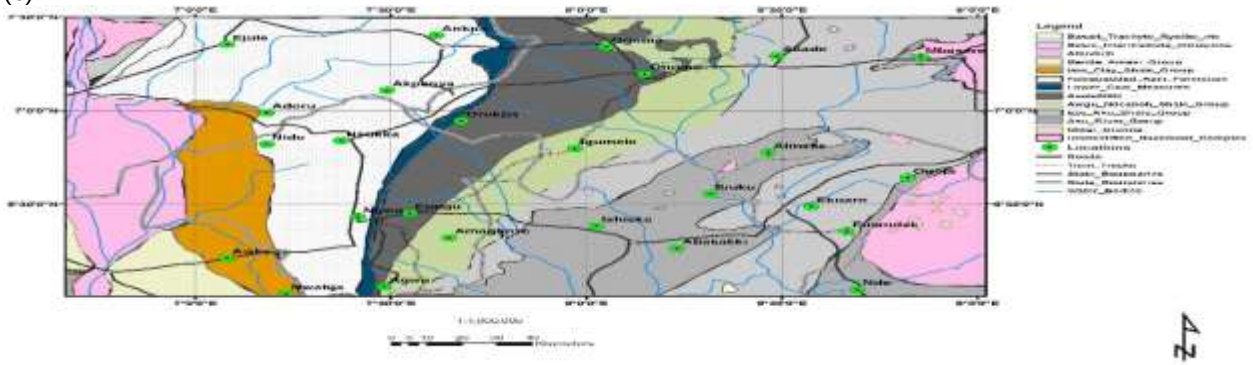

(c)

Figure 10. Correlation of (a) potassium abundance (b) total magnetic intensity and (c) geological maps of the study area.

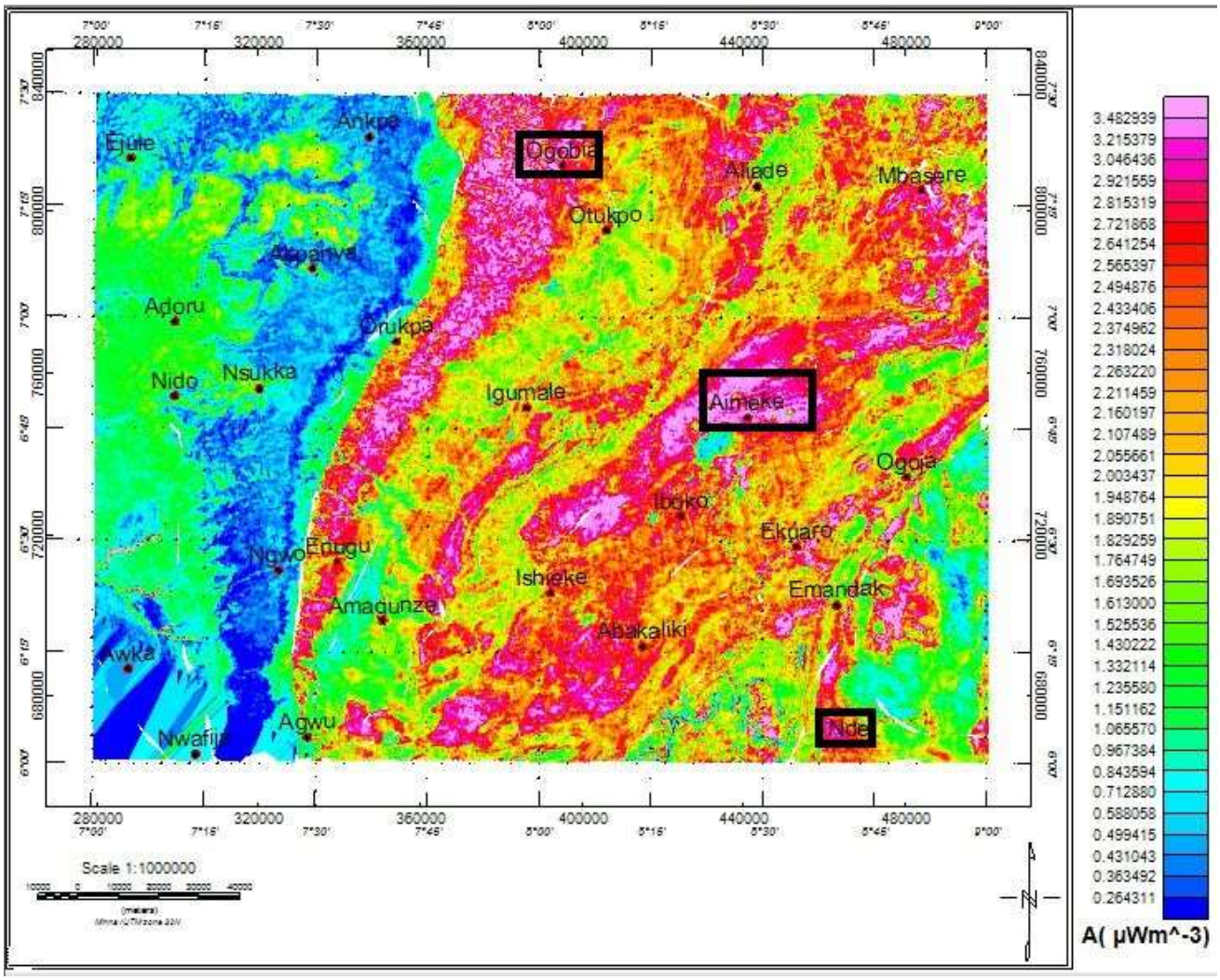

Figure 11. Airborne radioactive anomalies heat flow map showing hotspots in black rectangles.

Table 2. Average density for each rock unit.

Rock	Density (g/cm^3)
Unidentified basement complex	2.64
Older granite	2.81
Shale 1 (Asu River group)	3.10
Shale 2 (Eze Aku group)	2.90
Awgu Ndeaboh Shale group	2.80
Asata Nkporo group)	2.70
Lower coal measure	1.40
Falsebedded Ajali formation	1.60
Sandstones 2 (Bende Ameki Group)	2.10
Imo clay measure	1.65
Alluvium	1.96
Basic intermediate intrusion	2.79
Basalt trachyte rhyolite	2.60

Table 3. Radioactive heat production corresponding to each rock unit (in μWm^{-3}).

Rock units	Range		Average
	Minimum	Maximum	
Basalt Trachyte Ryolite	0.53	2.75	1.75
Basic intermediate intrusion	0.73	3.26	2.29
Alluvium	0.16	2.76	1.11
Bende Ameki Group	0.02	4.45	2.45
Imo clay measures	0.17	2.1	0.91
False bedded Ajali formation	0.09	3.26	0.79
Lower coal measures	0.03	2.09	0.95
Asata Nkporo Shale	0.01	5.43	2.47
Awgu Ndeaboh shale group	0.01	4.96	2.06
Eze Aku shale group	0.03	3.85	2.22
Asu river group	0.02	3.7	2.44
Older granite	0.03	4.3	2.04
Unidentified basement complex	0.01	3.4	1.76

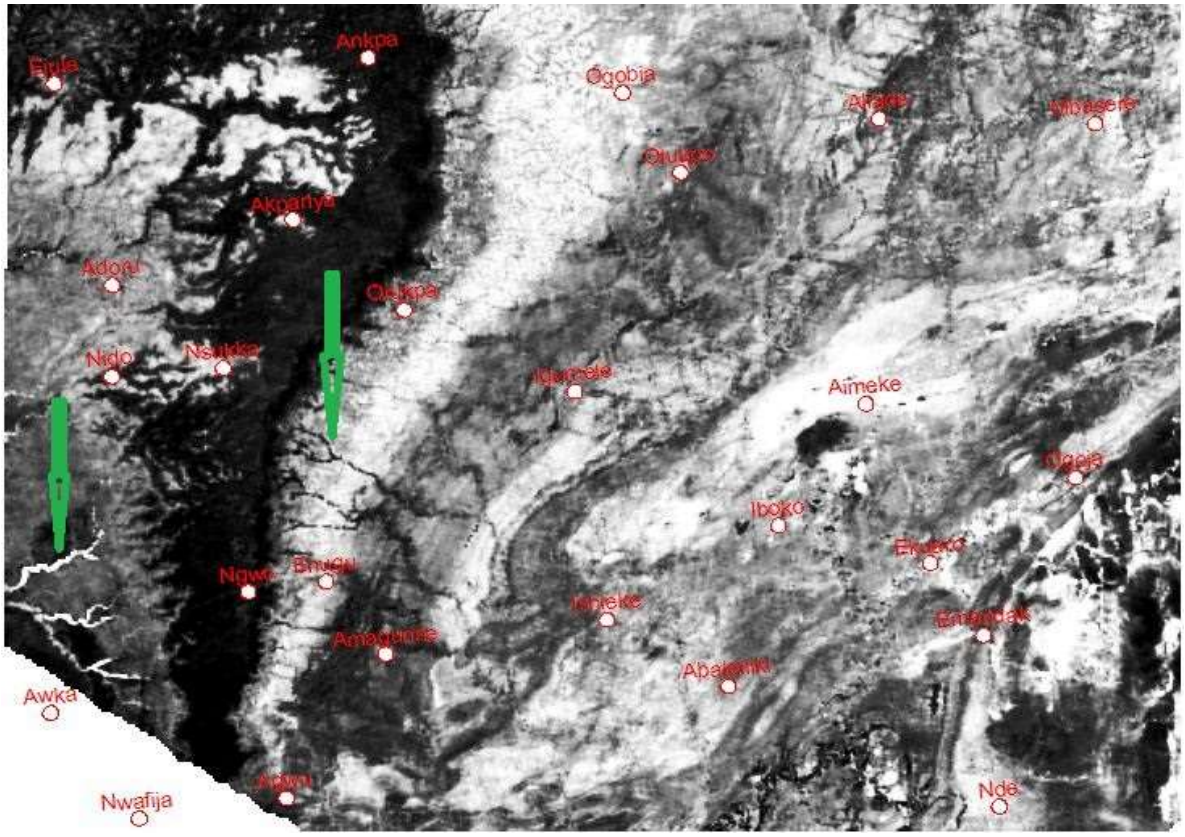

Figure 12. Radioactive heat map showing structural trends and fault lines in the green arrows.

potential. The radioactive results showed high concentration of uranium, thorium and potassium in Aimeke and Ogobia areas. Aimeke and Ogobia have high geothermal heat values. These areas are considered hotspots because of the high values of radioactive heat production.

Comprehensive ground radiometric and magnetic

surveys with soil test should be carried out at Ogobia and Aimeke which are considered to be hotspot. Also, detailed ground radiometric and magnetic surveys should be carried out at Ankpa because of the low radioactive heat values but high heat flow from the magnetic data.

CONFLICT OF INTERESTS

The authors have not declared any conflict of interests.

REFERENCES

Anudu GK, Randell AS, David IM (2014). Using high resolution aeromagnetic data to recognize and map intra-sedimentary volcanic rocks and geological structures across the Cretaceous middle Benue Trough, Nigeria. J. Afr. Earth Sci. 99:625-636.

Artemieva IM, Mooney WD (2001). Thermal Thickness and evolution of Precambrian Lithosphere, A Global Study Journal of geophysics Research 106(B8):16387-16414.

Bristow C, Williamson B (1989). Spectral Gamma ray logs: Core to log calibration, facies analysis and correlation problems in the Southern North Sea. Geol. Soc. Lond. Spec. Publ. 41:81-88.

Bücker C, Rybach L (1996). A simple method to determine heat production from gamma-ray logs. Mar. Pet. Geol. 13:373-375.

Davies S, McLean D (1996). Spectral gamma-ray and palynological characterization of Kinderscoutian marine bands in the Namurian of the Pennine Basin. Proc. Yorks. Geol. Polytech. Soc. 51:103-114.

Dentith M (2011). Magnetic methods, Airborne. In: Gupta, H.S. (Ed.), Encyclopedia of solid earth geophysics, Springer, Dordrecht, 1:761-766

Fairhead JD, Williams SE (2006). Evaluating normalized magnetic derivatives for structural mapping. SEG 2006 New Orleans Extended Abstract.

Fernández M, Marzan I, Correia A, Ramalho E (1998). Heat flow, heat production, and lithosphere thermal regime in the Iberian Peninsula, Tectonophysics 291:29-53.

Geosoft Inc (2011a). MAGMAP Filtering. Technical Documentation. Tutorial. Geosoft Inc., Canada. (accessed 20.03.12).

GETECH Group Plc (2007). Advanced processing and interpretation of gravity and magnetic data. GETECH (Geophysical Exploration Technology) Group Plc. Kitson House Elmete Hall Leeds, UK. 22p.

Grasty R (1979). Gamma ray spectrometric methods in uranium exploration – Theory and operational procedures. Geophys. Geochem. Search Met. Ores, 31:147-155.

Jessop AM (1990). Thermal geophysics, Elsevier, Amsterdam.

Jessop AM, Habart MA, Sclater JG (1976). The World heat flow data collection 1975. Geothermal services of Canada. Geotherm Services, 50:55-77.

Megwara JU, Emmanuel EU, Peter IO, Mohammed AD, Kolawole ML (2012). Geothermal and Radioactive heat studies of part of southern Bida basin, Nigeria and the surrounding basement rocks. 2(1):125.

Killeen P (1979). Gamma ray spectrometric methods in uranium exploration – Application and interpretation. Geophys. Geochem. Search Met. Ores 31:163-230.

MacDonald AM., Cobbing J, Davies J (2005). Developing groundwater for rural water supply in Nigeria. British Geological Survey Commissioned Report CR/05/219N.

Mero JL (1960). Uses of the gamma-ray spectrometer in mineral exploration. Geophysics, 25:1054-1076.

Myers K, Bristow C (1989). Detailed sedimentology and gamma-ray log characteristics of a namurian deltaic succession II: Gamma-ray logging. Geol. Soc. Lond. Spec. Publ. 136:1-7.

NOAA/NGDC (2010). World Magnetic Model – Epoch 2010: Main Field Inclination. National Oceanic and Atmospheric Administration (NOAA)/National Geophysical Data Centre (NGDC), Colorado USA.

Obaje NG (2009). Geology and mineral resources of Nigeria. Berlin: Springer Publishers, pp. 1-203.

Ojoh KA (1992). The Southern part of the Benue Trough (Nigeria) Cretaceous stratigraphy, basin analysis, paleo-oceanography and geodynamic evolution in the equatorial domain of the South Atlantic. NAPE Bull. 7:131-152.

Petters SW (1982). Central West African Cretaceous-Tertiary benthic foraminifera and stratigraphy. Palaeontographica Abt A 179:1-104.

Rajagopalan S (2003). Analytic signal vs. reduction to pole: solutions for low magnetic latitudes. Explor. Geophys. 34(4):257-262.

Reiter MA, Jessop AM (1985). Estimates of terrestrial heat flow in offshore Eastern Canada. Can. J. Earth Sci. 22:1503-1517.

Richardson KA, Killeen PG (1980). Regional radioactive heat production mapping by airborne gamma-ray spectrometry; in Current Research, Part B, Geological Survey of Canada, Paper 80-1B, pp. 227-232.

Rybach L, Schwarz GF (1995). Ground gamma radiation maps: Processing of airborne, laboratory, and in situ spectrometry data. First Break 13:97-104.

Salem A, Fairhead D (2011). Geothermal reconnaissance of Gebel Duwi area, Northern Red Sea, Egypt using airborne magnetic and spectral gamma ray data. Getech pp. 1-22.

Salem A, Abouelhoda EA, Aref AI, Sachio E, Keisuke U (2005). Mapping Radioactive Heat Production from Airborne Spectral Gamma-Ray Data of Gebel Duwi Area, Egypt. Proceedings World Geothermal Congress 2005 Antalya, Turkey, 24-29 April 2005.

Sanderson D, East B, Scott E (1989). Aerial radiometric survey of parts of North Wales in July 1989; Scottish Universities Research and Reactor Centre: Glasgow, UK.

Sheriff RE (2002). Encyclopedic Dictionary of Applied Geophysics, fourth ed. 13 Geophysical Reference Series. Society of Exploration Geophysicists, Tulsa USA, 429 p.

Tanaka A, Ishikawa Y (2005). Crustal thermal regime inferred from magnetic anomaly data and its relationship to seismogenic layer thickness: The Japanese islands case study. Phys. Earth Planet. Inter. 152:257-266.

Tanaka A, Okubo Y, Matsubayashi O (1999). Curie point depth base on spectrum analysis of the magnetic anomaly data in East and Southeast Asia. Tectonophysics, 306:461-470.

Thompson PH, Judge AS, Charbonneau BW, Carson JM, Thomas M.D (1996). Thermal regimes and diamond stability in the Archean Slave Province, Northwestern Canadian Shield, District of Mackenzie, Northwest Territories; in Current Research, 96-1E, Geological Survey of Canada, pp. 135-146.

Udensi EE, Osazuwa IB (2004). Spectral determination of depths to magnetic rocks under the Nupe Basin, Nigeria. Nigerian Association of Petroleum Explorationists (NAPE) Bull. 17:22-27.

Wijins C, Perez C, Kowalezyk P (2005). Theta map: Edge Detection in Magnetic Data. Geophysics 70:L39-L43.

academicJournals

Vol. 11(10), pp. 532-543, October 2017
DOI: 10.5897/AJEST2016.2252
Article Number: F2E344366053
ISSN 1996-0786

http://www.academicjournals.org/AJEST

African Journal of Environmental Science and Technology

Full Length Research Paper

Evidence for a gas-flaring source of alkanes leading to elevated ozone in air above West Africa

O. G. Fawole[1,2]*, X. Cai[1] and A. R. MacKenzie[1,3]

[1]School of Geography, Earth and Environmental Sciences, University of Birmingham, B15 2TT, UK.
[2]Department of Physics and Engineering Physics, Obafemi Awolowo University, Ile-Ife, Osun State, Nigeria.
[3]Birmingham Institute of Forest Research (BIFoR), University of Birmingham, B15 2TT, UK.

Received 18 November, 2016; Accepted 29 March, 2016

As part of the African Monsoon Multidisciplinary Analysis (AMMA) project, the FAAM BAe-146 research aircraft sampled the lower and mid-troposphere around the West Africa sub-region. Back trajectory analysis of the air parcels sampled on-board during the entire duration of the flights showed the history and fate of the air parcels. Data from flights B228 and B231 showed strongly enhanced carbon monoxide (CO) and ozone levels attributable to emissions of anthropogenic origin from the city of Lagos and gas flaring activities in the Nigeria oil fields. The elevated levels of ozone and CO observed at about 6 km above the sea-level on flight B231 were attributed to long-range transport of biomass burning plume from the East, around Sudan. The strongly enhanced mixing ratios of short-chained alkanes and CO (> 400 ppbv) observed from measurements on flights B228 and B231 are indicative of natural gas/combustion sources. Flight B222 sampled air parcels strongly impacted by emissions from Lagos but not from the Nigeria oil field and measured relatively lower mixing ratios of ozone, CO and short-chained alkanes species. Results from this study strongly suggests gas flaring emissions in the Niger Delta area to be a prominent contributor to the enhanced levels of short-chained alkane species observed in Lagos metropolis, especially during the West Africa Monsoon (WAM) months and, hence, a significant source of atmospheric aerosol in the sub-region.

Key words: African Monsoon Multidisciplinary Analysis (AMMA), gas flaring, West Africa Monsoon, alkanes, ozone, Niger Delta.

INTRODUCTION

African Monsoon Multidisciplinary Analysis (AMMA), an internationally funded program, was undertaken to enhance our understanding of the West African Monsoon (WAM) and the impact of its variability on the environment, atmospheric chemistry and socio-economy of the sub-region (Redelsperger et al., 2006). The program was designed to run between 2001 and 2009. During the Enhanced Observing Period (EOP) between 2005 and 2007, there was the implementation of specific land-based and sea-based measurements while 2006

*Corresponding author. E-mail: gofawole@oauife.edu.ng. Tel: +234(0)8033635453.

was the year of Special Observing Period (SOP) (Lebel et al., 2010). During the SOP, there were intensive surface and air (research aircraft and balloons) measurements.

The FAAM BAe-146 research aircraft was based in Niamey, Niger (Reeves et al., 2010), and made about 19 scientific flights (labelled B215 - B235) during SOP2 between July 17 and August, 17, 2006. Of particular interest in this study are BAe-146 flights that are suggested, by back-trajectories analysis, to have been significantly impacted by gas flaring emissions from the intense flaring activities in the Nigeria oil field, south of the country. Specifically, air parcels sampled on three of the flights (B222, B228 and B231) were suggested to have been impacted by anthropogenic emissions from the south of Nigeria, which compared to the North, is more industrialised and has higher population density.

The Niger Delta, the region of intense gas flaring in southern Nigeria, contains over 300 active flare sites (Elvidge et al., 2015) scattered around local communities and farm sites on a land mass of about 70,000 km^2 (Osuji and Onojake, 2004) (Figure 1d). In 2012, of the 325 active flare sites identified in the Nigeria oil field, 97 (~ 30%) ranked among the top 1000 largest flares identified globally. The heart of the Niger Delta is less than 300 and 400 km from Lagos (Nigeria) and Cotonou (Benin), respectively. With an average wind speed of 6 ms^{-1}, a common occurrence in the region, emissions from the region of intense gas flaring in the Niger Delta take about 13 and 18 h to be transported to Lagos and Cotonou, respectively. It should be noted that August marks the peak of the WAM when the Intertropical Convergence Zone (ITCZ) and Intertropical Front (ITF) are northernmost (Sultan and Janicot, 2003). Hence, significant inland transport of emissions from the region of intense flaring is highly favoured. Pollutants from gas flaring are highly buoyant when exiting the stack due to the exit temperature which could be >1900 K in a typical gas flare in the oil and gas industry. Nigeria, Africa's leading oil exporting country, still flares about a quarter of her annual natural gas production (Ite and Ibok, 2013). In 2006, as a result of an increase in Nigeria's daily oil production quota by the Organization of Oil Producing Countries (OPEC) (OPEC, 2015), there was an increase in the estimated amount of gas flared compared to the preceding years (Anejionu et al., 2015a; Fawole et al., 2016). The years 2005 and 2006 were years of intensive oil prospecting and production in Nigeria as a result of the increased quota of production by OPEC, with the achievement of the all-time high daily production in November, 2005. In 2006, the level of air pollution from gas flaring from the Niger Delta was more intense than preceding years due to the level of oil exploration and exploitation (Anejionu et al., 2015b).Despite the significant contributions of gas flaring to atmospheric aerosol loading (Johnson and Coderre, 2012; Weyant et al., 2016), emission factors for pollutants exiting the stacks are very scarce and the very few in the literature are significantly inadequate. For instance, black carbon, a chief climate forcer and a prominent pollutant from gas flaring (USEPA, 2012), is very poorly estimated. To adequately understand the contributions of gas flaring to atmospheric aerosol level and quantify their impact on the atmosphere on both region and global scales, there is the need to research into and establish emission factors that are representative of the huge level of emissions from typical gas flares.

Significantly enhanced CO and alkanes mixing ratios are indicative of fossil fuel combustion (De Gouw et al., 2004). Short-chain alkanes (C_3-C_6) have been use as indicators of fossil fuel combustion as they are less common from biomass burning sources (Seila et al., 1989). Volatile organic compounds such as cyclopentane and cyclohexane in ambient air have been strongly linked to gas flares, oil refineries, and natural gas sources (Gilman et al., 2013; Liu et al., 2008; Sanchez et al., 2008). The ability of an air mass to form ozone is strongly dependent on the ratio of NO_X to non-methane hydrocarbon (NMHC) it contains (Seinfeld and Pandis, 2016).

METHODOLOGY

Meteorological conditions over the West Africa region

The WAM is characterised by two prominent seasons, the dry (November-February) and the rain (March-October) seasons. Desert dust and biomass burning aerosols are predominant during the dry season while the onset of the WAM brings in the moist south-westerly wind which is associated with rainfall. The meteorological condition over West Africa is significantly influenced by the ITCZ which is the zone of convergence of the trade winds of the two hemispheres. The movement of the ITCZ shifts the belt of planetary winds and pressure systems both northwards and southwards depending on the period of the year. In Coastal area of West Africa, the rainy season is generally observed between April and July, and a second but shorter spell of rainy season in September and October (WMO, 2015). In West Africa, the Sahel and Coastal areas have annual rainfall range of 450 - 1050 and 1400 - 2700 mm, respectively.

In the West Africa sub-region, the shifts of the ITCZ and ITF, to a large extend, control the circulations in the lower troposphere. During the peak of the (WAM) between July and September, the ITCZ and ITF can shift as far as 12 and 20°N, respectively. At this period of the year, there is the formation of mesoscale convective systems (MCS) as a result of the position of the ITCZ and presence of elevated terrains to the east (Mari et al., 2011). Large organised MCS develop on a regular basis during the peak of the WAM enabling the rapid vertical uplift of gases and aerosols to the upper troposphere. Compared to preceding years, during the peak of the WAM in 2006, convective activity resulting from MCS was slightly enhanced (Janicot et al., 2008).

Back trajectory calculations

In this study, to understand the history of air masses sampled on

Table 1. Flight details of selected AMMA flights.

Flight	Date	Time of flight	Path of flight
B222	July 30, 2006	11:26 - 15:48	13.5 - 6.6° N; 2.4 - 3.4°E
B228	August 8, 2006	09:41 - 13:34 and 15:09 - 19:10	13.5 - 3.9°N; 2.3 - 2.6°E
B231	August 13, 2006	07:01 - 11:32	13.5 - 5.1°N; 1.3 - 2.5°E

the selected AMMA flights, trajectory ensembles associated with different measurement periods on selected AMMA flights were identified and assessed. A 7-day back trajectory along every second of the entire flight periods for flights B222, B228 and B231 was initiated. As a result of the large volume of time for each flight, each flight time was split into two almost equal parts (a and b) before the trajectory calculations. For example, the 24012 seconds on flight B321 was split into 12000 and 12012 s, and herein referred to as B231a and B231b, respectively. An analysis of every second of the flight duration rather than the 10 s time steps often used in similar studies in the literature were done because of the highly varying nature of plumes encountered on these flights as indicated by the broad range of the concentration of emissions measured on these flights.

Using the flight data (flight time, longitude, latitude and atmospheric pressure), 7-day back trajectories were calculated using the UK Universities Global Atmosphere Modelling Programme (UGAMP) offline trajectory model (Methven, 1997). This model is driven by six-hourly ERA-Interim (European Centre for Medium-Range Weather Forecasts Interim Re-Analysis) wind analyses data. Three dimensional meteorological data are interpolated to the trajectory locations. For each integration time, values of meteorological fields (temperature, potential temperature and pressure) are assigned as attributes to the particle in the trajectory. A detailed technical description of the UGAMP trajectory model can be found in Methven (1997) and Methven et al. (2001).

The trajectories were plotted using the National Center of Atmospheric Research (NCAR) Graphics/NCL trajectory plotting package, kmapline (Noone and Simmonds, 1999). Output of the trajectories calculation from UGAMP is imported into Openair as CSV files. Openair is an R package primarily developed for the analysis of air pollution measurement data (Carslaw and Ropkins, 2012). The trajectory density plot was done using the trajLevel option in the back trajectory function of the Openair package written in the R software (Carslaw and Ropkins, 2012). The trajLevel option in Openair considers the number of trajectories (that is, trajectory frequency) in a particular grid square (Carslaw, 2015).

Flight details and measurements

Three AMMA flights flew very near the flaring region in Nigeria and were suggested by trajectory analysis to have been impacted by gas flaring emissions from the Niger Delta area. Details of these flights are given in Table 1. The flight tracks are plotted on Google Earth (Figure 1a to c). Flight tracks data are obtained from the British Atmospheric Data Centre dataset (http://browse.ceda.ac.uk/browse/badc/ faam/data/2006). Active flare sites data shown in Figure 1d are obtained from the KML file in the supplementary data of Elvidge et al. (2015).

The FAAM BAe-146 flights involved in this analysis are flights B222, B228 and B231 which took place on July 30, August 8 and 13, 2006, respectively. To have an estimate of the extent of the contributions of the different regions to air parcel sampled, trajectory densities of the air parcels sampled on these flights were generated (Figure 2a to c). While flights B228 and B231 encountered plumes from the gas flaring region in the Niger Delta and urban plume from Lagos, plumes sampled on B222 were significantly impacted by urban emissions from Lagos but not from the Niger Delta. During AMMA flight campaigns, pollutants measured on several of the scientific flights were attributed to both biomass burning and urban-industrial emissions (Reeves et al., 2010). In the lower and mid-troposphere, at that time of the year (July to August), biomass burning aerosols are mainly due to long-range transport from central and south Africa into the West Africa sub-region; while inland flow and convective uplift of urban-industrial aerosol are substantially enhanced by the positions of the ITCZ and enhanced MCS, respectively.

Observations used in this analysis are mixing ratios of ozone (O_3), carbon monoxide (CO), NO_X (NO + NO_2) from the core chemistry payload, and VOCs (alkanes) from the non-core payload (Hopkins et al., 2009; Mari et al., 2011; Reeves et al., 2010). O_3, CO and NO_X were measured using TECO 49 UV photometer, TECO 42 chemiluminescence instrument and Aerolaser AL5002, respectively. The VOCs were collected in canister and then analysed by dual channel PTV-GC-FID (Programmed Temperature Vapourization - Gas Chromatography - Flame Ionization Detector), a technique used in the analysis of VOCs in the atmosphere, where their mixing ratios could be less than 1 pptv (McQuaid et al., 1998). On most of the AMMA flights, time scale of VOCs measurements ranges between 30 and 90 s.

RESULTS AND DISCUSSION

From the trajectory-density plots of flights B228b and B231b trajectories, more than 25% of the air parcels sampled on-board both flights had been impacted by anthropogenic emissions from Lagos (green boxes in Figure 2) and the oil fields in the Niger Delta area (black boxes in Figure 2). The trajectory-density plot of B222 shows that more than 25% of the air parcel sampled on this flight had been impacted by anthropogenic urban emissions from Lagos while less than 1% had been impacted by emissions from the oil fields in the Niger Delta. Figure 2 shows the trajectory-density plots for the (b) portions of the three flights considered in this study. The (b) portions of the flights have been considered because those were the portions of the flights that came within proximity of emissions from either Lagos or the Niger Delta region.

Using the trajectory density plots, the extent of the contributions of different region to aerosol loadings in air parcels sampled can be quantified. The (b) portions of the selected flights were chosen because at some time during the flight air parcels sampled during these

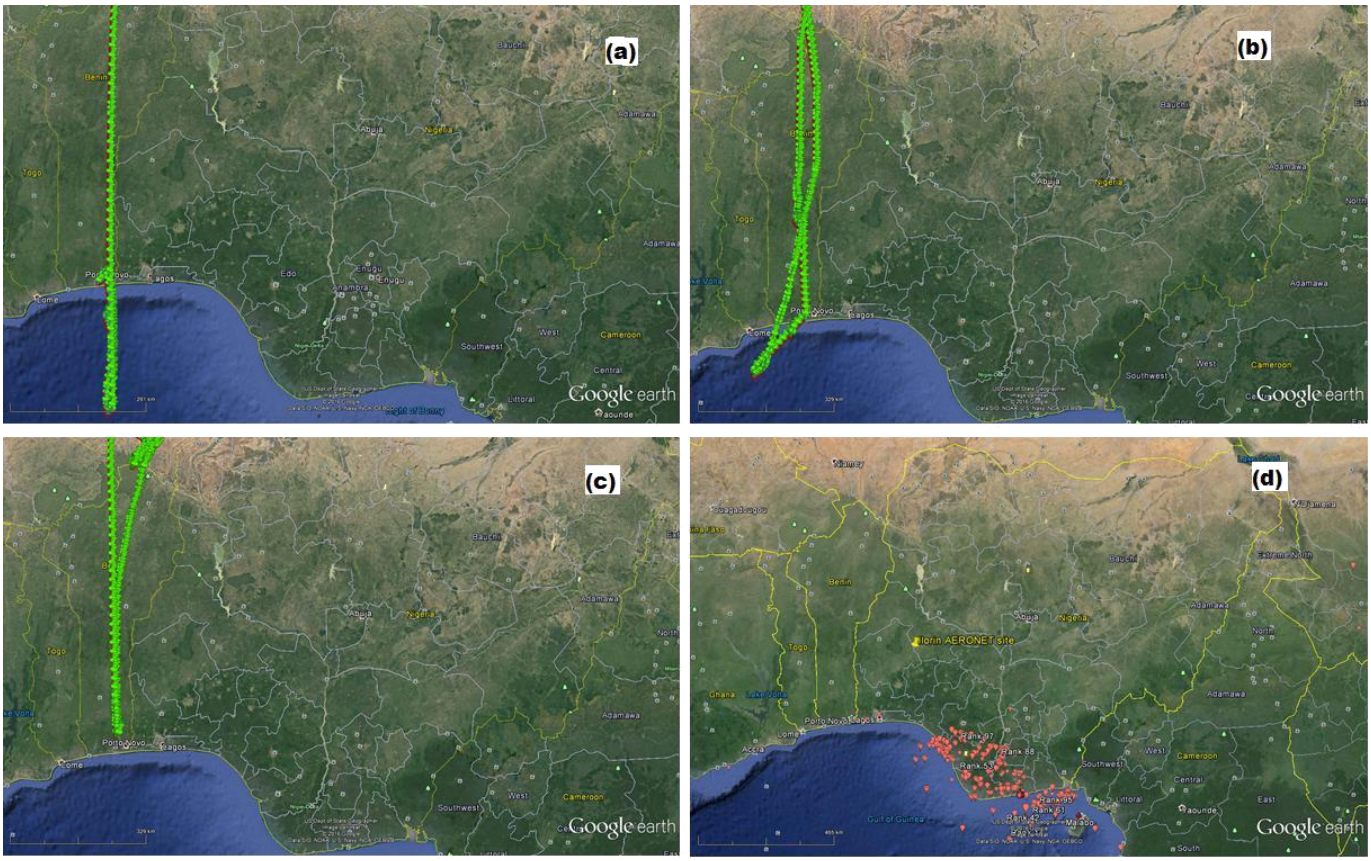

Figure 1. Flight track for (a) B228 (b) B231 (c) B222 and (d) active flare sites in the Niger Delta.

stretches of the flight were suggested by trajectory analysis to have been impacted by emissions from the oil fields in Niger Delta and urban emissions from Lagos. Elevated concentrations of carbon monoxide, ozone and alkane were observed during these portions of the flights. Plots of the 7-day back trajectory of entire air parcels sampled on the three selected AMMA flights are shown in Figure 3.

Case study I: Flight B228

Flight B228 took place on August 8, 2006 during the SOP 2 phase of the AMMA campaign in West Africa. The flight was from Niamey (Niger) to Cotonou (Benin), and then to Lagos to map emissions around the city. Figure 4 presents the plots of the mixing ratio of alkanes, carbon monoxide (CO), ozone, NO_X against flight time, and 7-day back trajectory at flight times with elevated measurements of these pollutants.

Here attempts are made to demonstrate that strongly elevated levels of NO_X, CO and O_3 (> 90 ppbv) were observed simultaneously in air parcels that have been impacted by both gas flaring emissions and urban aerosols in Lagos. For multiyear (1997-2003) analysis from the MOZAIC programme, the range of ozone observed within the planetary boundary layer (PBL) during August around Lagos is in the range of 30 to 70 ppbv (Sauvage et al., 2005).

Figure 4(b) shows the back trajectory plot for flight time between 43600 to 44700 s, a period of elevated ozone, NO_X and CO measurements shown in Figure 4a. As shown in Figure 4c, higher mixing ratios of NMHCs were also measured during this portion of the flight. These elevated measurements of ozone, CO and NO_X were observed around an altitude of 1.5 to 3 km (Figure 5a), which corresponds to the 700 to 800 hPa shown in the colour-coded pressure in the back trajectory plot in Figure 4b.

Of all BAe-146 flights during the AMMA flight campaign, concentration of ozone in excess of 90 ppbv was measured on B228 and B231 only. These are the only flights that measured air parcels that were suggested to have been significantly impacted by gas flaring emission from the Nigeria oil field, as shown in the trajectory density plot in Figure 2. With combustion

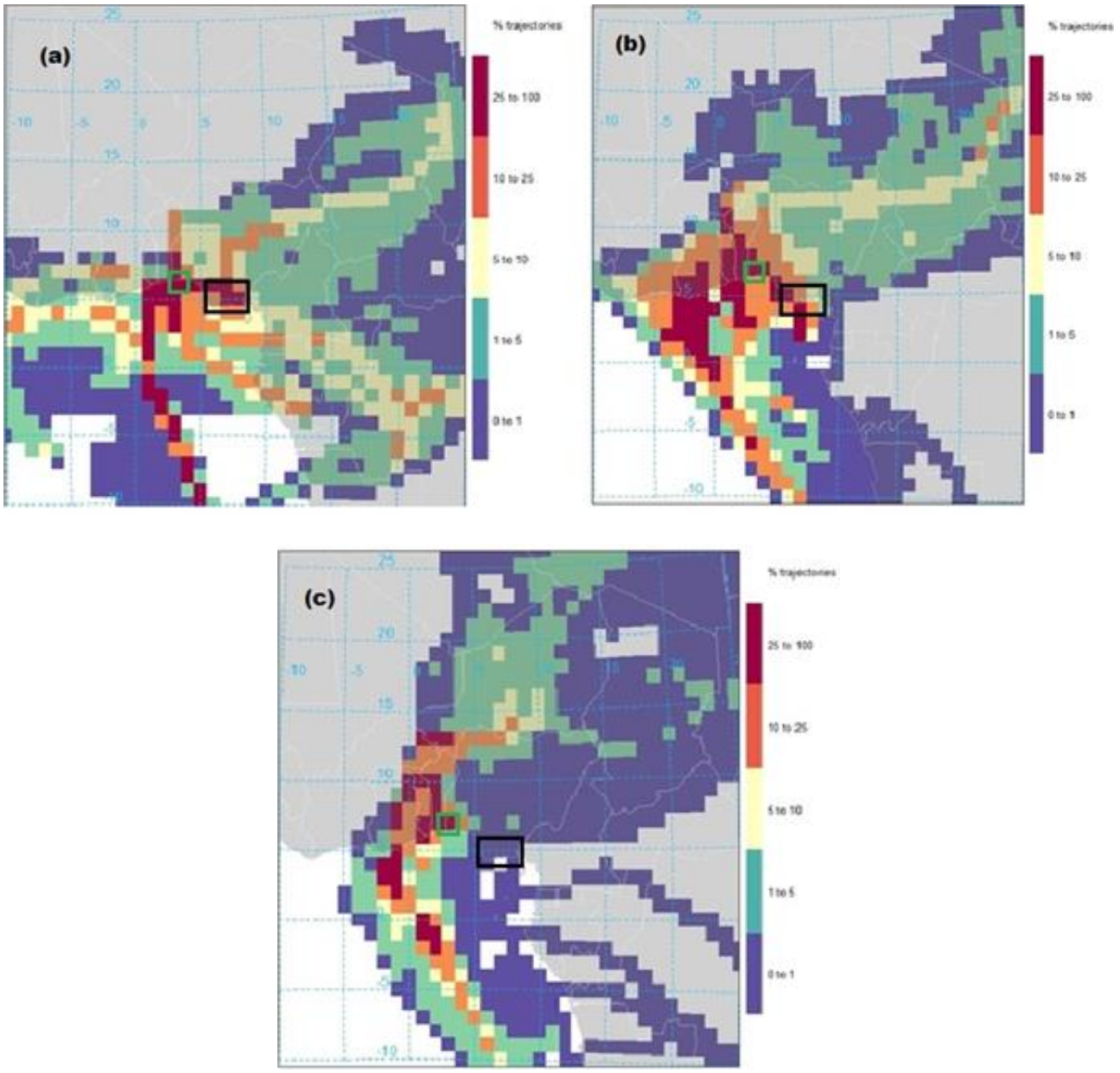

Figure 2. Trajectory-density plot for AMMA flights (a) B228b (b) B231b and (c) B222b. The black and green boxes show the region of intense gas flaring and the city of Lagos (Nigeria), respectively. The colour code shows the range of number of trajectories in each of the 1° × 1° gridded boxes.

temperature often >1900 K and fuel-rich combustion conditions, gas flaring is a significant source of atmospheric NO_X by both thermal NO_X and prompt NO_X processes (Fawole et al., 2016). Carbon monoxide (CO) and NMHCs are also common emissions from gas flaring, and their emission rates increase steadily with decreasing completeness of combustion process of the fuel gas. It should, however, be noted that while CO, O_3 and NO_X are measured every second, NMHCs measurements are averaged between 30 and 90 s.

During flight times between 43600 and 44700 s, there was significant enhancement of CO to up to 300 ppbv in the layer between 2 and 3 km; with accompanying enhanced NMHC measurements. The green vertical lines in Figures 4a and 4c shows the range of times within which elevated measurements of ozone, CO and NO_X were observed and the corresponding time-step for alkane species measurements on flight B228. Figure 4c

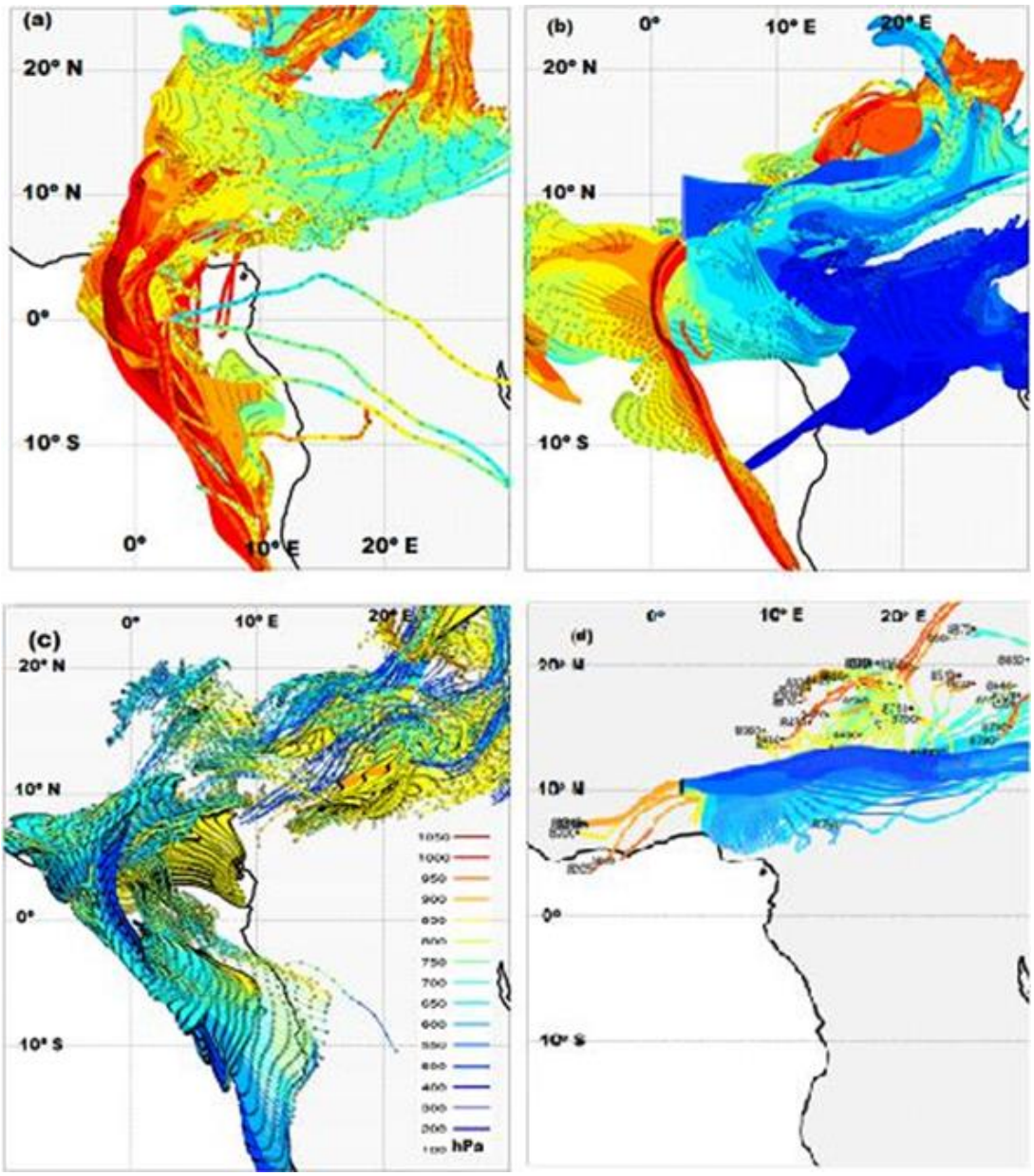

Figure 3. Trajectory plot for the entire duration of flights (a) B222b (b) B228b (c) B231b, and (d) back-trajectory plot for time of flight between 38200 and 39000 seconds on B231.

shows the time series plot of ethane, butanes, pentanes, and cycloalkanes with mixing ratio of over 250, 300 - 10000, 2000 and 300 - 2000 pptV, respectively. Such high mixing ratio of alkane species are indicative of natural gas sources, particularly from the oil and gas sector (Hopkins et al., 2009; Minga et al., 2010). These enhanced levels of CO and alkane together with elevated NO_X mixing ratio (> 2 ppbv) are suggested to be responsible for the elevated ozone level (120 ppbv) rather than long-range transport. Long-range transport of pollutants is not evident in the 7-day back trajectory plot shown in Figure 4b. Table 2 shows a summary of the statistics of the carbon monoxide (CO), ozone (O_3) and alkane species measured on-board flight B228.

Case study II: Flight B231

Flight B231 flew from Niamey to Cotonou and over the ocean around the Gulf of Guinea on August 13, 2006.

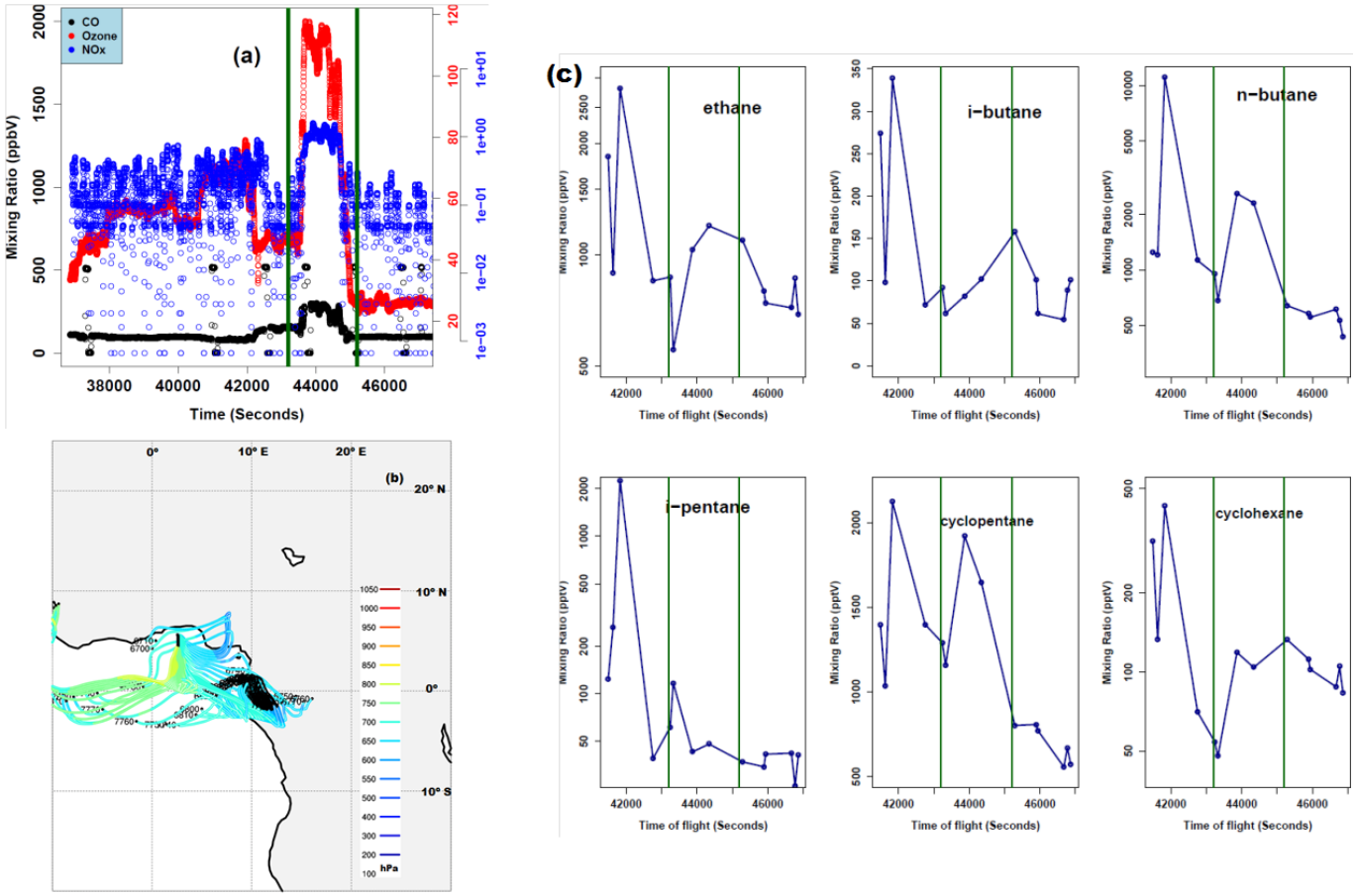

Figure 4. For flight B228b: (a) mixing ratio of CO, NO_X and O_3 against flight time; (b) back trajectory plot of time with elevated CO and O_3 in time step of 10 s; (c) mixing ratio of alkane species against flight time.

Table 2. Statistics of alkane species measured on flight B228.

Alkane species	Mean	Min	Max	Median
CO (ppbv)	127.2	0.043*	1999.9	98.4
Ozone (ppbv)	44.1	9.5	117.8	43.8
ethane (pptv)	1068.3	553.1	2817.5	865.8
i-butane (pptv)	120.3	54.3	338.9	94.8
n-butane (pptv)	1757.0	429.9	11143.6	813.6
i-pentane (pptv)	226.5	26.0	2252.1	42.6
cyclopentane (pptv)	1152.5	556.1	2123.1	1093.9
cyclohexane (pptv)	135	47.8	429.4	104.5

*Very low value might be due to equipment failure.

The 'b' portion of the flight (B231b) came within proximity of Nigeria and the air parcel sampled on-board was suggested to have been impacted by emissions from the gas flaring region in the Niger Delta and Lagos, Nigeria (Figure 2b). The back trajectory plots in Figures 7a and b are for flight times 31000 - 32000 and 34500 - 36000 s, respectively. These times correspond to the periods of elevated CO and ozone measurements; there was also a corresponding increase in NO_X measurements at these periods. Although, fewer and 20 to 30 s averages,

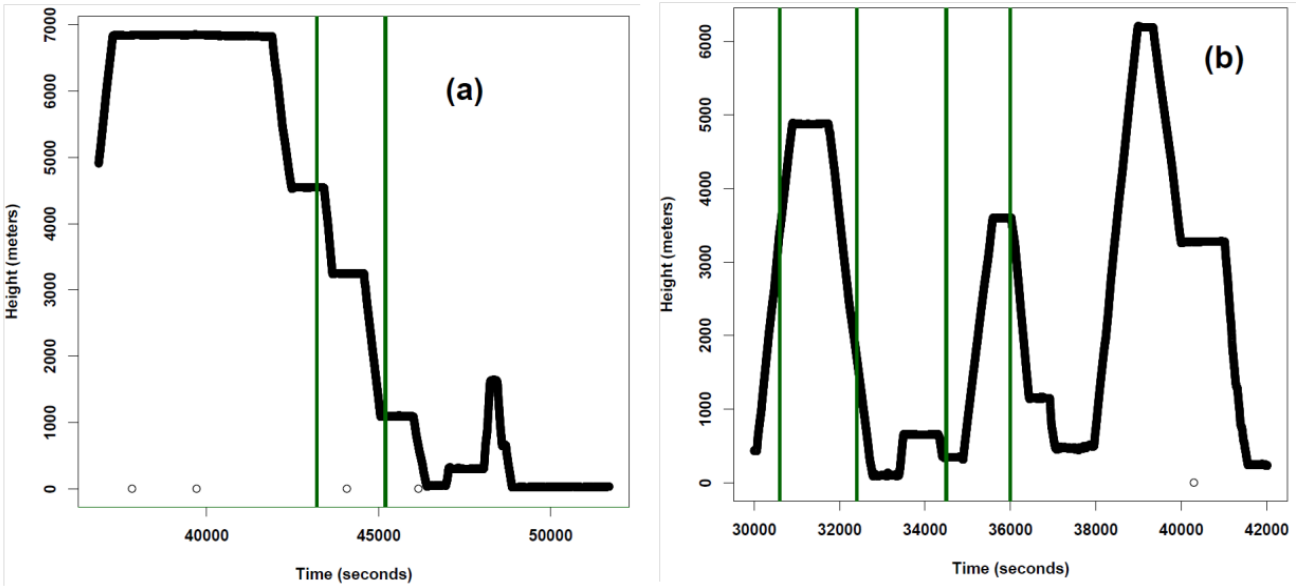

Figure 5. Variation of flight height with flight time for (a) B228b, and (b) B231b; vertical green lines show region of flight when elevated VOCs were sampled.

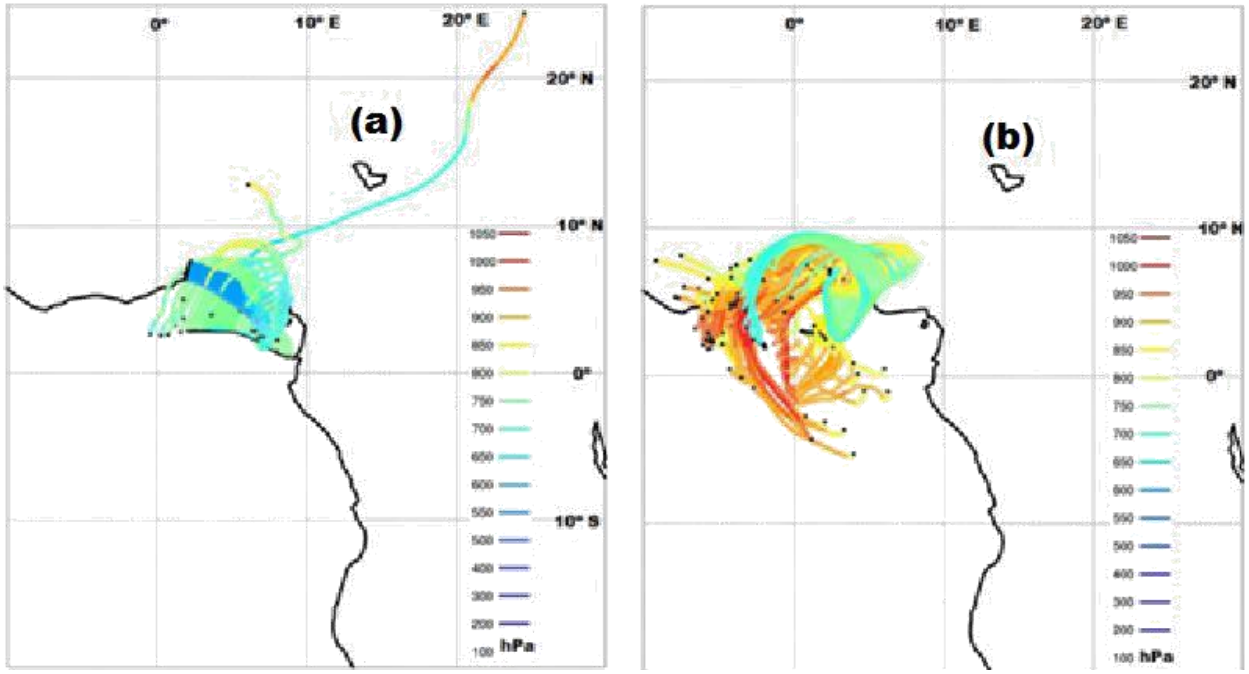

Figure 6. For flight B231b: (a) back trajectory plot of flight time 31000 to 32000 in time step of 10 s, and (b) back trajectory plot of flight time 34500 to 36000 in time step of 10 s.

NMHCs measurements shows significantly similar trends at these periods of elevated CO, ozone and NO_X measurements (Figure 6b). Heights at which air plumes from the intense gas flaring region were encountered during flight times 31000-32000 and 34500- 36000 s are between 3- 3.5 and 2-3 km, respectively. These heights correspond to that shown in the colour coded atmospheric pressures, in Figures 6a and b, 650- 800 and 750-850 hPa, respectively. These times, that is, 31000 - 32000 and 34500 - 36000 s, were on the to - and

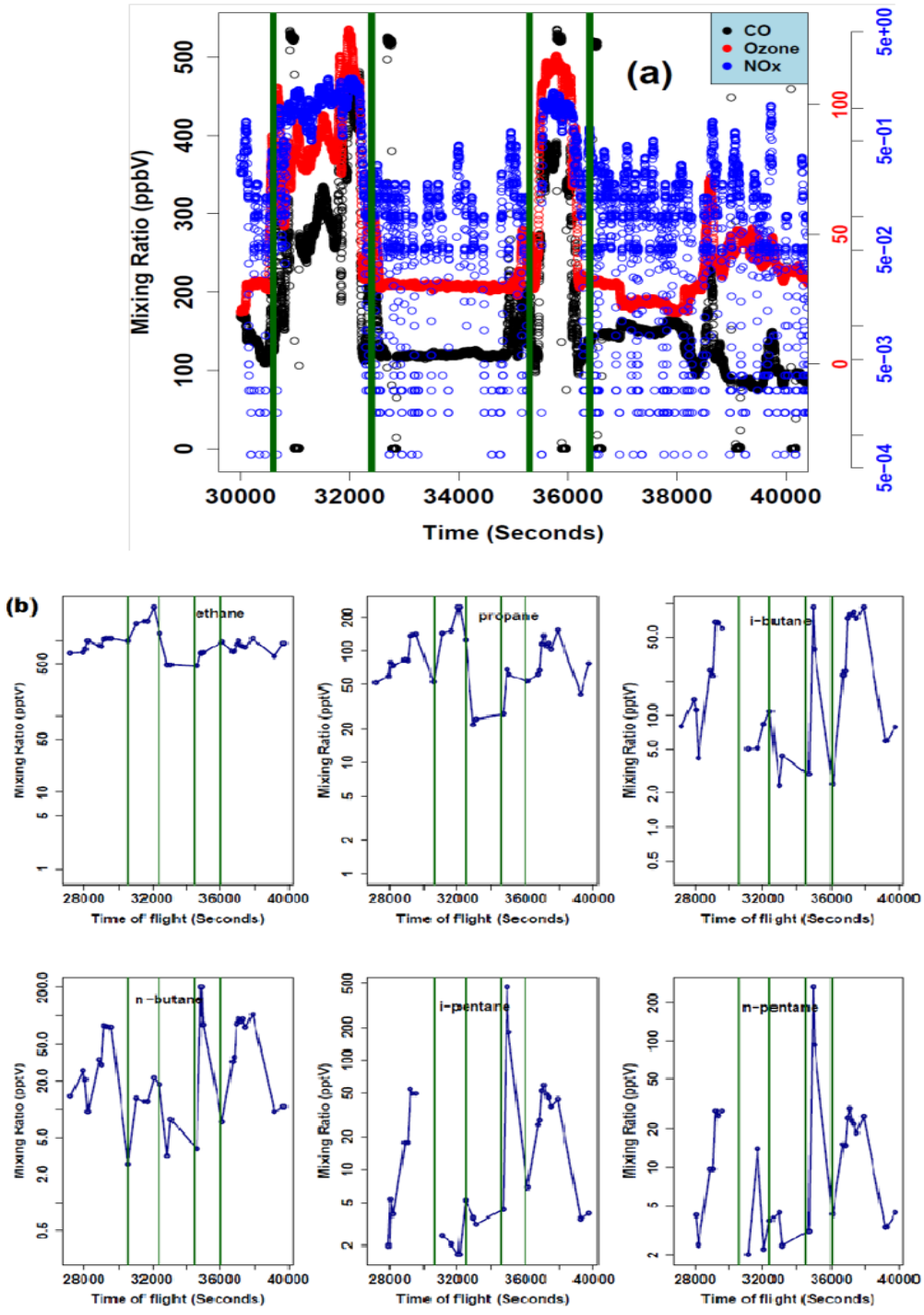

Figure 7. For flight B231b: (a) plot of mixing ratio of CO, NO_x and O_3 against flight time, and (b) mixing ratio of alkane species against measurement time.

fro - laps of the flight over the ocean around the Gulf of Guinea (Figure 1b).

The periods of strong enhancement of CO and NO_X occurred during flights times 31000-32000 and 34500-36000 s. During these enhancement periods of mixing ratios, CO mixing ratio was up to 480 and 440 ppbv, respectively while ozone was up to ~128 and 118 ppbv, respectively. These periods equally exhibited elevated NO_X mixing ratio up to ~2.5 ppbv. As shown in Figure 7b, mixing ratio for alkanes - ethane, propane, butanes and

Table 3. Statistics of alkane species measured on flight B231.

Alkane species	Mean	Min	Max	Median
CO (ppbv)	163.6	0.043*	535.1	123.1
Ozone (ppbv)	44.0	0*	128.9	31.7
ethane (pptv)	961.2	467.2	2758.1	859.3
propane (pptv)	94.2	22.0	248.2	81.1
i-butane (pptv)	33.3	0*	92.8	18.3
n-butane (pptv)	45.2	2.6	200.2	27.7
i-pentane (pptv)	40.5	0*	459.3	12.2
n-pentane (pptv)	22.7	0*	264.3	9.6

*value might be due to equipment failure.

Table 4. Statistics of alkane species measured on flight B222.

Parameter	Mean	Min	Max	Median
CO (ppbv)	118.1	0.043*	528.0	125.3
Ozone (ppbv)	27.0	0*	61.4	28.1
Ethane (pptv)	123.6	13.9	346.0	86.3
Propane (pptv)	27.1	3.1	91.6	22.6
n-Butane (pptv)	214.9	55.1	346.3	206.2
i-Pentane (pptv)	6.2	0*	21.1	5.0
n-Pentane (pptv)	7.7	3.9	19.8	6.4
Cyclopentane (pptv)	4.5	0*	7.2	4.5
Cyclohexane (pptv)	3.2	0.72	4.32	3.3

*Value might be due to equipment failure.

pentanes were also enhanced during these periods. The green vertical lines in Figures 7a and b shows the range of times within which elevated measurements of ozone, CO and NO_X were observed and the corresponding time-step for alkane species measurements on flight B231. Minga et al. (2010) suggested, from their simulation, that the only way to reach excessively high ozone concentration within few hours in their model was to increase amount of reactive VOCs to levels recorded around petrochemical facility. In their study to estimate emissions from Lagos (Hopkins et al., 2009) concluded that the substantial downwind enhancement of ethane is attributable to fugitive natural gas leakage. The enhanced CO measured simultaneously is indicative of a combustion source rather than a leak, which in this study, has been suggested to be gas flaring sources in the Niger Delta. Owing to the unique and significantly varying nature of gas flaring emissions, ratios of emissions often used as tracers for fossil fuel combustion could not be directly applied to emissions analysed in this study. Hence, a case is made for further studies to adequately characterise emissions from gas flares in the oil and gas sector, especially for VOCs.

Slight enhancement of ozone to up to 75 ppbv was measured around flight time between 38570 and 38700 seconds at a height of ~5 - 6 km. This was accompanied by a similar enhancement of CO up to ~220 ppbv, but there was no substantial enhancement in the levels of alkanes measured. This could be attributed to long range transport of biomass burning plume from the East, around Sudan (Figure 3d). Table 3 presents the statistics summary of CO, O_3 and alkane measured on flight B231.

Case study III: Flight B222

AMMA flight B222 flew around Benin on July 30, 2006 carrying out the mapping of biogenic emissions. As shown in the trajectory density plot in Figure 2c and Figure 3c, < 1 % of the air mass sampled on the flight is suggested to have been impacted by gas flaring emissions while >25% were impacted by anthropogenic emissions from Lagos. There is no significant enhancement in the mixing ratio of CO which was around 200 ppbv throughout the duration of the flight except for very few spikes (Figure 8a). Mixing ratios of ozone and NMHCs are also relatively low (Figure 8b and Table 4) in contrast to the other two flights that sampled air parcels

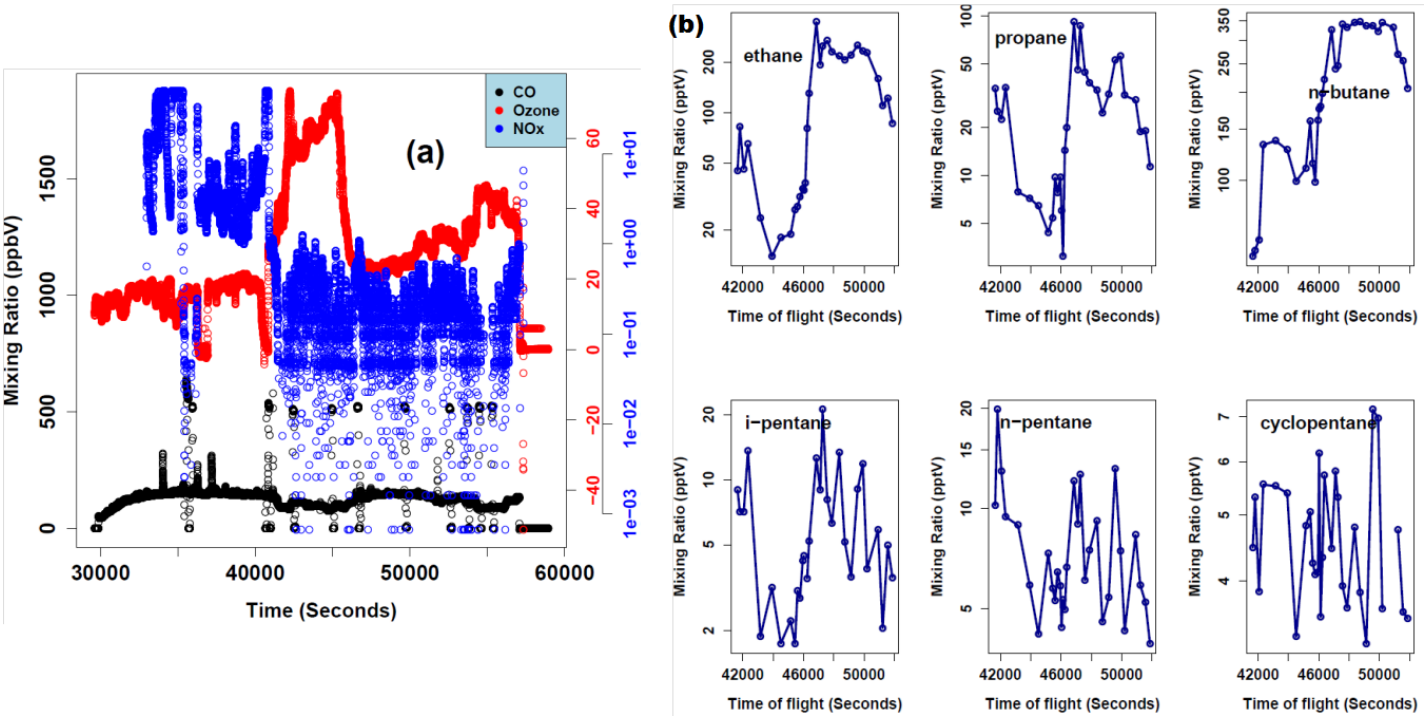

Figure 8. For flight B222: (a) plot of CO, NO_X and O_3 mixing ratios against flight time (b) mixing ratio of alkane species against measurement time.

that were suggested to have been impacted by emissions from both the region of intense gas flaring and Lagos, Nigeria. Table 4 presents the statistics summary of CO, O_3 and alkane species measured on flight B222.

Conclusion

During AMMA SOP 2, on 30 July, 8 and 13 August 2006, FAAM BAe-146 carried out three scientific flights that sampled air parcels around Benin and the ocean around the Gulf of Guinea during sections of the flights durations. Portions of the air parcel sampled were suggested to have been significantly impacted by anthropogenic emissions from the gas flaring activities in the Niger Delta region and the city of Lagos. These flights sampled air parcels within the lower and mid-troposphere. On flights B228 and B231, there were portions of the flight with strongly enhanced mixing ratios of carbon monoxide (CO) and ozone. These enhancements were attributed to emissions from the region of intense gas flaring in the Niger Delta and Lagos, Nigeria because of the highly enhanced levels of short-chained alkane species and histories of air parcel sampled which is obtained from the back trajectory analysis. At a height of about 6 km, slight enhanced mixing ratios of CO and ozone observed is attributable to long-range transport of pollutants. Air parcels sampled on flight B222 was suggested to be strongly impacted by emissions from Lagos but almost insignificantly by emissions from the Niger Delta, hence, the relatively low mixing ratios of CO, ozone and short-chained alkanes. Analysis of short-chained alkanes species and cycloalkanes are limited by the number and cycles of NMHCs measurements on these flights. With our understanding of the extent of contributions of gas flaring in this region to levels of ambient pollutants coupled with limited and insufficient data to characterise emission from this source (gas flaring), we make a strong case for the need for further in-depth studies to understand the emissions, atmospheric transport and behaviour of emissions from this unique stationary source of aerosol pollutant under the impact of the peculiar climatic conditions of the West Africa region.

CONFLICT OF INTERESTS

The authors have not declared any conflict of interests.

ACKNOWLEDGEMENT

The authors acknowledge Kevin Keay of the University of Melbourne for the support he offered with kmapline and

Openair and the anonymous reviewers for their helpful criticisms and comments. Olusegun G. Fawole is highly grateful to the UK government for funding his PhD studies through the UK Commonwealth Scholarships Commission (CSCUK) NGCA-2013-70.

REFERENCES

Anejionu OC, Blackburn GA, Whyatt JD (2015a). Detecting gas flares and estimating flaring volumes at individual flow stations using MODIS data. Remote Sens. Environ.158:81-94.

Anejionu OC, Whyatt JD, Blackburn GA, Price CS (2015b). Contributions of gas flaring to a global air pollution hotspot: Spatial and temporal variations, impacts and alleviation. Atmos. Environ. 118:184-193.

Carslaw D (2015). The openair manual–open-source tools for analysing air pollution data. Manual for version 1.1-4, King's College, London.

Carslaw DC, Ropkins K (2012). Openair—an R package for air quality data analysis. Environ. Model. Softw. 27:52-61.

De Gouw J, Cooper O, Warneke C, Hudson P, Fehsenfeld F, Holloway J, Hübler G, Nicks D, Nowak J, Parrish D (2004). Chemical composition of air masses transported from Asia to the US West Coast during ITCT 2K2: Fossil fuel combustion versus biomass-burning signatures. J. Geophys. Res. Atmos. 109(D23).

Elvidge CD, Zhizhin M, Baugh K, Hsu FC, Ghosh T (2015). Methods for Global Survey of Natural Gas Flaring from Visible Infrared Imaging Radiometer Suite Data. Energies, 9(1):14.

Fawole O, Cai XM, MacKenzie A (2016). Gas flaring and resultant air pollution: A review focusing on Black Carbon. Environ. Pollut. 216:182-197.

Gilman J, Lerner B, Kuster W, De Gouw J (2013). Source signature of volatile organic compounds from oil and natural gas operations in northeastern Colorado. Environ. Sci.Technol. 47(3):1297-1305.

Hopkins JR, Evans MJ, Lee JD, Lewis AC, Marsham JH, McQuaid J, Parker DJ, Stewart DJ, Reeves CE, Purvis RM (2009). Direct estimates of emissions from the megacity of Lagos. Atmos. Chem. Phys. 9(21):8471-8477.

Ite AE, Ibok UJ (2013). Gas Flaring and Venting Associated with Petroleum Exploration and Production in the Nigeria's Niger Delta. Am. J. Environ. Protect. 1(4):70-77.

Janicot S, Thorncroft CD, Ali A, Asencio N, Berry GJ, Bock O, Bourles B, Caniaux G, Chauvin F, Deme A (2008). Large-scale overview of the summer monsoon over West Africa during the AMMA field experiment in 2006, Ann. Geophys. pp. 2569-2595.

Johnson MR, Coderre AR (2012). Compositions and greenhouse gas emission factors of flared and vented gas in the Western Canadian Sedimentary Basin. J. Air Waste Manag. Assoc. 62(9):992-1002.

Lebel T, Parker DJ, Flamant C, Bourlès B, Marticoréna B, Mougin E, Peugeot C, Diedhiou A, Haywood J, Ngamini JB (2010). The AMMA field campaigns: multiscale and multidisciplinary observations in the West African region. Quart. J. Royal Meteorol. Soc. 136(S1):8-33.

Liu Y, Shao M, Fu L, Lu S, Zeng L, Tang D (2008). Source profiles of volatile organic compounds (VOCs) measured in China: Part I. Atmos. Environ. 42(25):6247-6260.

Mari CH, Reeves CE, Law KS, Ancellet G, Andrés-Hernández MD, Barret B, Bechara J, Borbon A, Bouarar I, Cairo F (2011). Atmospheric composition of West Africa: highlights from the AMMA international program. Atmos. Sci. Lett. 12(1):13-18.

McQuaid JB, Lewis AC, Bartle KD, Walton SJ (1998). Sub-ppt atmospheric measurements using PTV-GC-FID and real-time digital signal processing. J. High Resolut. Chromatogr. 21(3):181-184.

Methven J (1997). Offline trajectories: Calculation and accuracy. UGAMP.

Methven J, Evans M, Simmonds P, Spain G (2001). Estimating relationships between air mass origin and chemical composition. J. Geophys. Res. Atmos. 106(D5):5005-5019.

Minga A, Thouret V, Saunois M, Delon C, Serça D, Mari C, Sauvage B, Mariscal A, Leriche M, Cros B (2010). What caused extreme ozone concentrations over Cotonou in December 2005? Atmos. Chem. Phys. 10(3):895-907.

Noone D, Simmonds I (1999). A three-dimensional spherical trajectory algorithm. In: H. Ritchie (Editor), Research Activities in Atmospheric and Oceanic Modelling, Report No. 28, WMO/TD-No. 942. World meteorological Organization, Geneva, pp. 26-27.

OPEC (2015). OPEC annual statistical bulletin, Organisation of Petroleum Exporting Countries, Austria.

Osuji LC, Onojake CM (2004). Trace Heavy Metals Associated with Crude Oil: A Case Study of Ebocha-8 Oil-Spill-Polluted Site in Niger Delta, Nigeria. Chem. Biodivers. 1(11):1708-1715.

Redelsperger JL, Thorncroft CD, Diedhiou A, Lebel T, Parker DJ, Polcher J (2006). African Monsoon Multidisciplinary Analysis: An international research project and field campaign. Bull. Am. Meteorol. Soc. 87(12):1739-1746.

Reeves C, Formenti P, Afif C, Ancellet G, Attié JL, Bechara J, Borbon A, Cairo F, Coe H, Crumeyrolle S (2010). Chemical and aerosol characterisation of the troposphere over West Africa during the monsoon period as part of AMMA. Atmos. Chem. Phys. 10(16):7575-7601.

Sanchez M, Karnae S, John K (2008). Source characterization of volatile organic compounds affecting the air quality in a coastal urban area of South Texas. Int. J. Environ. Res. Public Health 5(3):130-138.

Sauvage B, Thouret V, Cammas JP, Gheusi F, Athier G, Nédélec P (2005). Tropospheric ozone over Equatorial Africa: regional aspects from the MOZAIC data. Atmos. Chem. Phys. 5(2):335.

Seila RL, Lonneman WA, Meeks SA (1989). Determination of C2 to C12 ambient air hydrocarbons in 39 US cities from 1984 through 1986, Computer Sciences Corp., Research Triangle Park, NC (USA).

Seinfeld JH, Pandis SN (2016). Atmospheric chemistry and physics: from air pollution to climate change. John Wiley & Sons.

Sultan B, Janicot S (2003). The West African monsoon dynamics. Part II: The “preonset” and “onset” of the summer monsoon. J. Clim. 16(21):3407-3427.

USEPA (2012). Report to congress on Black Carbon. EPA-450/R-12-001, United States Environmental Protection Agency, Research Triangle Park, NC.

Weyant CL, Shepson PB, Subramanian R, Cambaliza MO, Heimburger A, McCabe D, Baum E, Stirm BH, Bond TC (2016). Black carbon emissions from associated natural gas flaring. Environ. Sci. Technol. 50(4):2075-2081.

WMO (2015). The climate in Africa: 2013, World Meteorological Organization, Switzerland (WMO-No. 1147).

academicJournals

Vol. 11(10), pp. 544-555, October 2017
DOI: 10.5897/AJEST2015.2069
Article Number: 9DD957366057
ISSN 1996-0786

http://www.academicjournals.org/AJEST

African Journal of Environmental Science and Technology

Full Length Research Paper

Increased streamflow dynamics and implications for flooding in the Lower River Benue Basin

Roland Clement Abah[1,3]* and Brilliant Mareme Petja[2,3]

[1]National Agency for the Control of AIDS, Central Area, Abuja, Nigeria.
[2]Water Research Commission (WRC), Rietfontein Pretoria, South Africa.
[3]University of South Africa, Pretoria, South Africa.

Received 31 December, 2015; Accepted 29 March, 2016

The paper dealt with increased streamflow dynamics and implications for flooding in the Lower River Benue Basin. The study utilised data collected over a period of more than fifty years (1955-2012) from three hydrological stations operated by the Nigerian Hydrological Services Agency (NIHSA). The average discharge at Umaisha was 4,919.47 cubic metres per second (m^3/s). Average discharge at Makurdi hydrological station was 3,468.24 m^3/s. The monthly average discharge for Katsina Ala did not record any amount over 2000 m^3/s in any month of year from 1955-2012. The rating curves for Umaisha and Makurdi showed a smooth streamflow with Umaisha surpassing the average discharge at 661 cm. Makurdi surpassed the average streamflow of the station at 654 cm. River Katsina Ala rating curve showed a rough streamflow. The trend of discharge rate for the three hydrological stations showed a rise over the years assessed and staggering discharge rates were recorded during peak periods in some years. Evidence provided show increasing streamflow variability and flood risk due to rainfall intensity and release of excess dam water from Lagdo dam in Cameroun. In order to prevent and control flood damage, useful recommendations have been proffered.

Key words: Discharge rate, water resources management, streamflow monitoring, river basin, flooding, River Benue Basin.

INTRODUCTION

It is important to assess drainage systems to embark on effective water management which has become quite significant in the light of climate change evidence in literature. Understanding streamflow dynamics is important if related challenges such as droughts and floods are to be managed adequately. It has been stated in literature that streamflow monitoring received increased attention in the 1970s in Nigeria. However, many flow monitoring stations are faced with faulty equipment while some have been abandoned (Akpoborie et al., 2012).

Nigeria is endowed with numerous rivers and streams.

*Corresponding author. E-mail: rolann04@yahoo.com.

The biggest water bodies with vast flood plains are the rivers Niger and Benue. Most of the major floods which occur annually in Nigeria occur within the floodplains of the rivers Niger and Benue and their numerous tributaries. Despite the importance of streamflow dynamics in the major flood plains in Nigeria, the subject has received little attention in literature unlike other parts of the world (Akpoborie et al., 2012; Nwilo et al., 2012; Adelalu, 2012; Ehiorobo et al., 2013). It has therefore become essential to assess streamflow dynamics in river basins around the world including the Lower River Benue Basin in Nigeria given the risk of increased flooding globally due to global warming. This study therefore aims to assess the level of increased streamflow in the lower River Benue basin in order to further highlight the risk of flood increase.

METHODOLOGY

Study area

The area of study is located between Latitudes 7° 13'N and 8°00'N and Longitudes 8°00'E and 9°00'E within the Lower River Benue Basin. Most parts of the study area fall within the boundaries of Benue State. According to Ayoade (2004) and Climate-data (2015), the climate of Makurdi and Katsina Ala and Otukpo which are located within the Lower River Benue Basin are the tropical wet and dry type, according to Koppen's Aw classification, with double maxima. The rainy season usually lasts from April to October with an average annual rainfall of 1,332 mm (Makurdi), 1,547 mm (Katsina Ala), and 1496 mm (Otukpo).

The land is generally low lying (averaging 100 to 250 m) and a gently undulating landscape (Kogbe, 1989). The River Benue is the dominant geographical feature in the state. River Benue rises from the Adamawa Plateau of Central Cameroon, then flows west across Central Nigeria, and joins River Niger as the main drainage feature in the area. It is one of the few large rivers in Nigeria. The Katsina-Ala is the largest tributary of the River Benue, while smaller rivers include Mkomon, Amile, Kpa, Okpokwu, Duru, Loko Konshisha, Ombi Mu, Be, Apa Ogede and Aya. The flood plains of the River Benue are characterized by extensive swamps and ponds which have potential for dry season irrigated farming. Though Benue State has high drainage density, many of the streams are seasonal.

The largest water body in the Lower River Benue Basin is the River Benue which meets with the River Niger about 483 km from the coast at a confluence point in Lokoja, Kogi State. The width of the River Benue varies from about 488 to 976 m. It is navigable during the wet season from May to September for a length of more than 965 km (Uchua and Ndukwe, 2011). The River Benue is about 1,440km long with a surface area of 129,000 ha. The floodplain of the River Benue Basin is about 181,000 ha making it an important economic resource for the region (Ita et al*.,* 1985). Table 1 provides more information on the River Benue Basin while Figure 1 shows the location of the Lower River Benue Basin.

Many tribes inhabit the Lower River Benue Basin. These tribes include Tiv, Idoma, Etilo, Jukun, Egede, Hausa, Yoruba and Ibo with the Tivs being dominant. The main livelihood activity is subsistence agriculture. Other occupations include the civil service, commerce and manufacturing industries. Subsistence agriculture is practiced extensively at the periphery, including some open lands within major towns. Irrigation gardening, sand harvesting and burnt bricks production are carried out along the banks of the River Benue. Local fishing is another important economic activity on the River Benue. Makurdi town has a few medium scale industries such as a plastics factory and a fertilizer blending plant. It has an airport, a soft drink bottling company, a brewery, and fruit concentrate company. Commercial activities include the many markets and grain milling plants.

The physiography of the Lower River Benue Basin was determined from satellite imagery of the area using ArcGIS software. The survey provided a basis for identifying the sources of surface-water. The paper utilised data collected over a period of more than fifty years (1955-2012) from three hydrological stations (Umaisha, Makurdi, and Katsina Ala) operated by the Nigerian Hydrological Services Agency (NIHSA). The data for Umaisha hydrological station was from 1980 when the equipment was commissioned by NIHSA. Some years witnessed days of incomplete data due to faulty equipment. The River Benue discharge rate was analysed from hydrologic data. The hydrological parameters of particular interest were discharge rate and rating curve, water level, drainage networks, flood peaks, and damming potentials.

In order to present the contribution of rainfall to flood risk and increased streamflow dynamics, 40 years rainfall data on Makurdi from 1973 to 2013 was sourced from the Nigerian Metrological Agency Abuja and analysed for intensity, trends and variation. Analysis of data was carried out in Microsoft Excel and the Statistical Package for Social Sciences (Version 17). Flood risk simulation data was sourced from the annual flood outlook report in Nigeria which is prepared by NIHSA using Geospatial Stream Flow Model (GeoSFM) and Soil and Water Assessment Tool (SWAT) modelling software.

RESULTS AND DISCUSSION

Rainfall characteristics

The average daily rainfall for the period 1973-2013 was 133.8 mm with a median of 108.7 mm. The highest value for daily rainfall recorded was 149 mm on the 3rd of August 2000. The annual rainfall average recorded for the period 1973-2013 was 1194.1mm with a median of 1207.9 mm. The highest amount was recorded in 1999 (1617.1 mm). The year with the lowest amount of rainfall was 2003 (761.5 mm). The annual rainfall totals for Makurdi is presented in Figure 2.

The number of rainy days from 1973 to 2013 averaged 85.7 days. The annual rainy days from 1973 to 2013 is presented in Figure 3. The year with the highest number of rainy days was recorded in 1977 (159 days). The lowest number of rainy days was recorded in 1983 (56 days). The number of total annual rainy days is decreasing.

The relationship between total number of rainy days and annual rainfall totals is presented in Figure 4. Figure 4 shows that the year 1977 which had the highest number of rainy days had produced an annual rainfall total of 1387.1 mm. The year 1978 which had a total number of 156 rainy days produced an annual rainfall total of 1326.2 mm, and 56 rainy days in 1983 produced an annual total of 930.3 mm.

Even though the number of rainy days seems to be decreasing, the annual rainfall totals is not decreasing. There are several years in which less than a hundred days of rainfall produced annual rainfall totals over 1200

Table 1. Attributes of the River Benue Basin

Geographical attributes	Data
Source	Adamawa mountains, northern Cameroon
Total length	1,440 km
Catchment area	64,000 km^2
Water area	Bankfull (In Nigeria): 1,290 km^2; flooded: 3,100 km^2 (Floodplain: 1 810 km^2)
Major tributaries	Mayo-Kebbi (Cameroon), Faro, Gongola, and Katsina Ala (Nigeria)
Volume of Discharge at Mouth	1 920 m^3/s (mean max.) 32 m^3/s (mean min.)

Source: Food and Agriculture Organisation (FAO, 1990).

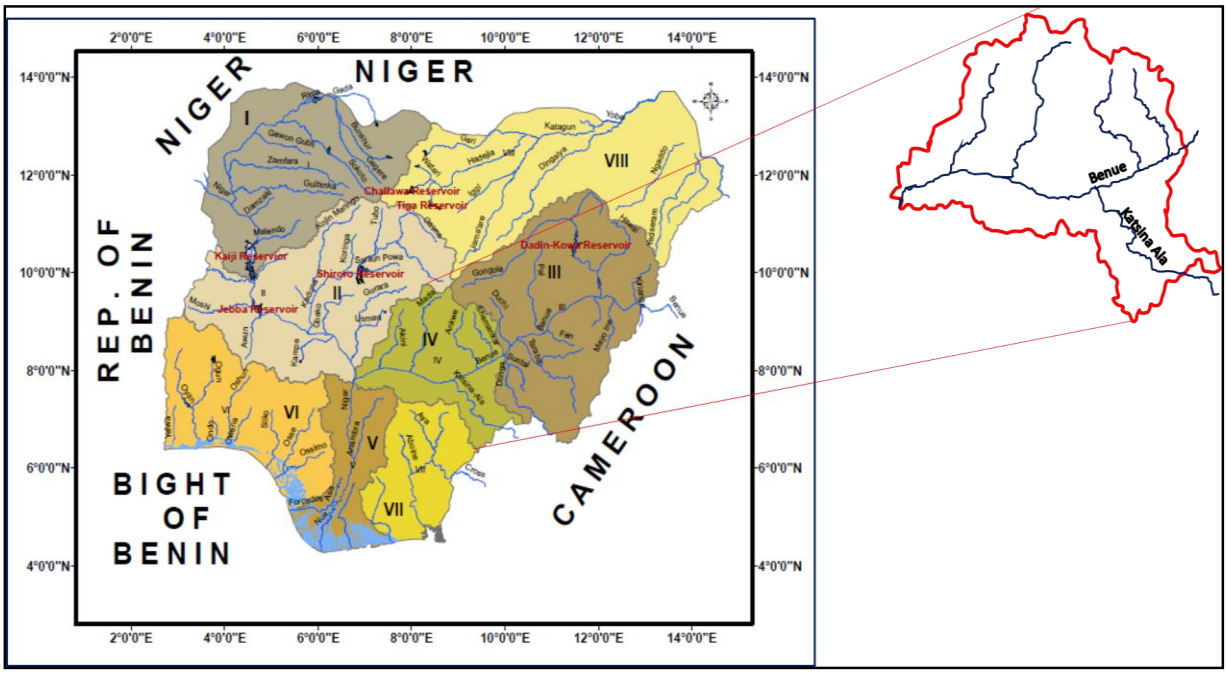

Figure 1. Location of the Lower River Benue Basin (NIHSA, 2014).

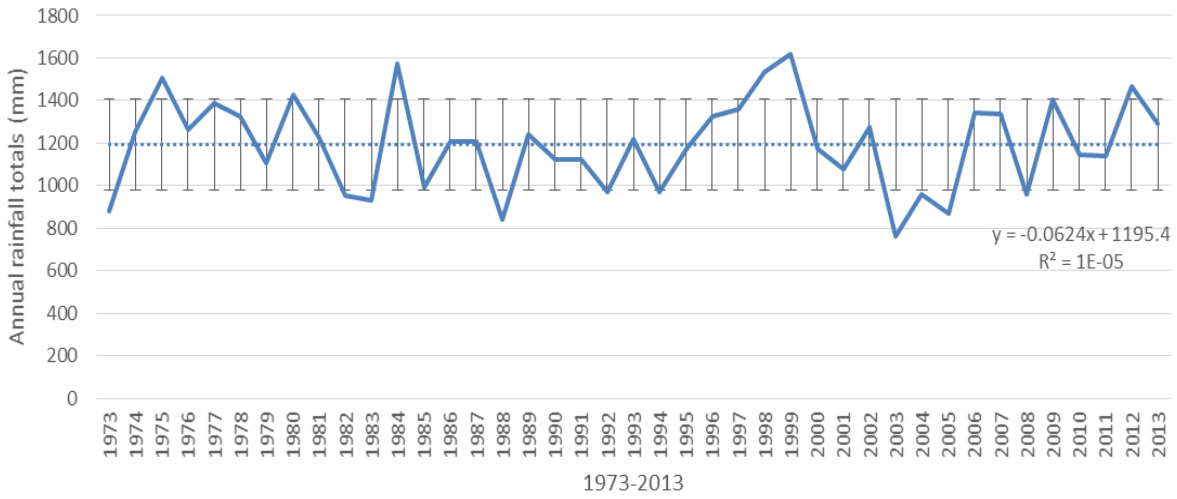

Figure 2. Annual rainfall averages for Makurdi (1973 - 2013).

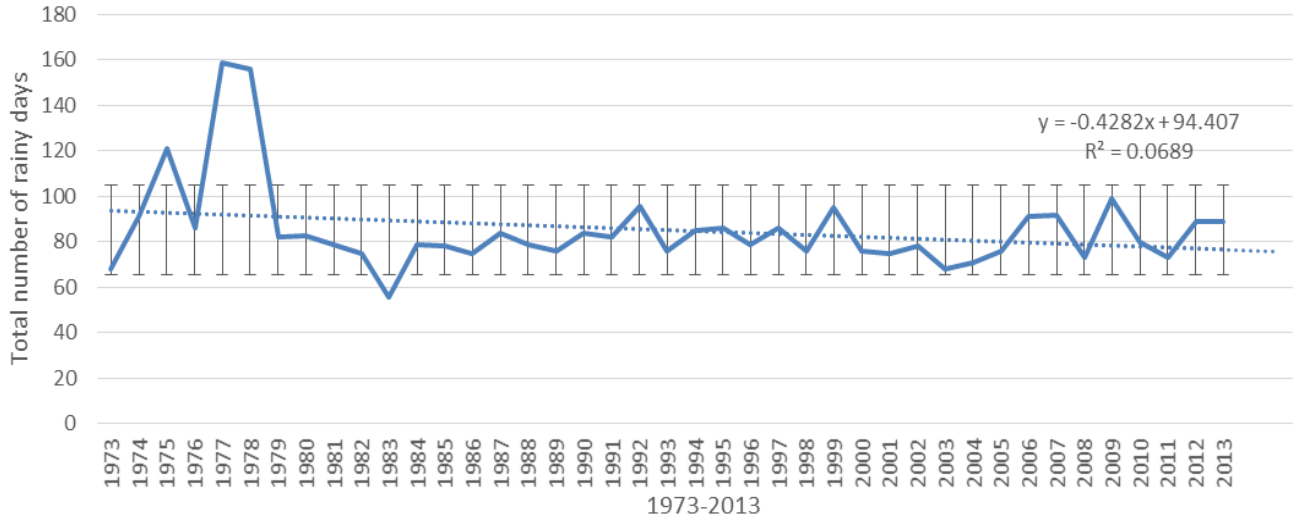

Figure 3. Total number of rainy days in Makurdi (1973 - 2013).

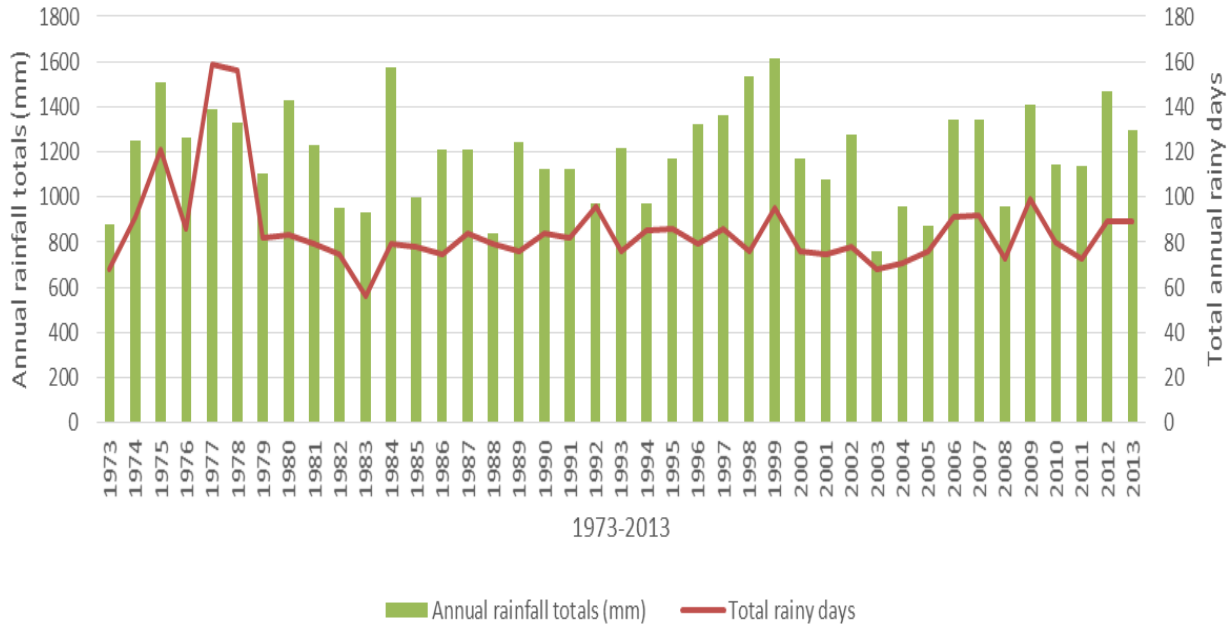

Figure 4. Annual rainfall totals and total number of rainy days in Makurdi (1973 - 2013).

mm which is above the annual average of 1194.1 mm from 1973 to 2013. The year 2012 which was most recently notable for rainfall intensity and severe flooding, recorded a total of 1407 mm of rain in 89 days.

Drainage discharge rate

The instantaneous daily discharge data (1955 to 2014) was collected from three hydrological stations in the Lower River Benue Basin that were readily available. The stations are Umaisha (1980-2014), Makurdi (1955-2014), and river Katsina Ala (1955-2012). The Umaisha hydrological station is located close to the confluence of the River Benue and River Niger, while the others are located in Makurdi and Katsina Ala L.G.As. Although the entire data collected was for the period of January 1955 to May 2014, a few omissions exist due to faulty measuring equipment and the more recently commissioned Umaisha hydrological station.

The average discharge at Umaisha from January 1980 to May 2014 was 4,919.47 m^3/s. The maximum discharge

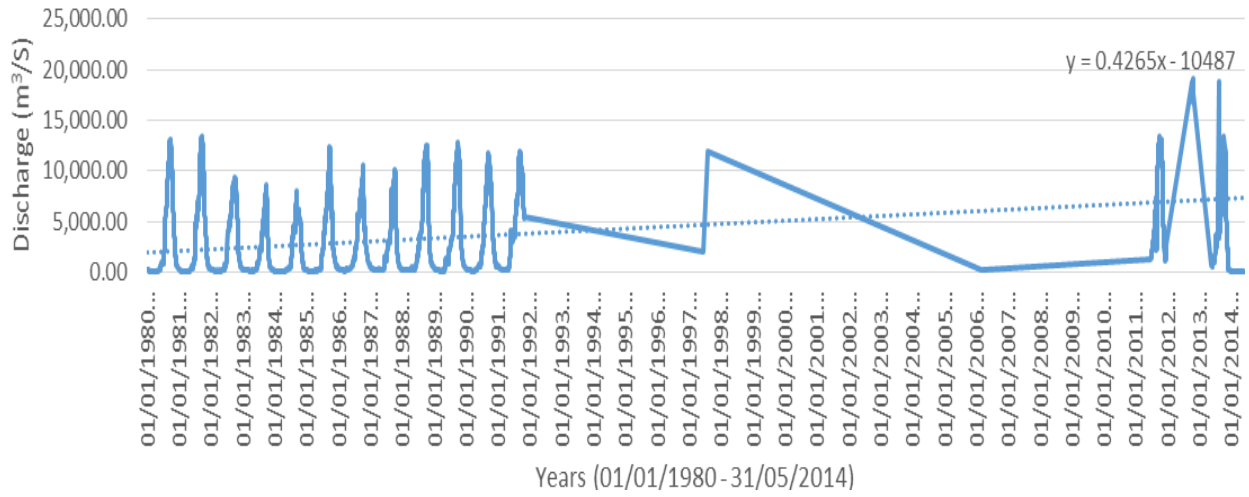

Figure 5. Daily flow hydrograph of the River Benue at Umaisha station from 1980-2014.

Figure 6. Daily streamflow hydrograph of River Benue at Makurdi in 2012.

for the period was 19,120 m^3/s which was recorded on the 15/10/2012. The line chart in Figure 5 shows the discharge amounts at Umaisha from 01/01/1980 to 31/05/2014. The linear forecast trend line shows the trend of discharge is gradually rising.

Average discharge at Makurdi hydrological station was 3,468.24 m^3/s. The peak flow discharge of 16,400 m^3/s was recorded in three days 19th, 29th, and 30th in the month of September 2012 while the peak flow of 2011 was 9,436 m^3/s. The average flow derived for Makurdi which was 3,468.24 m^3/s was surpassed in June. Figure 6 shows the instantaneous daily discharge of the River Benue for the 2012.

The lowest discharge rate in the River Benue was recorded in 1983 while the highest discharge rate occurred in 2012. The total flow in 2012 was not equalled between 1961 and 2011 (50 years). The second highest discharge rate of 15,975 m^3/s was recorded in September 1969. There was high inflow during the month of June before the arrival of peak flow periods of July and September from Upper Benue Basin. The high inflow in July, August and September 2012 led to River Benue overflowing its banks and submerging land areas and settlement in Upper and Lower Benue Basins. In addition, there was a high discharge into River Benue from Lagdo Reservoir in Cameroun in July and subsequent months. Thus, high flow in River Benue is due to both inflow from Lagdo dam in Cameroun and inflows from the Upper and Lower Benue Basins. Figure 7 shows the discharge amounts at Makurdi hydrological station from 01/01/1955

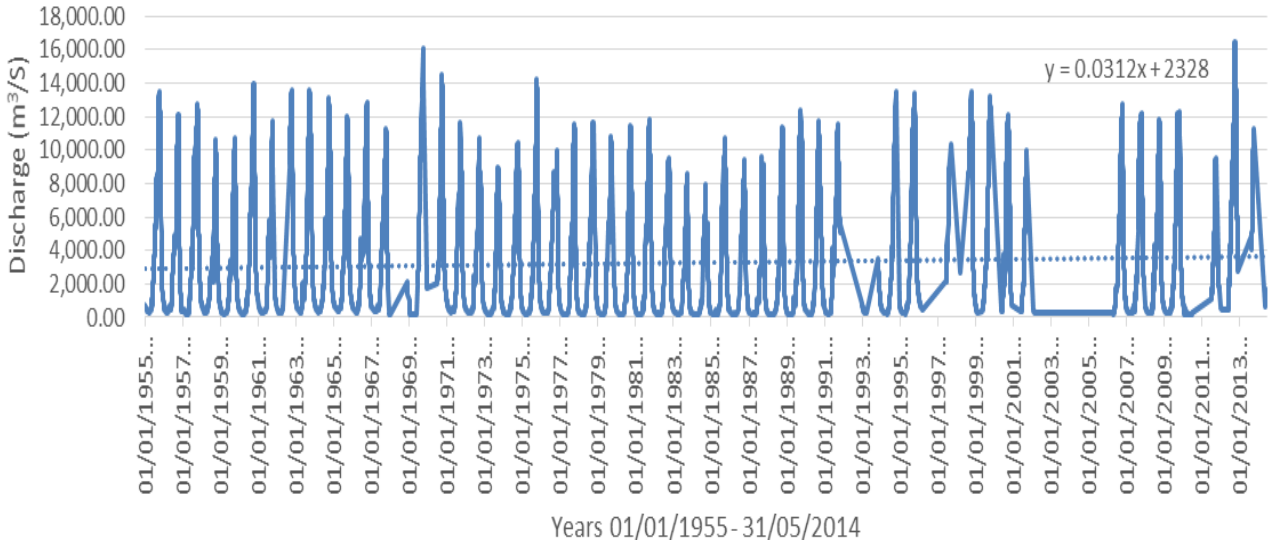

Figure 7. Daily flow hydrograph of River Benue at Makurdi station from 1955-2014.

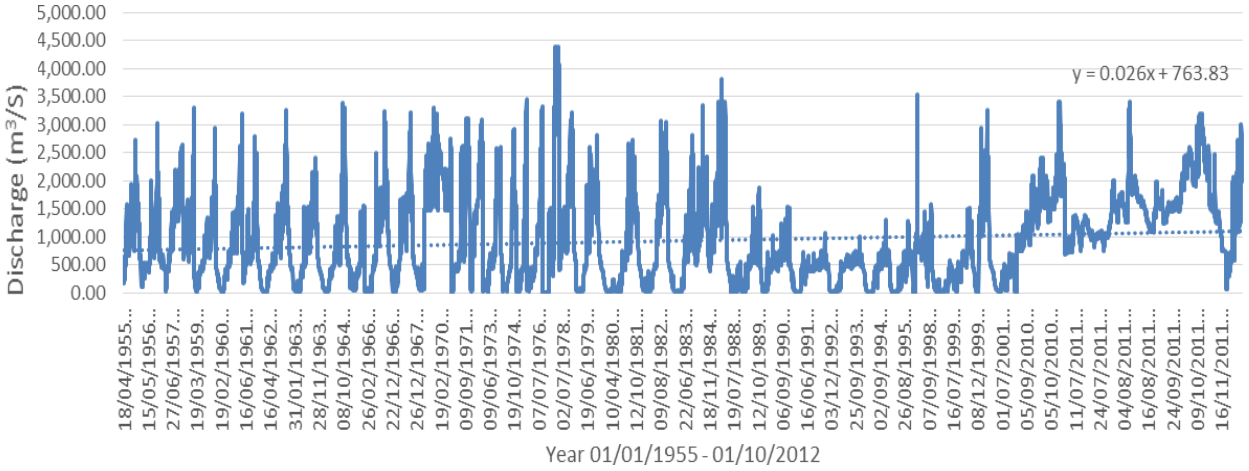

Figure 8. Daily flow hydrograph of the River Katsina Ala from 1955-2012.

to 31/05/2014. The linear forecast trend shows a gradual rise over the years.

At River Katsina Ala hydrological station, the average discharge from January 1955 to May 2014 was 933.12 m^3/s. The maximum discharge for the period was 4,401 m^3/s which was recorded on the 20/10/1977. The line chart in Figure 8 shows the discharge amounts at River Katsina Ala from 01/01/1955 to 01/10/2012. The linear forecast trend shows a gradual rise in discharge.

The averages of monthly total discharge for the period 1980 to 2014 for Umaisha hydrological station (Figure 9) reveals that the River Benue recorded the highest discharge amounts in the months of September (10,556.95 m^3/s) and October (11,651.88 m^3/s). The months of July to November recorded significant discharge amounts from 1980 to 2014 at Umaisha.

The average monthly total discharge for Makurdi was quite similar to Umaisha. In addition to the high discharge amount in September (10,390.17 m^3/s) and October (10,370 m^3/s), amounts over 2000 m^3/s was recorded between July and November (Figure 10). However, unlike Umaisha, the highest monthly average discharge amount in Makurdi was September.

The monthly average discharge for Katsina Ala hydrological station (Figure 11) is not entirely similar to that of Makurdi and Umaisha. The station did not record any discharge amount over 2000 m^3/s in any month of year from 1955 to 2012. The months of September (1518.76 m^3/s) and October (1781.85 m^3/s) recorded the highest monthly average discharge amounts. The lower amounts from Katsina Ala are understandable because it is a smaller river and a tributary of River Benue.

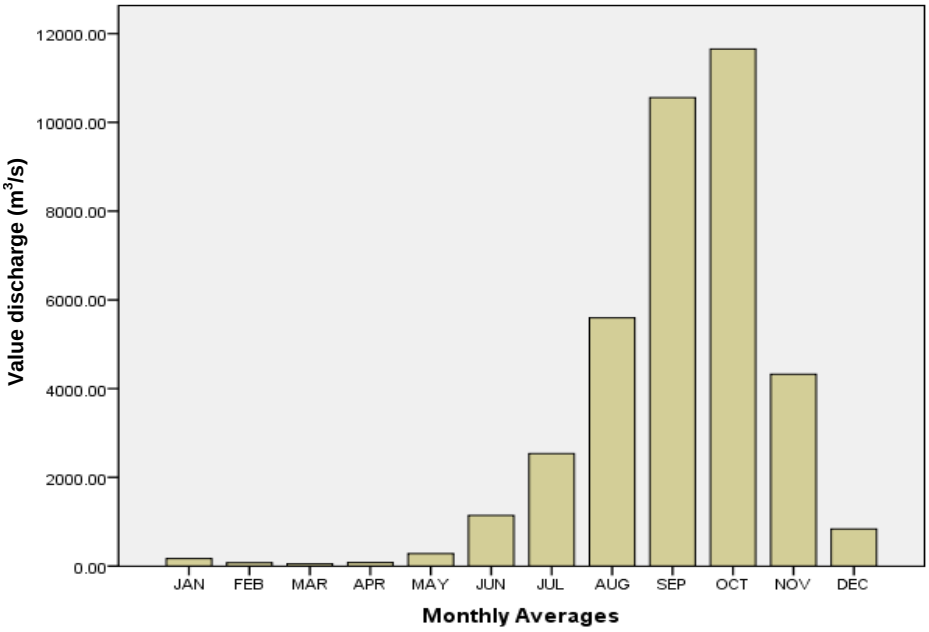

Figure 9. The averages of monthly total discharge for Umaisha (1980-2014).

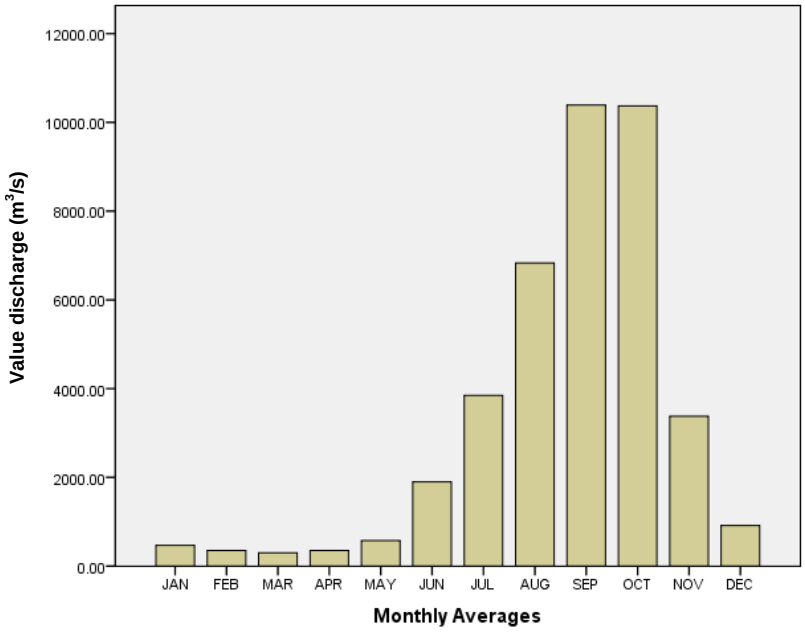

Figure 10. The averages of monthly total discharge for Makurdi (1955-2014).

All the averages of monthly totals of the three hydrological stations where correlated to test if a significant relationship existed between them. The result is presented in Table 2. The monthly discharge averages for Umaisha, Makurdi and Katsina Ala correlated positively with significant values ($p< 0.01$).

The rating curve for the Umaisha, Makurdi, and Katsina Ala were produced (Figures 12 and 13). The rating curves for Umaisha and Makurdi showed a smooth streamflow with Umaisha surpassing the average discharge at 661 cm (Figure 12). Makurdi surpassed the average streamflow of the station at 654 cm (Figure 13). River Katsina Ala rating curve showed a rough streamflow. The River Katsina Ala has several rapids and

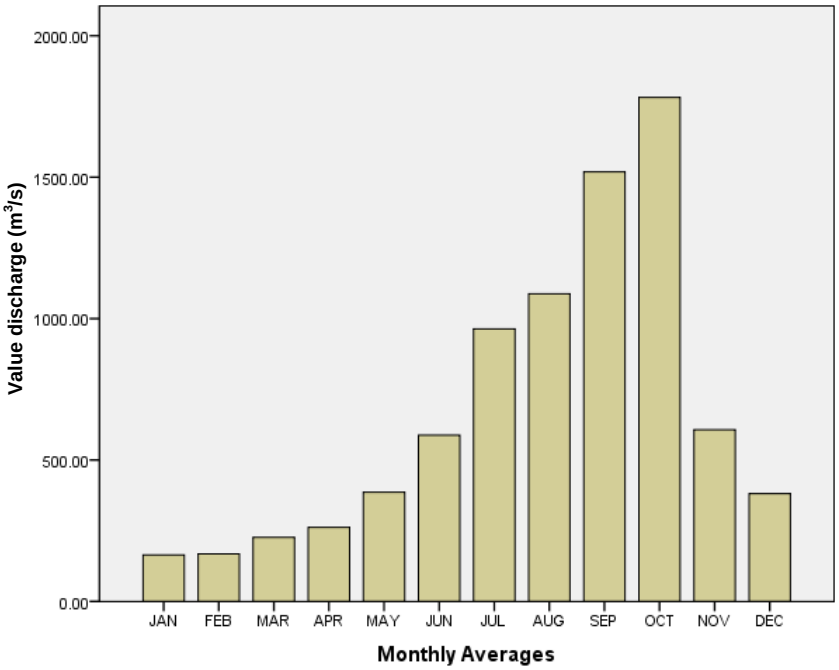

Figure 11. The averages of monthly total discharge for Katsina Ala (1955-2012).

Table 2. Pearson's product correlation of averages of monthly totals discharge for Umaisha, Makurdi, and Katsina Ala.

Parameter			Umaisha discharge (m^3/s)	Makurdi discharge (m^3/s)	Katsina Ala discharge (m^3/s)
Umaisha (m^3/s)	Discharge	Pearson Correlation	1	0.985**	0.958**
		Sig. (2-tailed)		0.000	0.000
		N	12	12	12
Makurdi (m^3/s)	Discharge	Pearson Correlation	0.985**	1	0.979**
		Sig. (2-tailed)	0.000		0.000
		N	12	12	12
Katsina Ala (m^3/s)	Discharge	Pearson Correlation	0.958**	0.979**	1
		Sig. (2-tailed)	0.000	0.000	
		N	12	12	12

**: Correlation is significant at the 0.01 level (2-tailed).

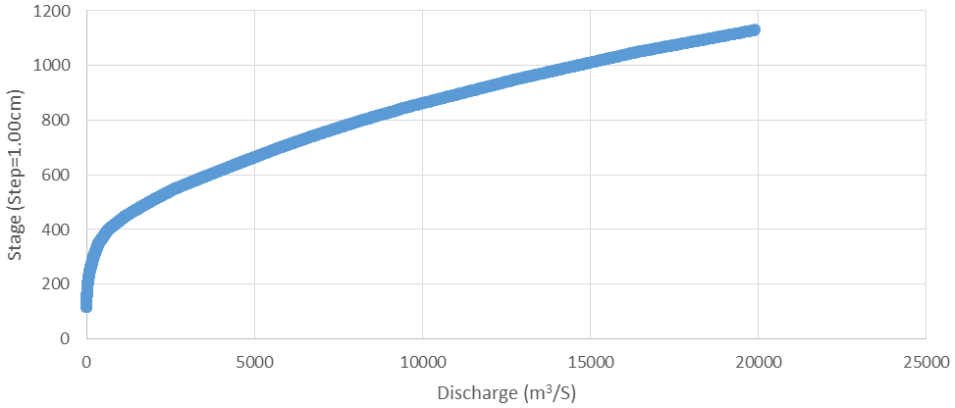

Figure 12. Streamflow rating curve for Umaisha hydrological station.

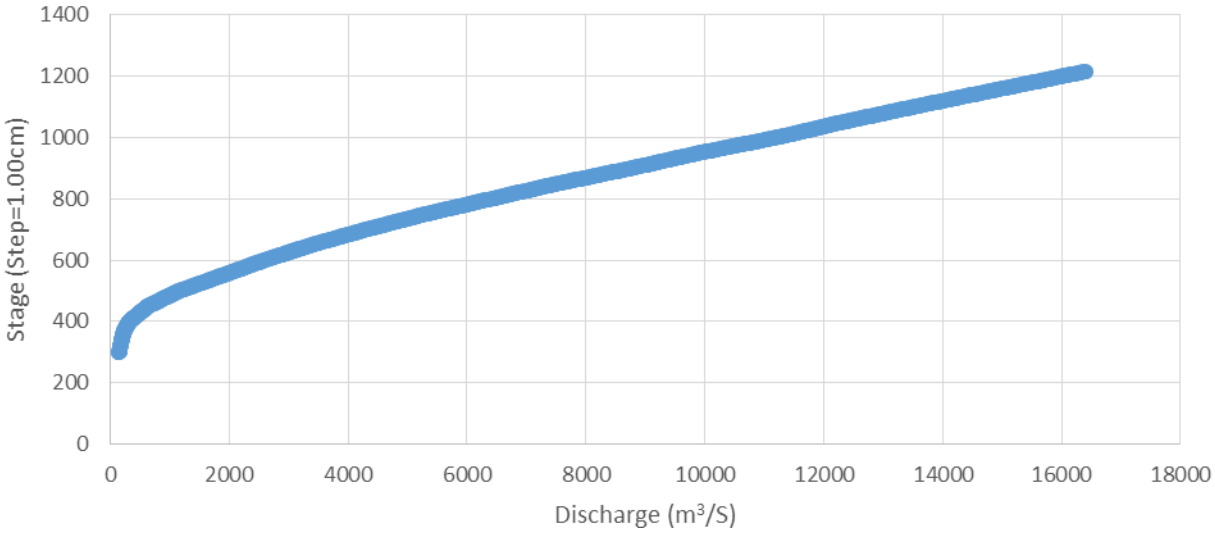

Figure 13. Streamflow rating curve for Makurdi hydrological station.

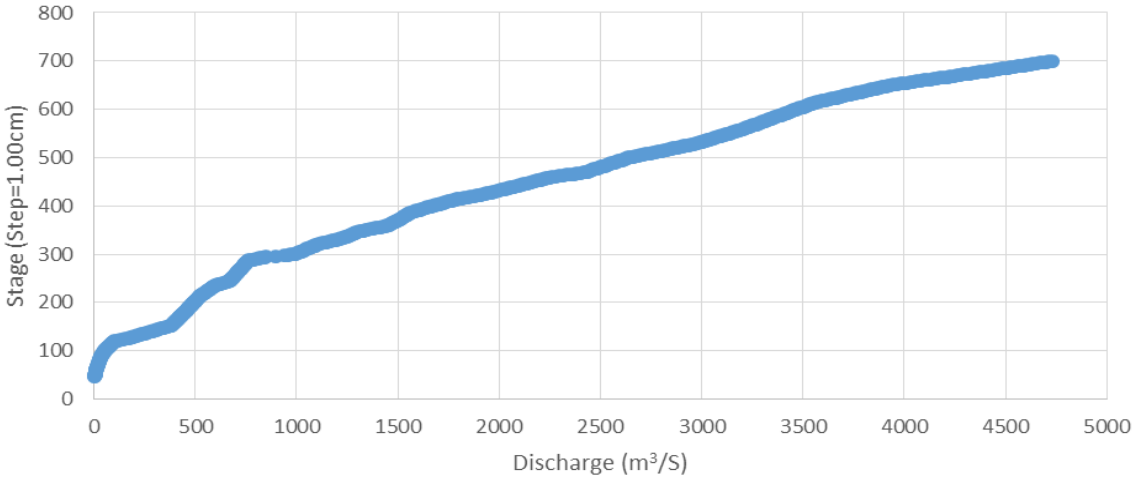

Figure 14. Streamflow rating curve for Katsina Ala hydrological station.

this may have reflected in the rating curve of the hydrological station. The streamflow of River Katsina Ala surpassed average discharge rate at 297 cm (Figure 14).

The drainage map which shows the stream networks of the study area is presented as Figure 15. A total of eleven streams which include River Katsina Ala and River Guma where identified. All these streams are viable throughout the year and provide potential opportunities for local dams and irrigation farming across the study area. There is currently no modern constructed dam in the Lower River Benue Basin.

Increased flood risk in the Lower River Benue Basin

The Nigeria Hydrological Services Agency (NIHSA), in accordance with its statutory mandate to issue flood forecasts, monitors the trend of floods in Nigeria annually. NIHSA releases an annual flood outlook report which provides information to prepare Nigerians living in flood risk areas to be at alert in the event of floods which could damage property and human life.

According to NIHSA (2014), the flow simulation for River Katsina Ala hydrological station for 2014 produced a Julian discharge of 1,368.78 m^3/s. The Julian day for 2013 (1,801.86 m^3/s) was higher than that of 2012 (1,515.46 m^3/s) for Katsina Ala station (Figure 16).

The 2012 Julian day discharge rate for Makurdi was 26, 088.72 m^3/s. This was not reflected earlier in the daily streamflow hydrograph for Makurdi as it was obtained from another report and no date was given for the Julian day by NIHSA (2014). The Julian day for 2013 for Makurdi hydrological station was 16,435.65 m^3/s while the 2014 prediction put the Julian discharge at 15,732.45

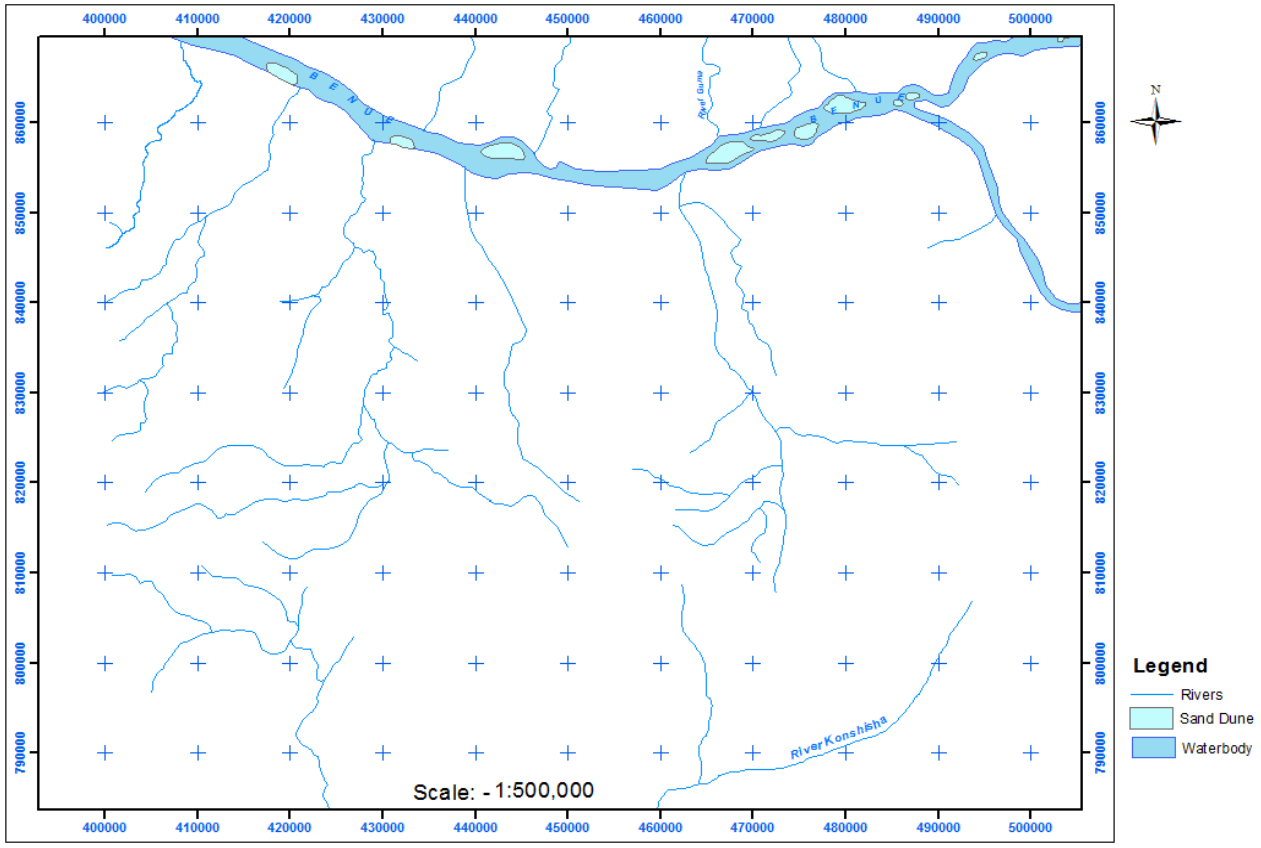

Figure 15. Drainage network of the study area.

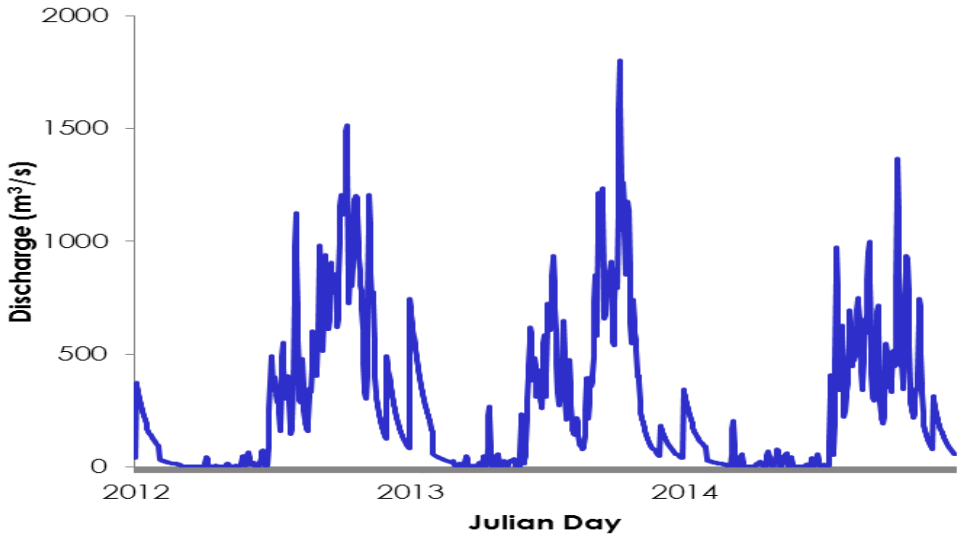

Figure 16. Flow simulation (2014) for River Katsina Ala (NIHSA, 2014).

m^3/s (Figure 17).

The flood plains in the Lower River Benue Basin have been very beneficial to agriculture and this has given rise to high density settlements along the River Benue and its major tributaries such as Umaisha, Makurdi, Tarka, and Katsina Ala (Akpan-Idiok et al., 2013). The occurrence of

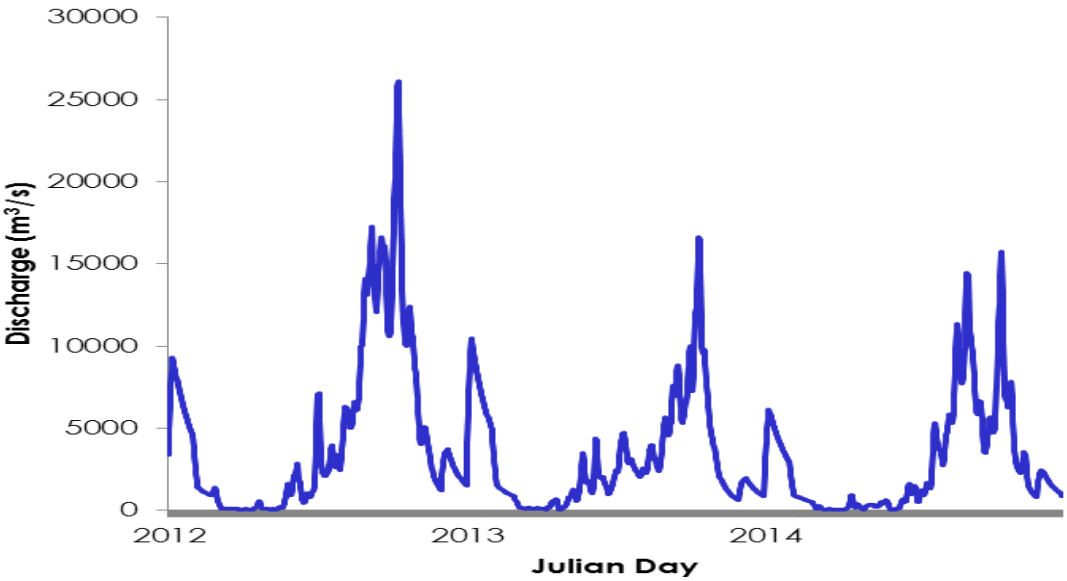

Figure 17. Flow simulation (2014) for River Benue at Makurdi (NIHSA, 2014).

several streams in a basin provides challenges and opportunities as well as tremendous societal significance especially in surface hydrology (Cuo et al., 2014). One of such challenges is the fluctuation in stream volume which overflows during peak seasons. The resulting floods have potential to cause fatalities and huge damage to assets and farms. The gradual rise in discharge rate, and increased fluctuation of streamflow in the Lower River Benue Basin has been mentioned elsewhere (Adelalu, 2012). These phenomena can be explained by rainfall intensity from the rainfall data presented and release of upstream dam waters from the Lagdo dam in northern Cameroun. The influence of the Lagdo dam on flooding on the River Benue is well documented in literature and in local and online media. The causes of flooding in the Lower River Benue Basin has been discussed in Ologunorisa and Tor (2006), Abah (2012), and Ojigi et al. (2013). The profound changes on the hydrological environment around the world have been attributed to climate change (Ehiorobo et al., 2013). The impact of changing climate on streamflow is receiving attention from scholars globally. Aich et al. (2014) studied impact of climate in four African river systems and found a tendency for increased streamflow in three of the four basins. Aich et al. (2014) called for increased attention to river systems in Africa due to risk of increasing high flows. Therefore, rainfall intensity due to changing climate has a significant impact on the streamflow results presented.

Urban growth and development due to land use changes can also influence streamflow. According to Tyubee and Anyadike (2012), a decrease of 19% (4 km^2) occurred in the area of water in Makurdi the Benue State capital from 1991(21 km^2) to 2006 (17 km^2). Forest areas witnessed a decline by 28% (37 km^2) for the same period from 1991(133 km^2) to 2006 (96 km^2). Undergrowth and wetland areas decreased by 32% (119 km^2) between 1991 (370 km^2) and 2006 (251 km^2). Similarly, cultivated areas shrunk by 14% (19 km^2) from 1991 (138 km^2) to 2006 (119 km^2) in 2006. All these changes in land use were attributed to urban growth and development by Tyubee and Anyadike (2012), as built-up areas witnessed an increase of 130% (179 km^2) from 1991 (138 km^2) to 2006 (317 km^2). Tyubee and Anyadike (2012) stated that degradation of wetlands, water channels and deforestation due to increased urban population and unregulated land use contributes to flooding. Increased built-up areas have the potential to increase run-off after intensive rainfall.

A severe flooding event occurred in Nigeria in 2012 as intensive rainfall and river overflow caused extensive flooding in the flood plains of the River Benue and River Niger. The flooding of 2012 was escalated by the discharge of floodwaters from the Lagdo dam in Cameroon into the River Benue. Obiora (2014) conducted a study on 120 farmers in Benue State to assess the impact of the 2012 floods on these farmers. According to Obiora (2014), these farmers lost houses and storages (60.0%), farmlands (60.0%), and human lives (10.0%). In order to survive the losses from the floods, 35.0% of the respondents resorted to begging alms and another 30.0% migrated to neighbouring communities. Obiora (2014) stated that 70% of respondents had no survival strategies and resigned to fate. A total of 112, 362 people were internally displaced by the 2012 floods and a total area of 932.46 km^2 was inundated by the 2012 floods (Ojigi et al., 2013). The annual occurrence of flooding in the study area is

adequately reported in literature (Ologunorisa and Tor, 2006; Abah, 2012; Ojigi, 2013; Shabu and Tyonum, 2013). In order to control flood damage in the study area, the government of Benue State should explore these modern measures:

1. Development of dams and reservoirs which are currently lacking.
2. Improved streamflow prediction and flood warning mechanisms
3. Clearing debris from water channels and drainages for river and rainfall run-offs.
4. Re-dredging of silted streams and construction of new drainages.
5. Mid-term and long-term plans to relocate people living along river banks and those that have livelihood activities on the flood plains of the Lower River Benue Basin.

Conclusion

The paper has assessed streamflow characteristics and has observed a high rate of variation in discharge rate and increased streamflow variability on the main streams in the Lower River Benue Basin. Policy makers in the region may wish to plan adequately to steer away development from the flood plains of the River Benue and its tributaries and mainstream flood control measures into future development plans.

CONFLICT OF INTERESTS

The authors have not declared any conflict of interests.

REFERENCES

Abah RC (2012). Causes of seasonal flooding in flood plains: A case of Makurdi, Northern Nigeria. Int. J. Environ. Stud. 69(6):904-912.

Adelalu TG (2012). Climate variability and river Benue discharge in Jimeta, Yola area, Nigeria. Hydrology for Disaster Management. Spec. Publ. Niger. Assoc. Hydrol. Sci. pp. 375-382.

Aich V, Liersch S, Vetter T, Huang S, Tecklenburg J, Hoffmann P, Koch H, Fournet S, Krysanova V, Müller EN, Hattermann FF (2014). Comparing impacts of climate change on streamflow in four large African river basins. Hydrol. Earth Syst. Sci. 18:1305-1321,

Akpan-Idiok AU, Ukabiala ME, Amhakhian OS (2013). Characterization and classification of River Benue floodplain soils in Bassa Local Government Area of Kogi State, Nigeria. Int. J. Soil Sci. 8:32-46.

Akpoborie IA, Asiwaju-Bello AY, Efobo O (2012). Streamflow variability in Ossiomo River catchment and implications for basin-wide water resources management. Hydrology for Disaster Management. Spec. Publ. Niger. Assoc. Hydrol. Sci. pp. 338-350.

Ayoade JO (2004). Introduction to climatology for the tropics. Revised edition. Spectrum Books limited, Ibadan.

Cuo L, Zhang Y, Zhu F, Liang L (2014). Characteristics and changes of streamflow on the Tibetan Plateau: A review. J. Hydrol. Reg. Stud. *2*:49-68.

Ehiorobo JO, Izinyon OC, Ilaboya IR (2013). Effect of climate change on the river flow regimes in the mangrove and tropical rain forest of the Niger Delta region of Nigeria. Res. J. Eng. Appl. Sci. 2(4):256-261

Food and Agricultural Organisation - FAO (1990). Source book for the inland fishery resources of Africa. CIFA Technical FAO Rome. 18(2):411.

Ita EO, Sado EK, Balogun JK, Pandogari A, Ibitoye B (1985). Inventory survey of Nigeria inland waters and their fishery resources. I. A preliminary checklist of inland water bodies in Nigeria with special reference to ponds, lakes, reservoirs and major rivers. Kainji Lake Research Institute Tech. Rep. Ser. 14. New Bussa, Nigeria.

Kogbe AC (Ed.) (1989). Geology of Nigeria. Rock View Ltd, Jos.

National Hydrological Service Agency NIHSA (2014). Annual flood outlook report. Federal Ministry of Water Resources, NIHSA, Abuja, Nigeria.

Nwilo PC, Olayinka DN, Adzandeh AE (2012). Flood Modelling and Vulnerability Assessment of Settlements in the Adamawa State Floodplain using Remote Sensing and Cellular Framework Approach. Glob. J. Hum. Soc. Sci. Res. 12(3).

Obiora CJ (2014). Survival strategies for climate change induced stress among women farmers in Benue State, Nigeria. Res. Hum. Soc. Sci. 4(2):87-90.

Ojigi ML, Abdulkadir FI, Aderoju M (2013). Geospatial mapping and analysis of the 2012 flood disaster in central parts of Nigeria. Conference paper presented at the 8th National GIS Symposium. Dammam, Saudi Arabia. April 15-17.

Ologunorisa T, Tor T (2006). The changing rainfall pattern and its implication for flood frequency in Makurdi, Northern Nigeria. J. Appl. Sci. Environ. Manage. 10(3):97-102.

Shabu T, Tyonum TE (2013). Residents coping measures in flood prone areas of Makurdi town, Benue State. Appl. Eco. Environ. Sci. 1(6):120-125.

Tyubee BT, Anyadike RNC (2012). Analysis of surface urban heat island in Makurdi, Nigeria. African Climate Change Fellowship Program (ACCFP). Available online at: www.goes-r.gov.

Uchua KA, Nduke GE (2011). Agricultural landuse planning based on terrain characteristics using remote sensing and geographic information system in the lower river Benue floodplain Nigeria. J. Sus. Dev. Environ. Prot. 1(3):67-72.

African Journal of Environmental Science and Technology

Related Journals Published by Academic Journals

- *Journal of Ecology and the Natural Environment*
- *Journal of Bioinformatics and Sequence Analysis*
- *Journal of General and Molecular Virology*
- *International Journal of Biodiversity and Conservation*
- *Journal of Biophysics and Structural Biology*
- *Journal of Evolutionary Biology Research*

academicJournals